


12-2017

# Investigating Fate of Silver Nanoparticles in Wastewater Biofilms

Connie Marie Walden  
*University of Arkansas, Fayetteville*

Follow this and additional works at: <http://scholarworks.uark.edu/etd>

 Part of the [Civil Engineering Commons](#), and the [Environmental Engineering Commons](#)

---

## Recommended Citation

Walden, Connie Marie, "Investigating Fate of Silver Nanoparticles in Wastewater Biofilms" (2017). *Theses and Dissertations*. 2549.  
<http://scholarworks.uark.edu/etd/2549>

This Dissertation is brought to you for free and open access by ScholarWorks@UARK. It has been accepted for inclusion in Theses and Dissertations by an authorized administrator of ScholarWorks@UARK. For more information, please contact [scholar@uark.edu](mailto:scholar@uark.edu), [ccmiddle@uark.edu](mailto:ccmiddle@uark.edu).

# Investigating Fate of Silver Nanoparticles in Wastewater Biofilms

A dissertation submitted in partial fulfillment  
of the requirements for the degree of  
Doctor of Philosophy in Engineering

by

Connie Marie Walden  
University of Arkansas  
Bachelor of Science in Civil Engineering, 2012  
University of Arkansas  
Master of Science in Civil Engineering, 2014

December 2017  
University of Arkansas

This dissertation is approved for recommendation to the Graduate Council.

---

Dr. Wen Zhang  
Dissertation Director

---

Dr. Julian Fairey  
Committee Member

---

Dr. Franck Carbonero  
Committee Member

---

Dr. Lauren Greenlee  
Committee Member

## **Abstract**

As industrial advances make everyday life easier for human kind, the processes by which we need to maintain sanitary conditions for both water and wastewater treatment will become increasingly complex. Innovations in food packaging and textile design incorporate engineered nanoparticles (ENPs) to increase antimicrobial properties of clothing, maintain product color, and keep food in packaging from spoilage. For most products, ENPs released will enter the sanitary sewer system, and ultimately wastewater treatment plants. Biofilms grow universally on surfaces where a protective layer of extracellular polymeric substances (EPS) shields attached cells from stressors. In wastewater treatment, complex biofilms are utilized as a biological process for nutrient removal. Along with manufacturing innovations, the technology to study wastewater processes also continues to advance. Understanding complex biological communities requires detailed expertise in metagenomics for identifying bacteria present in a unit process of interest. This dissertation seeks to address both issues with respect to biofilm processes. First, a review of ENPs and their interaction with wastewater microbial communities lays groundwork for understanding the current state of knowledge. Then, a comparison of multiple methods to identify wastewater biofilms will help to understand the proper application of metagenomics to study changing biofilms in the presence of ENPs. Finally, multiple bench scale reactors and a quartz crystal microbalance are used to quantify ENP accumulation in wastewater biofilm. These studies advance the field of biofilm research by aiding in understanding how new technologies impact the biological treatment processes applied in wastewater treatment, as well as improve on the metagenomic identification of biofilm communities in these environments.

## **Acknowledgments**

I would like to extend deepest gratitude to my advisor, Dr. Wen Zhang, for unwavering support and countless late-night revisions of each manuscript. I would not have been able to work this program and have a balanced home life without her understanding and encouragement. Besides my advisor, I would like to thank the rest of my advisory committee, Dr. Julian Fairey, Dr.

Franck Carbonero, and Dr. Lauren Greenlee for providing thoughtful input throughout the years.

I also acknowledge and am forever thankful for financial support provided by the University of Arkansas Graduate School Doctoral Academy Fellowship for the past four years, and the Hearst Foundation Fellowship through the Women in Engineering program.

I am grateful to the other graduate students including Clint Mash, Johnnie Chamberlin and undergraduate Casey Gibson whom helped with gathering data, maintaining the laboratory, and sharing a laugh when things went terribly wrong. A special shout to Thien Do, whose insistence on a dozen training sessions on multiple devices not only made me chuckle, but also pull out my hair.

## **Dedication**

This dissertation is dedicated to my parents for somehow molding me into the person I strive to be every day. And to my husband, thank you for riding this train to the end.

## Table of Contents

<b>Chapter 1: Introduction</b> .....	1
1. Problem Statement .....	2
2. Objectives and Approach .....	3
2.1. Objective 1 .....	3
2.2. Objective 2 .....	3
2.3. Objective 3 .....	4
3. Document Organization .....	4
4. References .....	6
<b>Chapter 2: Biofilms versus activated sludge: considerations in metal and metal oxide nanoparticle removal from wastewater</b> .....	7
1. Introduction .....	8
1.1. Application and use of Me(O)NPs .....	9
1.2. Presence of Me(O)NPs in wastewater .....	11
2. Agglomeration/Aggregation of Me(O)NPs in wastewater .....	14
3. Interaction between Me(O)NPs and activated sludge .....	19
3.1. Removal of Me(O)NPs with activated sludge .....	19
3.2. Toxicity of Me(O)NPs and its impact on nutrient removal .....	21
3.3. Impact on subsequent processes .....	23
4. Interactions between ENPs and Biofilm .....	24
4.1. Entrapment of Me(O)NPs .....	26
4.2. Factors affecting removal of Me(O)NPs .....	28
5. Me(O)NPs impact upon wastewater treatment design .....	30

5.1. Implications of Me(O)NPs in wastewater treatment processes.....	30
5.2. Considerations in regulating Me(O)NP removal from wastewater.....	33
<b>Chapter 3: Assessing impacts of DNA extraction methods on next generation sequencing of water and wastewater samples.....</b>	<b>55</b>
1. Introduction.....	57
1.1 Materials and Methods.....	59
1.1.1. Study sites and sampling.....	59
1.1.2. Sample processing.....	59
1.1.3. DNA extractions.....	60
1.1.3.1. QIAamp DNA Mini Kit.....	60
1.1.3.2. QIAamp DNA Stool Mini Kit.....	61
1.1.3.3. MO BIO PowerSoil DNA Kit.....	61
1.1.3.4. MO BIO PowerWater DNA Kit.....	61
1.1.4. 16S rRNA amplification and Illumina sequencing.....	61
2. Results and Discussion.....	62
2.1 Alpha diversity.....	63
2.1.1 Relative abundance.....	64
2.1.1.1 Freshwater lake.....	64
2.1.1.2 Trickling filter reactor.....	64
2.1.1.3 Moving bed bioreactor.....	65
2.1.2 Beta diversity.....	66
2.1.2.1 Lake community.....	66
2.1.2.2 MBBR biofilm community.....	67

2.1.2.3 MBBR planktonic community.....	67
2.1.2.4 TF biofilm community.....	67
2.1.2.5 TF planktonic community.....	67
2.1.3 Full dataset analysis.....	68
2.1.4 Conclusion.....	68
<b>Chapter 4: Bioaccumulation of silver nanoparticles in wastewater biofilm .....</b>	<b>104</b>
1. Introduction.....	106
2. Materials and Methods.....	108
3. Results and Discussion .....	113
3.1 CBR exposure tests.....	115
3.2 Flow cell exposure tests.....	116
4. Conclusion .....	120
<b>Chapter 5: Real-time interaction of mixed species biofilm with silver nanoparticles using QCM-D.....</b>	<b>138</b>
1. Introduction.....	140
2. Materials and Methods.....	143
3. Results and Discussion .....	147
4 Conclusion.....	151
<b>Chapter 6: Conclusion.....</b>	<b>165</b>



## List of Tables

### Chapter 2.

**Table 1.** Summarized results of studies focusing on the fate of Me(O)NPs in wastewater treatment design .....37

**Table 2.** Studies focusing on the toxicity of Me(O)NPs in activated sludge .....39

**Table 3.** Summarized results of studies focusing on the implications of Me(O)NPs in wastewater treatment processes .....40

### Chapter 3.

**Table 1.** Experimental matrix detailing various sampling locations and DNA extraction methods compared among sample types.....70

**Table 2.** Sequencing and metagenomic final sequence totals after quality filtering, removal of chimeras, and uniqueness filtering .....71

**Table S1.** LIBSHUFF analysis output.....95

### Chapter 4.

**Table 1.** CBR effluent characteristics after multiple retention times.....125

**Table S1.** Particle size analysis for stock Ag-NP solution.....136

**Table S2.** Particle size analysis for stock Ag-NPs in wastewater .....137

### Chapter 5.

**Table 1.** Mixed model wastewater biofilm species characteristics. ....153

**Table 2.** Frequency and dissipation rates of change for mixed model biofilm under exposure to different concentrations of Ag-NPs. ....154

## List of Figures

### Chapter 2.

**Figure 1.** Typical fate of Me(O)NPs in WWTPs for both activated sludge and biofilm processes .....36

### Chapter 3.

**Figure 1.** Comparison of alpha diversity indices (simpson, chao, ace, and shannon index) between all sample types and kits .....72

**Figure 2.** The relative abundance of microbiota variations at phylum level among location types across extraction methods.....73

**Figure 3.** Un-weighted Pair Group Method with Arithmetic mean (UPGMA) hierarchical clustering using Euclidean similarity index to interpret the distance matrix produced from  $\beta$ -diversity analysis.....74

**Figure 4.** Principal components analysis (PCoA) of each community for all extraction methods where samples diverged into 4 distinct ellipses .....75

**Figure S1.** Similarity tree at 0.07 distance for freshwater Lake sample set.....84

**Figure S2.** PCoA analysis of Lake samples relating each method through eigenvectors (Pearson method) .....85

**Figure S3.** Similarity tree at 0.07 distance for MBBR wastewater biofilm environment .....86

**Figure S4.** 3D PCoA analysis of MBBR biofilm samples relating each method through eigenvectors (Pearson method) .....87

**Figure S5.** Similarity tree at 0.07 distance for MBBR suspended environment .....88

**Figure S6.** PCoA analysis of MW samples relating each method through eigenvectors (Pearson method). .....89

**Figure S7.** Similarity tree at 0.07 distance for TB environment .....90

**Figure S8.** PCoA analysis of TB samples relating each method through eigenvectors (Pearson method) .....91

**Figure S9.** Similarity tree at 0.07 distance for TW environment .....92

**Figure S10.** PCoA analysis of TW samples relating each method through eigenvectors (Pearson method). .....93

<b>Figure S11.</b> Rarefaction curves for sub-sampled dataset (n=762) at each sampling location and extraction methods .....	94
--	----

#### Chapter 4.

<b>Figure 1.</b> Biovolume measurement of fluorescently stained model biofilm in the CBR after Ag-NP exposure .....	121
---	-----

<b>Figure 2.</b> Reactive oxygen species detected before and after Ag-NP exposure to biofilms .....	122
---	-----

<b>Figure 3.</b> Confocal laser scanning microscope image of biofilm stained with propidium iodide and Hoescht 33358.....	123
---	-----

<b>Figure 4.</b> Sorption of Ag-NPs to differently formed model wastewater biofilms .....	124
---	-----

<b>Figure S1.</b> Custom flow cell image.....	130
---	-----

<b>Figure S2.</b> SW selection through biofilm formation assay .....	131
--	-----

<b>Figure S3.</b> UV-vis spectra of Ag-NP stock solution.....	132
---	-----

<b>Figure S4.</b> TEM image of Ag-NP stock solution.....	133
--	-----

<b>Figure S5.</b> TEM images of Ag-NPs.....	134
---	-----

<b>Figure S6.</b> Morphology of model biofilm species .....	135
---	-----

#### Chapter 5.

<b>Figure 1.</b> TEM image analysis of Ag-NPs in synthetic wastewater. The inset table summarizes the analysis particle counts and mean diameter from ImageJ .....	155
--	-----

<b>Figure 2.</b> Change in frequency and change in dissipation for biofilm during Ag-NP exposure. ....	156
--	-----

<b>Figure 3.</b> $\Delta D/\Delta f$ over time for (a) Ag-NPs alone (b) during biofilm formation.....	157
---	-----

<b>Figure 4.</b> $\Delta D/\Delta f$ over time for each Ag-NP concentration tested. (a) 20 ppb (b) 127 ppb for 30 minutes and 127 ppb final step-down for the final 10 minutes (c) 300 ppb (d) 666 ppb (e) 1160 ppb (f) 1632 ppb.....	158
---	-----

<b>Figure 5.</b> Confocal laser scanning microscope image slice from z-stacked measurements of the final attached biofilm to the quartz crystal sensor .....	159
--	-----

**Figure S1.** TEM image of Ag-NP stock solution.....161

## **List of Published Papers**

### **Chapter 2**

Walden, C. and W. Zhang, 2016. "Biofilms Versus Activated Sludge: Considerations in Metal and Metal Oxide Nanoparticle Removal from Wastewater." *Environmental Science & Technology*, 50 (16), 8417-8431.

### **Chapter 3**

Walden, Connie, F. Carbonero, and W. Zhang. 2017. "Assessing impacts of DNA extraction methods on next generation sequencing of water and wastewater samples." *Journal of Microbiological Methods* 141 (Oct) 10-16.

**Chapter 1**  
**Introduction**

## 1. Problem Statement

Bacteria near surfaces tend to form biofilms with a robust matrix of excreted polysaccharides, nucleic acids, cells and proteins (Metcalf, and, & Eddy, 2003). When biofilms develop, the cells are protected by this matrix. Biofilms thrive in the environment, surviving anywhere an interface and water are in contact. Multiple advantages arise from this protection, including resistance to antibiotics and chlorine (Watnick & Kolter, 2000). Biological treatment processes in wastewater utilize bacteria (planktonic or attached) for the breakdown of nutrients and compounds that are regulated in wastewater effluents. The most common today, activated sludge processes, require removal of sand and grease before treatment, while also involves downstream clarification and mixed liquor recycle. As activated sludge processes depend on a balance between sludge age and hydraulic retention time, treatment plant upgrades to meet new standards may require an infeasible increase in basin volumes due to land availability limitations (Capdeville & Rols, 1992). As land availability decreases and wastewater effluent standards become more stringent, biofilm processes are an excellent option for treatment plant upgrades and small communities. Examples include biofiltration, moving bed biofilm reactors, and membrane biofilm reactors.

The United States Environmental Protection Agency (US EPA) sets limits for conventional pollutants such as biochemical oxygen demand, total suspended solids, fecal coliform, and pH in wastewater effluents under the Clean Water Act section 304(b) (US EPA, 2015). Emerging pollutants, such as engineered nanoparticles (ENPs) have yet to be regulated in the United States. ENPs are less than 100 nm in diameter, and given the large surface area to volume ratio, react differently than larger particles of the same element. Most commonly found in anti-microbial textiles and food packaging, the washing of such products inevitably results in

ENPs entering wastewater treatment facilities. Certain ENPs have toxic effects on nitrifying bacteria and anaerobic processes (Ma, Zhong, Han, & Wang, 2013). However, with silver nanoparticles (Ag-NPs), the toxic threshold is measured at unrealistically high concentrations (Thuptimdang, Limpiyakorn, & Khan, 2017). Therefore, the possibility of silver accumulation in biofilm without toxic effects is possible.

The following dissertation focused on the overall interaction between biofilm biological processes and ENPs. Our goal is to study the interaction between complex biofilms and Ag-NPs as model ENPs. The dissertation addresses (1) current publications on the impacts of ENPs in wastewater systems; (2) application of next generation sequencing for reproducible biofilm community identification; (3) quantification of ENP accumulation in mixed wastewater biofilms; and (4) fundamental response of biofilm in the presence of Ag-NPs as a model ENP.

## **2. Objectives and Approach**

### **2.1 Objective 1**

The first objective is to summarize the current research on metal and metal oxide nanoparticles (Me(O)NPs). Research into wastewater-ENP interactions will be divided into two key categories: activated sludge and biofilm processes. The known fate and impact of common Me(O)NPs will be summarized within each of these biological processes. Then, the advantages and disadvantages will be weighed in terms of ENP removal and toxicity to bacteria communities. Key gaps concerning biofilm-NP interactions will identify groundwork for the rationale of the following biofilm – ENP studies.

### **2.2 Objective 2**

The second objective is to study the effects of DNA extraction method on biofilm community analysis with next generation sequencing (NGS) technology. Biofilms in wastewater



systems are complex and require metagenomic analysis for identifying key species present. Four locations will be sampled, including planktonic and biofilm species, and tested with four DNA extraction methods. The most efficient method will be applied in future studies regarding ENP – biofilm interactions with environmental biofilms.

### **2.3 Objective 3**

The third objective is to quantify accumulation of ENPs, as well as the biofilms structural response to ENP exposure. A mixed model biofilm will be developed and tested for functionality and reproducibility in a CDC Biofilm Reactor (CBR). Following, a flow cell will be used for ENP exposure tests to quantify ENP accumulation and detachment from this model system. Finally, a quartz crystal microbalance with dissipation monitoring will measure changes in frequency and dissipation as the model biofilm is exposed to different concentrations of ENPs (QCM-D). The biofilm structural response will be interpreted from resonant frequency shifts and dissipation rates of change.

### **3. Document Organization**

Chapter 2 addresses Objective 1 and reviews both activated sludge and biofilm processes in terms of ENP toxicity, fate, and advantages in each type of system. Few studies are published on biofilm – ENP interactions, so extrapolations were made from more broadly conducted studies in biofiltration and soil environments.

Chapter 3 addresses Objective 2. The most efficient DNA extraction method for NGS processing was identified when comparing across multiple wastewater environments. We show diversity variations across extraction methods and similarities among sampling sites. Ultimately, two extraction methods proved most reliable when comparing all sites in terms sequencing coverage, phylum identification, and community mapping.

Chapter 4 and Chapter 5 address Objective 3. A mixed model biofilm was tested in a CBR and proved resistant to functionality changes while in the presence of Ag-NPs as a model ENP. Further, flow cell tests revealed accumulation occurs minimally, and does not show to be affected by influent Ag-NP concentration fluctuations. QCM-D experiments show biofilm structural responses to multiple Ag-NP concentrations by comparing  $\Delta D/\Delta f$  ratios over time.

## References

Capdeville, B., & Rols, J. (1992). Introduction to biofilms in water and wastewater treatment *Biofilms—Science and Technology* (pp. 13-20): Springer.

Ma, W., Zhong, D., Han, H., & Wang, P. (2013). A review: inhibition of Ag NPs on wastewater treatment. *Desalination and Water Treatment*, 51, 7012–7017.

Metcalf, and, & Eddy, I. (2003). *Wastewater engineering : treatment and reuse*: Fourth edition / revised by George Tchobanoglous, Franklin L. Burton, H. David Stensel. Boston : McGraw-Hill, [2003] ©2003.

Thuptimjang, P., Limpiyakorn, T., & Khan, E. (2017). Dependence of toxicity of silver nanoparticles on *Pseudomonas putida* biofilm structure. *Chemosphere*, 188, 199-207. doi:10.1016/j.chemosphere.2017.08.147

US EPA, O. (2015, 2015). National Recommended Water Quality Criteria.

Watnick, P., & Kolter, R. (2000). Biofilm, city of microbes. *Journal of bacteriology*, 182(10), 2675-2679.

## Chapter 2

### Biofilms Versus Activated Sludge: Considerations in Nanoparticle Removal from Wastewater

## **Abstract**

The increasing application of metal and metal oxide nanoparticles [Me(O)NPs] in consumer products has led to a growth in concentration of these nanoparticles in wastewater as emerging contaminants. This may pose a threat to ecological communities (*e.g.*, biological nutrient removal units) within treatment plants and those subject to wastewater effluents. Here, the toxicity, fate, and process implications of Me(O)NPs within wastewater treatment, specifically during activated sludge processing and biofilm systems are reviewed and compared. Research showed activated sludge achieves high removal rate of Me(O)NPs by the formation of aggregates through adsorption. However, recent literature reveals evidence that inhibition is likely for nutrient removal capabilities such as nitrification. Biofilm systems were much less studied, but show potential to resist Me(O)NP inhibition and achieve removal through possible retention by sorption. Implicating factors during bacteria-Me(O)NP interactions such as aggregation, surface functionalization, and the presence of organics are summarized. At current modeled levels, neither activated sludge nor biofilm systems can achieve complete removal of Me(O)NPs, thus allowing for long-term environmental exposure of diverse biological communities to Me(O)NPs in streams receiving wastewater effluents. Future research directions are identified throughout to minimize the impact of these nanoparticles released

### **1. Introduction.**

Metal and metal oxide nanoparticles [Me(O)NPs] can enter the aquatic environment through multiple pathways (*e.g.*, agrochemicals, (Khot et al., 2012) construction, (*Opportunities and Risks of Nanotechnologies*, 2007) air pollution (Stone et al., 2007)) with the most prevalent by way of domestic and/or industrial wastewater. Me(O)NPs could pose a threat to aquatic organisms when released into surface waters (Bondarenko et al., 2013). Findings in recent

studies regarding nanoscale impacts on WWTPs indicate that more attention should be focused on the increasing presence of these contaminants in residential and commercial wastewater (Eduok et al., 2013). A previous review of possible outcomes for ENP fate through a WWTP carefully laid out what can happen at each process, however, a lack of sufficient literature at that time left quantifiable fate and negative microbial impacts to speculation (Brar et al., 2010). A more recent review also summarized Me(O)NP fate in wastewater, but focused solely on activated sludge or methane production, still asking what conditions increase or decrease ENP toxicity (Wang and Chen, 2015). Other alternatives to activated sludge in biological wastewater treatment were rarely investigated for the interaction with Me(O)NPs, such as biofilm systems. This review directly compares the advantage and disadvantage between activated sludge and biofilm systems in regard to Me(O)NP fate, toxicity, and removal from wastewater. Here, known impacts of Me(O)NPs upon conventional WWTPs and biofilm systems are presented and discussed to critically review the efficacy of these design processes for nanoparticle removal. Finally, an overall comparison will be summarized between activated sludge and biofilm systems, attempting to answer this overarching question – “can biofilm systems offer better Me(O)NP removal from wastewater than activated sludge?” Knowledge gaps and future opportunities for further studies are identified throughout.

### **1.1 Application and use of Me(O)NPs.**

The Project on Emerging Nanotechnologies (Vance et al., 2015) (independently collaborating with industry, researchers, and government in the United States) defines nanoparticles as one of four categories: engineered, incidental, natural, or generic while identifying over 1800 consumer products which are nanotechnology-based. ENPs are manufactured explicitly with a structure between approximately 1 nm and 100 nm, exhibiting nano-sized properties different from their larger counterparts (Auffan et al., 2009). The large specific surface areas of ENPs (surface area

to volume ratio) result in a high reactivity. Manufactured ENPs of concern include metals (Ag, Au), metal oxides (TiO<sub>2</sub>, ZnO, CeO<sub>2</sub>, SiO<sub>2</sub>, and Al<sub>2</sub>O<sub>3</sub>), carbon materials (fullerenes), and other types of materials such as nanocomposites and quantum dots (Aldeek et al., 2011; Boxall et al., 2009; *Opportunities and Risks of Nanotechnologies*, 2007).

ENPs in application are commonly incorporated into consumer product lines in four general ways: dispersed in fluid or gel, attached to surfaces, embedded in polymers, or applied in industrial processing (*e.g.*, mechanical polishing fluids) (Westerhoff et al., 2013). Only recently have ENPs become more widely applied in the manufacturing industry such as food packaging (Boxall et al., 2009), cosmetics (Fernández-García and Rodríguez, 2011), paints (Burton, 2012), textiles (Benn and Westerhoff, 2008), and human medicines (Aitken et al., 2006). One of the major beneficial applications of certain Me(O)NPs (Silver, Iron and Copper) includes their bactericidal effects in personal care products, textiles, and hospitals, especially in combination with antibiotics targeting pathogenic microorganisms (Lee et al., 2008; Ravishankar Rai and Jamuna Bai, 2011; Ruparelia et al., 2008). In addition, certain metal oxides are regularly included in a variety of sunscreens, cosmetics, paints, and coatings (OECD, 2014). Due to the lack of regulations pertaining specifically to nanoparticles in the United States, industries are not forthcoming with quantities produced or added to products such as anti-bacterial clothing (Ag-NPs) or sunscreens (nano-TiO<sub>2</sub>). Through modeling from known and assumed datasets, polyester fibers used in textile manufacturing contain estimated concentrations of Ag-NPs from 100 g Mg<sup>-1</sup> to 238.5 g Mg<sup>-1</sup> (grams per Megagram). This would amount to 2.6 – 6.3 Mg of Ag-NPs produced globally just from one industry (Boldrin et al., 2014). Nano-TiO<sub>2</sub> global quantities in sunscreen has been estimated to be from 14.3 Mg to 143 Mg, in 2008 alone (Boxall et al., 2009). Other engineered oxides of significant commercial interest include: nano-CeO<sub>2</sub>, nano-Al<sub>2</sub>O<sub>3</sub>,

nano-ZnO, and nano-SiO<sub>2</sub>. Although Si is a metalloid, nano-SiO<sub>2</sub> is commonly grouped with metal oxides owing to its stability and similar chemical behavior to such oxides as TiO<sub>2</sub> and Al<sub>2</sub>O<sub>3</sub>, and will therefore be discussed here as a metal oxide (Brar et al., 2010; Mu et al., 2011; Sahai, 2002; Tso et al., 2010). In an effort to overcome the lack of reported quantities, estimated values for the production of three Me(O)NPs in the United States were extrapolated from phone surveys, proxy data, and company information (Hendren et al., 2011). Nano-TiO<sub>2</sub>, Ag-NPs, and nano-CeO<sub>2</sub> were modeled at upper bounds of production totaling 34,000, 18, and 635 Mg, respectively. Based on this model, the amount of TiO<sub>2</sub>-NP annual production is comparable to trichloroethylene (TCE), the most frequently reported groundwater contaminant, with previously estimated total release of 19,000 Mg (US EPA National Center for Environmental Assessment, 2001). Quantities this large seize attention as toxicity studies have recognized Me(O)NPs such as nano-TiO<sub>2</sub> and Ag-NPs to be potentially hazardous to human health (OECD, 2014; Ratte, 1999). Due to their prevalent use and potential toxic impact, Me(O)NPs are focused on in this review.

### **1.2 Presence of Me(O)NPs in wastewater.**

As Me(O)NPs described above are included within short-lived or one-time use consumer products (*e.g.*, food packaging, sunscreens), certain Me(O)NPs can inevitably be released into the environment. Me(O)NPs bound onto or into textiles, plastics, etc. are not easily controlled from entering the environment. Consequently, concerns for negative environmental impacts and human exposure safety are raised. Their qualities are dependent on variations of factors including: surface area, surface charge (zeta potential), agglomeration/aggregation status in the relevant media, pH of the media, bulk density/particle density, composition/surface coatings, crystal structure, particle size and size distribution, photocatalytic activity, porosity, redox potential, and water solubility (United Kingdom Department of Environment, Food, and Rural



Affairs, 2011). As a result, it is difficult to predict the amount of Me(O)NPs dispersed into the air, soil or water environments. The intended lifetime of the product, the quantity of ENP included within, and the actual use intended for that product (e.g. one time use cleaning supplies versus paints) all influence ENP release (Mitrano et al., 2015). One direct consequence of ENP release is the increase in Me(O)NP concentrations in domestic and/or industrial wastewater. A 2014 exposure model for the EU predicted the most prominent paths for nano-TiO<sub>2</sub> and Ag-NPs entering wastewater (4,500 and 6.4 Mg in 2012) are from production, manufacturing, and consumption (Sun et al., 2014). Although this exposure model considers average datasets from EU households, it extracts material fate from current knowledge in the literature. WWTPs serve as a key barrier between anthropogenic sources and environmental distribution of harmful contaminants into ecosystems, Me(O)NPs included. However, the efficacy of ENP removal at various levels of wastewater treatment remain elusive. Reuse of tertiary treated wastewater for various purposes such as drinking water, irrigation water, and/or cooling water is now a reality – the United States Environmental Protection Agency (EPA) published many examples of current water reuse practice in Region 9 district (serving Arizona, California, Hawaii, Nevada, Pacific Islands and Tribal Nations), and reuse will continue to rise as traditional fresh water sources become increasingly stressed (Fachvereinigung Betriebs- und Regenwassernutzung e.V. (fbr), 2005). Two existing water reuse systems (Orange County, CA and Berlin, Germany) use treated wastewater to replenish groundwater reserves which feed potable distribution systems (Kirkegaard et al., 2015). With advanced treatment (ultrafiltration and reverse osmosis), Orange County faces worst case concentrations of 0.04, 147, and 0.28 µg L<sup>-1</sup> of Ag-NPs, nano-TiO<sub>2</sub>, and nano-ZnO, respectively, in potable water. Lacking advanced treatment, worst case concentrations in Berlin's potable water are estimated at 3.3, 13 and 0.25 µg L<sup>-1</sup> (Ag-NPs, nano-TiO<sub>2</sub>, and nano-

ZnO). This study estimated worst case scenarios by way of mass flow analysis based on current knowledge of nanoparticle fate and removal in water treatment systems. These values are likely to change as the knowledge base for nanoparticle fate in the water reuse cycle is expanded. Now, these metals are not currently regulated in water at such low levels. However, without effective treatment and source water protection, the presence of Me(O)NPs and subsequent release into the ecosystem have a possible effect of bioaccumulation in crops and aquatic species (Bour et al., 2015).

Despite the need for efficient (*i.e.*, removal to acceptable toxicity limits) if not complete (100%) Me(O)NP removal, modern WWTPs are not designed to treat ENPs specifically, unlike other regulated contaminants such as solids, microorganisms and nutrients. Several treatment processes within WWTPs can remove Me(O)NPs to a certain degree, including sedimentation, biological treatment, and sludge processing (Figure 1) (Brar et al., 2010). Among these, activated sludge has shown efficient Me(O)NP removal from wastewater; however, complete removal has yet to be achieved (Westerhoff et al., 2013). Other approaches in biological wastewater treatment have the potential to offer a promising solution for effective Me(O)NP removal without losing the treatment capability of regulated contaminants, such as biofilm reactors. Biofilm systems have been recognized for their scalability, robustness, and usefulness in removing a wide array of contaminants from domestic and industrial wastewater (Schlegel and Teichgräber, 2000; Matamoros et al., 2016). However, while the use of Me(O)NPs in commercial products has expanded exponentially in recent years (Boldrin et al., 2014; Boxall et al., 2009), little is known and understood about how Me(O)NPs interact with, and can be removed by wastewater biofilms. After compiling the few studies conducted to date, results have shown promise in removing model Me(O)NPs due to biofilm resistance to ENP toxicity and biofilm contribution in retaining

ENPs in filtration units (Choi et al., 2010; Jiang et al., 2013). In addition, in either activated sludge or biofilm systems, mechanisms such as accumulation, adsorption, and oxidative transformations (Dwivedi et al., 2015) can both improve and inhibit treatment process efficiency, and will be discussed in detail (Choi et al., 2008; Devlin et al., 2015; Hou et al., 2015a; Ma et al., 2015). Innovations or significant improvements may be required to retrofit the current wastewater treatment design for desired Me(O)NP removal.

## **2. Agglomeration/Aggregation of Me(O)NPs in wastewater.**

The most distinct characteristic of Me(O)NPs, their nano-scale particle size, is influenced by aggregation or agglomeration. For this review, an IUPAC definition of agglomeration and aggregation will be used (A.D. McNaught and A. Wilkinson, 2007). In short, agglomeration references weak, reversible physical interactions; aggregation references strongly bonded interactions (Grillo et al., 2015; Sokolov et al., 2015; Zhou et al., 2015). Nanoscale particles demonstrate different chemical properties than their larger equivalents, where the tendency to (or not to) aggregate influences the ecotoxicity of these ENPs significantly. Illustrated elsewhere (Auffan et al., 2009), mechanisms occurring at the surface of an inorganic particle include oxidation, Fenton reaction, surface acido-basicity, adsorption of compounds, dissolution, redox, electron transfer, and ROS generation. From an environmental perspective, Auffan et al. showed that although engineered Me(O)NPs are defined as less than 100 nm in size, size dependent shifts in crystallinity at diameters of 30 nm or less modify the environmental reactivity in certain ENPs (*i.e.*, nano-TiO<sub>2</sub>, Au-NPs) (Auffan et al., 2009). Therefore, researchers must be cautious that the Me(O)NPs fall within this critical size range during impact studies. In one instance, when examining the impact of Me(O)NPs on anaerobic digestion, measured average sizes of nano-Al<sub>2</sub>O<sub>3</sub>, nano-SiO<sub>2</sub>, nano-TiO<sub>2</sub>, and nano-ZnO ranged from 110±40 nm to 185±40 nm at the start of experimentation, which are well above the nano range and may not have exhibited the

quantum size properties exclusive to these Me(O)NPs as argued, even though the purchased size was labeled below 100 nm (Mu et al., 2011). Aggregation of Me(O)NPs during the intended experiment may alter the interfacial reactivity and should be considered.

Fundamentally, Me(O)NP agglomeration/aggregation is controlled through their structural characteristics and surrounding environments. Agglomeration of Me(O)NPs includes homoagglomeration (two same particles) and heteroagglomeration (different particles). As wastewater influent and activated sludge consist of a variety of suspended particles with a wide particle size distribution, aggregation (*e.g.*, irreversible formation of complexes between different particles) dominates reaction processes. The aggregation of ENPs is influenced by two main factors: surface functionalization (sometimes referred to as the corona) and the presence of organics. Several surface coatings reported with medical applications (*i.e.*, drug delivery) include: bovine serum albumin (BSA), polyethylene glycol (PEG), polyvinyl alcohol (PVA), polyvinylpyrrolidone (PVP), and polyethyleneimine (PEI) (Jokerst et al., 2011; PEN, 2012; Sekine et al., 2013; Yu et al., 2014). The anticoagulant trisodium citrate (CIT) and organic polymer polydimethylsiloxane (PDMS) are also commonly used as stabilizers and in chemical imaging applications (Piella et al., 2016; Wang et al., 2011). These coatings are not impermeable, but retain discontinuities throughout the coating shell. These discontinuities provide environmental access of the Me(O)NP core to surrounding microorganisms or ligands present (Levard et al., 2012), while also possibly contributing to how the Me(O)NP interacts with organics.

The type of functionalization can impact the removal through aggregation during wastewater treatment. Typically, Me(O)NPs retain surface functionalization to aid resistance from agglomeration within media such as lotions or soaps. Surface functionalized Me(O)NPs are, by

design, stabilized in suspension and resistant to removal by agglomeration. However, this addition of coating can complicate Me(O)NP's removal within WWTP. At nanoscale diameters, the settling of Me(O)NPs becomes closely balanced with repulsive forces and Brownian motion (Howard, 2010). Jarvie et al. applied small angle neutron scattering experimentation with nano-SiO<sub>2</sub> (as a representative of engineered oxide NPs), proving that surface functionalization is a major factor in flocculation behavior during primary treatment (Jarvie et al., 2009). They observed uncoated nano-SiO<sub>2</sub> were not removed by sedimentation within the primary sludge, but continued within the effluent stream, whereas surface functionalized nano-SiO<sub>2</sub> rapidly flocculated. Nano-SiO<sub>2</sub> has a low pH<sub>pzc</sub> which may be a controlling factor for this unusual particle behavior. Contrary to nano-SiO<sub>2</sub>, other Me(O)NPs have been observed to have higher removal efficiencies without surface coatings (Barton et al., 2014b). Barton et al. calculated the relative affinity of Me(O)NPs with various surface property for aggregation in activated sludge using the Smoluchowski equation. Results showed 95-100% of unfunctionalized nano-TiO<sub>2</sub> and nano-CeO<sub>2</sub> were removed from suspension, followed by 90% of nano-ZnO and polyvinylpyrrolidone (PVP)-functionalized Ag-NPs, 85% citrate-functionalized nano-CeO<sub>2</sub>, and 70% gum arabic (GA)-functionalized Ag-NPs (Barton et al., 2014a). They indicated removal percentages varied based on surface functionalization, and higher relative affinity to heterogeneous particles corresponded to higher removal of Me(O)NPs.

As the surface coating plays an important part in removal of Me(O)NPs, new evidence of chemical interactions also suggests that the potential toxicity and fate of certain Me(O)NPs is likely to be dictated by other Me(O)NPs present as well. In the case of highly soluble, unstable nano-ZnO interacting with stable nano-TiO<sub>2</sub>, the dissolution of nano-ZnO combines with a secondary reaction of adsorption of Zn<sup>2+</sup> ions to nano-TiO<sub>2</sub> (Tong et al., 2014). Toxicity of nano-

ZnO is attributed to the release of  $Zn^{2+}$  ions into suspension in the literature, but the presence of nano-TiO<sub>2</sub> with available surface sites for adsorption may lessen the quantities of  $Zn^{2+}$  ions in aqueous environments (Wu et al., 2010). Based on these evidences, surface coating effects on aggregation are a key variable in Me(O)NP removal from suspension.

Meanwhile, the presence of dissolved organic matter in wastewater from soluble microbial products interferes with particle-particle attachment, thus altering the agglomeration and deposition behavior of Me(O)NPs (Grillo et al., 2015). Organic matter can increase Me(O)NP stability in suspension by adsorption to the Me(O)NP surface, resulting in longer residence time in the water column (Baalousha et al., 2008; Quik et al., 2010). Since organic matter adsorbs to particles and reduces coagulation, the stability of agglomerates can be dependent on the amount of organic matter present (Walker and Bob, 2001). For Me(O)NPs, Baalousha et. al found NZVI agglomerates only at specific pH (pH values starting from 5 – 6 and peaking at 8.5), however, agglomeration occurs at lower pH (pH values ranging 4 – 5) in the presence of organics (Baalousha et al., 2008). This study further showed that organic matter adsorbs to NZVI and increases agglomeration, but those agglomerates are more compact than NZVI agglomerates formed without the presence of organic matter, and therefore actually settle at a slower rate. Similar patterns have been observed for the most studied Me(O)NPs. For nano-CeO<sub>2</sub>, NZVI, nano-Al<sub>2</sub>O<sub>3</sub>, nano-TiO<sub>2</sub>, and nano-ZnO in the water column, organic matter can adsorb to these ENP strongly and decreases the zeta potential (an indicator for liquid-phase adsorption) (Domingos et al., 2009; Quik et al., 2010; Yang et al., 2009; Zhang et al., 2008). Therefore, a reduction of overall agglomeration can be expected during interaction with organic matter. Even though the impact of both surface functionalization and organic matter was confirmed, it is still difficult to predict the extent of agglomeration in solutions. It has been observed as particle

concentrations increase in aqueous media, the hydrodynamic diameter of nano-ZnO and nano-TiO<sub>2</sub> also increased (Chih-ping Tso et al., 2010; Tong et al., 2014). However, this trend might derail in environmental samples such as sewage samples. A 2011 study recorded an upper limit of 1233 mg L<sup>-1</sup> for nano-TiO<sub>2</sub> within the influent of a WWTP (Westerhoff et al., 2011).

Concentration this high would then by assumption warrant many agglomerates larger than 100 nm, however TEM results found the average TiO<sub>2</sub> particle was 4 to 30 nm in diameter and spherically shaped, aggregating with biomass instead of other Me(O)NPs.

To better predict aggregation of nanoparticles, models have been developed and discussed in detail (Barton et al., 2014b; Conway et al., 2015; Trefalt et al., 2014; Wang et al., 2015; Zhou et al., 2015). Calculating such behavior as aggregation requires applying the classic Derjaguin, Landau, Verwey, and Overbeek (DLVO) theory. In short, the repulsive electric double layer forces and attractive van der Waals forces are both considered, where investigators can apply DLVO theory to quantify the net interaction between particles. This net interaction allows for analysis of aggregation and/or deposition rates of similar or a variety of particles. DLVO theory technically only applies to single particle-particle interactions, not particle-aggregate interactions, which are more complex. Recent theory applications with DLVO explore the more complex properties associated with aggregation such as differences in particle charge (Trefalt et al., 2014). Unfortunately, the complex environment in activated sludge does not result in electric double layer compression for nano-TiO<sub>2</sub> or nano-ZnO, so aggregation rates cannot be predicted with DLVO theory in wastewater (Zhou et al., 2015). This suggests experimental approach is necessary to confirm the aggregation of Me(O)NPs in wastewater environments.

### **3. Interaction between Me(O)NPs and activated sludge.**

Activated sludge treatment (aerobic, anaerobic, and/or anoxic environments) takes advantage of microbial substrate utilization for nutrient removal from wastewater, and has been put into practice for over 100 years. Through advancements in chemical and biological treatment processes, nutrient concentrations in WWTP effluent are significantly reduced to lower and lower levels each decade. Here, a close examination was performed on the literature regarding the fate of these nanoparticles during activated sludge processing. Potential mechanisms for removal of Me(O)NPs in WWTPs vary among processes (Figure 1). Previous studies varied in spiked quantities of the chosen Me(O)NPs. Environmentally relevant quantities are debated, depending on the particular environment (*e.g.*, waste streams or soil solutions) as well as interpretation of current surveys of effluents. The sewage sludge survey report published by EPA has been used as a standard for choosing Me(O)NP quantities for study in waste streams, however its data relies on total concentrations, regardless of particle size (Mu et al., 2011; US EPA, 2015a). For example, quantities as low as  $1 \mu\text{g L}^{-1}$  and as high as  $1233 \mu\text{g L}^{-1}$  for nano-TiO<sub>2</sub> have been studied in aerobic processes (Limbach et al., 2008; Ma et al., 2014). A recent summary arising from research on predicted or measured concentrations shows that measured nano-TiO<sub>2</sub> concentrations in wastewater effluent are somewhat low ( $\mu\text{g} - \text{ng L}^{-1}$ ) resulting in difficulties with direct quantitative analysis when concentrations approach minimum detection limits in these cases (Wang and Chen, 2015). Nonetheless, the elucidation of the interaction between Me(O)NPs and activated sludge will be beneficial in the long term.

#### **3.1 Removal of Me(O)NPs with activated sludge.**

Research focusing on the transport and fate of Me(O)NPs in wastewater treatment processes focus upon activated sludge due to its widespread application (Table 1) and have shown that



adsorption to colloidal particles is the dominant removal mechanism for Me(O)NPs within the activated sludge process (Brar et al., 2010; Park et al., 2013). Taking nano-TiO<sub>2</sub> as an example, they were shown to primarily adsorb to activated sludge and silicate particles during wastewater treatment, and recently reported concentrations of nano-TiO<sub>2</sub> in effluents ranged from 10 to 50 µg L<sup>-1</sup> (Kiser et al., 2009). The adsorption of nano-TiO<sub>2</sub> is strong; there is preliminary evidence that 98.3% (on average of 10 municipal WWTPs in Arizona) of nano-TiO<sub>2</sub> are sequestered within the waste activated sludge as observed by applying HNO<sub>3</sub>/H<sub>2</sub>SO<sub>4</sub> digestion standard method (Westerhoff et al., 2011). The authors observed that the detected titanium morphology in wastewater is expected to fall within one of the following categories: 100-200 nm spheres of TiO<sub>2</sub> (Type I), aluminosilicates (Type II), or mixed environmental silicates less aluminum (Type III). Titanium may also appear as nonparticulate titanium salts (Powell et al., 1996). This study of 10 WWTPs concluded that titanium recovered was partly from food additives and partly from the environment. However, there is no marker for anthropogenic Ti-based ENPs to date. Given that these WWTPs were not sampled prior to the application of nano-TiO<sub>2</sub> in consumer products, the portion of titanium from the environment or from consumer products remains unknown. The adsorption of nano-TiO<sub>2</sub> will occur in solid phases instead of ionic forms at temperate environmental conditions due to the low solubility of nano-TiO<sub>2</sub> (Antignano and Manning, 2008). At 1 mg L<sup>-1</sup> of nano-TiO<sub>2</sub>, total nitrogen and phosphorous removal efficiencies were not significantly affected, even in the long term (70-day exposure) (Zheng et al., 2011a). The removal of nano-TiO<sub>2</sub> through adsorption to biomass is an efficient and non-inhibiting mechanism. Bench batch experiments with Ag-NPs in activated sludge also showed these Me(O)NPs were well removed through adsorption to biomass (>90%) (Benn and Westerhoff, 2008; Kiser et al., 2010).

In activated sludge, the more soluble complexes of Me(O)NPs (such as Ag-NP and nano-ZnO) will exhibit dissolution and form new moieties depending on the organic ligands available or open surface sites on other aggregates (R. Ma et al., 2013a). PVP-Ag-NPs were observed to all convert to silver sulfides in bench scale tests; Nano-ZnO converted to one of the following species: ZnS,  $Zn_3(PO_4)_2$ , and zinc associated iron oxy/hydroxides. In biosolids, PVP-Ag-NPs ionized and were observed to adsorb to nano-TiO<sub>2</sub> rutile present in the mesocosms (Kim et al., 2012). The Me(O)NPs exhibiting low solubility at neutral pH (such as nano-TiO<sub>2</sub> and nano-SiO<sub>2</sub>) are more prone to serve as sorption sites for released ions. In laboratory scale activated sludge reactors, nano-CeO<sub>2</sub> (pristine and citrate functionalized) are confirmed to also be associated with biosolids in the solid phase, but as Ce<sub>2</sub>S<sub>3</sub> most likely (Barton et al., 2014a; Liu et al., 2015; Lombi et al., 2012).

### **3.2 Toxicity of Me(O)NPs and the impact on nutrient removal.**

In bench scale and simulated wastewater treatment processes, Me(O)NPs are observed to negatively affect biological treatment on account of toxic effects upon beneficial microorganisms that contribute to COD and nutrient reduction (Alito and Gunsch, 2014; Hou et al., 2015b, 2012). Toxic effects of Me(O)NPs to cells in general are attributed to the formation of excess reactive oxygen species (ROS) such as hydroxyl radical or hydrogen peroxide induced by Me(O)NPs (Vejerano et al., 2015). Toxicity studies of Me(O)NPs use either microbial colony counts, toxicity assays, or correlation with the formation of ROS. In Table 2, multiple studies revealed Me(O)NPs cause significant inhibition to important microbial groups such as nitrifying and heterotrophic bacteria in activated sludge. Although toxicity tests with model species are important initial steps, response from the complex and unique microbial communities within activated sludge are far different from single model species tested (Sun et al., 2013).

Me(O)NPs from sewer systems to the WWTP are expected to have partially changed in speciation, which has a significant impact on analyzing the cause of inhibitory effects of Me(O)NPs. With reference to nano-ZnO, XAS data from bench scale sewer system experiments predicts this Me(O)NP present mainly as Zn sulfide, but also as Zn carbonate species, Zn phosphate, and bound to organic ligands in the waste stream (Brunetti et al., 2015; Kaegi et al., 2013). In relation to Ag-NPs, speciation is even more complex. Note the bench scale experiments in Table 2 start with pure Me(O)NPs, with the assumption of no chemical speciation before entering the biological processes. However, it is not likely the case in real wastewater. Including the possibility of chemical speciation at the start of laboratory experiments will clarify the species responsible for the toxic effects. For example, by monitoring oxygen uptake rates of activated sludge, the toxicity responses observed from the addition of soluble Zn, nano-ZnO, and bulk ZnO were all significantly different for BOD biodegradation and nitrification. (Liu et al., 2011) In that connection, several different Ag-NPs (gum arabic and citrate coated Ag-NPs along with Ag as AgNO<sub>3</sub>) followed the expected pattern of binding to activated sludge and settling with precipitates, however all three types of Ag particles inhibited COD removal and nitrification at differing percentages (Alito and Gunsch, 2014).

Sometimes Me(O)NPs can promote nutrient reduction of wastewater from activated sludge. A reactive antimicrobial species, Cu-NPs, causes concern due to potential toxic effects copper can have on ecosystem stability (Yoon et al., 2007), yet exhibited advantageous effects upon BNR processes. (Chen et al., 2012) When examining the fate of Cu-NPs during BNR, total phosphorous (TP) removal efficiencies stayed at approximately 98% regardless of Cu-NP concentrations (Chen et al., 2012). By increasing Cu-NPs from 0 to 5 mg L<sup>-1</sup>, the average TN removal efficiency raised from 60.6% to 72.8% due to the effects the copper had on suppressing

the activity of glycogen accumulating organisms. The generation of the greenhouse gas  $N_2O$  decreased from  $0.441 \text{ mg L}^{-1}$  to  $0.174 \text{ mg L}^{-1}$  at concentrations of 0 and  $5 \text{ mg L}^{-1}$  Cu-NPs, respectively. This experiment was performed in bench scale sequencing batch reactors operated for 90 days, however, the contradictory result deserves further investigation. The inhibition of BNR by the presence of Me(O)NPs can be the primary hurdle to overcome in wastewater treatment, even though the majority of Me(O)NPs are adsorbed and removed by activated sludge. As a result, we will discuss shortly how biofilm processes can present as a favorable alternative in wastewater treatment due to their increased resistance to Me(O)NP toxicity (Choi et al., 2010; Sheng et al., 2015; Thuptimdang et al., 2015).

### **3.3 Impact on subsequent processes.**

Sludge settling is an important stage in the activated sludge process to ensure the effluent quality as well as sludge recycling operation. Though adsorption of Me(O)NPs onto activated sludge can be effective, dissolution of Me(O)NPs during clarification can add more metal ions to wastewater, inducing toxicity to essential microbial communities (Benn and Westerhoff, 2008). Using  $4 \pm 1 \text{ nm}$  nano-ZnO particles, a multivariate study on dissolution compared the effects of varying pH (Bian et al., 2011). Through TEM imaging, the observed concentration of  $Zn^{2+}$  ions in solution increased as particle size decreased in a non-linear, somewhat exponential, relationship. With low pH, dissolution is likely to result from interacting with free protons in solution. At higher pH ( $pH > 9$ ), soluble hydroxyl complexes are expected (e.g.  $Zn(OH)_{2(aq)}$ ). Dissolution was hypothesized as a possible interference for particle removal. In simulated sedimentation experiments with Ag-NPs at typical residence times (30 minutes), 94% of Ag-NPs remained in the upper layers of the waste flows (Hou et al., 2012) as precipitates  $Ag_2S$  and  $AgCl$ ,

supporting that in non-aerated clarification basins at pH = 7.3, Ag-NPs will not add to toxicity, but nor will they be removed prior to biological treatment.

Once removed from wastewater with biosolids, the accumulation of Me(O)NPs can negatively impact further solids handling processes. Anaerobic digestion is susceptible to distresses due to toxic substances (Tchobanoglous et al., 2003). Me(O)NPs can pose inhibiting effects on this solids stabilization process. Studies examining the fate of nanoparticles during anaerobic digestion/composting or sludge treatment concluded chemical speciation of Me(O)NPs is key at this stage. Ag-NPs, as model Me(O)NPs, convert to sulfides at concentrations up to 50 mg/kg (Lombi et al., 2012; R. Ma et al., 2013b). Lombi et al. presented that these silver sulfides are stable for up to six months in processed biosolids. Thus, higher concentrations of sulfides are sequestered as Ag-NP concentrations rise in anaerobic sludge. The consequences of rising concentrations of Me(O)NPs affecting anaerobic stability are hypothesized and summarized elsewhere (Wang and Chen, 2015). To include another example here, ZnO-NPs removed with activated sludge are converted to three forms in biosolids following the release of  $Zn^{2+}$  ions: sulfides, Fe-oxy/hydroxides, and  $Zn_3(PO_4)_2$  (R. Ma et al., 2013a). The negative impacts upon solids processing due the formation of  $Ag_2S$  or  $ZnS$  within waste sludge will be another barrier engineers must consider in future designs or plant upgrades.

#### **4. Interactions between ENPs and Biofilm.**

Biofilms are ubiquitous in aquatic environments such as soil solution, surface waters, and piping systems (Wingender et al., 2012). A microbial biofilm consists of microorganisms in a matrix of EPS which include proteins, polysaccharides and nucleic acids (de Faria et al., 2014).

Amphiphilic compounds (i.e. phospholipids) have also been observed in significant amounts in activated sludge and sewer biofilms (Sand and Gehrke, 1999). Designs applying attached growth

mechanisms are more commonly used in the industrial waste sector due to their compact design, low quantities of sludge production, and resistance to shock loads (Schlegel and Teichgräber, 2000). Primary options for attached growth include MBBRs, upflow or downflow submerged fixed film reactors, and membrane bioreactors (Schlegel and Teichgräber, 2000; Tchobanoglous et al., 2003). The main advantage of biofilm processes over activated sludge is attributed to the protective layer of EPS. It is agreed that biofilms are thus more resistant to higher levels of nanoparticles than planktonic cells (Battin et al., 2009; Choi et al., 2010; Sheng and Liu, 2011). As an example of this resistance, using *Escherichia coli* (*E. coli* PHL628), the minimum Ag-NPs concentration to inhibit bacterial growth for planktonic and biofilm cultures were 10 and 38 mg L<sup>-1</sup>, respectively. The biofilm cultures exhibited an almost four-fold resistance to Ag-NP concentrations (Choi et al., 2010). A similar exposure study with *Pseudomonas putida* found minimal reduction in ATP activity in mature biofilms exposed to Ag-NPs (Thuptimdang et al., 2015). Scaling up, when exposing Ag-NPs to biofilm forming bacteria sampled from an RBC WWTP, no significant changes in heterotrophic plate counts have been observed at Ag-NP concentrations reaching 200 mg L<sup>-1</sup> (Sheng and Liu, 2011). These results imply that a mature, mixed culture biofilm has a greater ability to resist inhibition from Me(O)NPs, and should be considered when conducting mesocosm experiments in wastewater treatment design. As discussed, biofilms in WWTPs are more resistant to Ag-NP inhibitory effects (W. Ma et al., 2013), but more detailed studies are needed to understand the impacts of biosorption into wastewater biofilm structures and influences on increased detachment. Interactions between ENP and biofilm are complex and expected to vary with environmental conditions. Several aspects of biofilm-ENP interactions are unique in wastewater treatment. To begin, for ENP removal from wastewater, biomass concentration, contact time, and nanoparticle type can

govern the removal process through contact in suspension (Park et al., 2013). For biofilms, sorption to an attached matrix is attributed strongly to charge or size of the Me(O)NP (Ikuma et al., 2015; Nevius et al., 2012). Previously illustrated mechanisms of biofilm-nanoparticle interactions include adhesion, potential toxicity, migration, and detachment (Ikuma et al., 2015; Jing et al., 2014; Wang and Chen, 2015). Also, the stability of biofilms can be disrupted in the presence of Me(O)NPs. For example, Ag<sup>+</sup> ions released from the dissolution of Ag-NPs will be more toxic to a biofilm than Ag-NPs prior to speciation (Zook et al., 2011). These considerations need to be taken into account when studying the ‘trapping capacity’ and elucidation of specific ENP-biofilm interactions. Given the unique nature of wastewater biofilms, the following sections will extrapolate findings from other types of biofilm studies to predict likely nanoparticle-biofilm interactions in wastewater. Assumptions were made based on the similarities between previous studies and wastewater biofilm. For example, studies in groundwater remediation or wastewater filtration focus on interaction between Me(O)NPs and biofilms growing on porous media; resembling biofilm can also be found on similar media in trickling filters for wastewater treatment.

#### **4.1 Entrapment of Me(O)NPs.**

Wastewater biofilms may serve as an environmental sink for Me(O)NPs, depending on the wastewater constituents (*i.e.*, organic ligands), the concentration and species/surface functionalization of Me(O)NPs, as well as microbial species within biofilms. Biofilms of model species are commonly used to study the biofilm-Me(O)NP interaction in columns where the presence of biofilm does affect entrapment. For example, model biofilm *E. coli* in porous media columns were used to examine the effects biofilm has on transport theories with nano-ZnO (Jiang et al., 2013). Jiang et al. established that the biofilm present lowered all breakthrough

curves as ionic strengths were increased, indicating that electrostatic force plays an important part in Me(O)NP transport in porous media. Compared to non-biofilm coated columns, since breakthrough plateaus were lower with biofilm columns, retained concentrations of nano-ZnO were also greater. Along the same line, NZVI retention, only in the presence of *Pseudomonas aeruginosa* biofilm, also increased at higher ionic strength (Lerner et al., 2012).

Resistance to nanoparticle impacts allow biofilms to remain intact as Me(O)NPs interact with the surface and diffuse within. For example, 50 mg L<sup>-1</sup> of suspended ZnO-NPs only inhibited the outer 200 µm of biofilm within 2 hours, however the inner layers exhibited increased respiratory activity through microelectrode surveillance (Hou et al., 2014). Exposure of *Shewanella oneidensis* biofilms, a metal reducing bacteria, to nano-TiO<sub>2</sub> revealed no change in viability (agreeing with previous studies) but significant decreases in growth rates correlating with the addition of nano-TiO<sub>2</sub> (Maurer-Jones et al., 2013). TEM showed the nano-TiO<sub>2</sub> were not taken into bacterial cells, but located in the EPS matrix close to the cells. This species significantly increased riboflavin secretion (which aides in the transformation of metals). Again, using a model bacterial species with a stable Me(O)NP is an excellent approach in the newly developing field of nanotoxicology, but to design engineered systems such as WWTP, it is necessary to understand the response of mixed environmental cultures with Me(O)NPs. For instance, when examining river biofilms (periphyton), nano-CeO<sub>2</sub> are stabilized by extracellular polymeric substances (EPS) regardless of pH, but dissolution increases over time in the dark at pH=6. (Kroll et al., 2014) Kroll found EPS induces a size increase in Ag-NPs, which implies that periphyton may be subjected to a fluctuation of engineered and naturally formed Ag-NP and Ag<sup>+</sup> ions. With citrate coated Ag-NPs, for example, slower ion release rates will occur as the hydrodynamic diameter becomes larger (Zhang et al., 2011). The ability of biofilms to sequester Me(O)NPs is



an area of interest in much need of exploration. As it is possible and likely for biofilms to accumulate Me(O)NPs, we next discuss what can affect this interaction.

#### **4.2 Factors affecting removal of Me(O)NPs.**

Biofilm development/growth dynamically evolves through attachment, maturation, and detachment (Stoodley et al., 2002), and they can affect the interaction with Me(O)NPs in aqueous environment. In an investigation of Ag-NPs and biofilm interactions, the viability of *Pseudomonas putida* biofilms were not affected in the presence of Ag-NPs with Suwannee River fulvic acid (SRFA) (Fabrega et al., 2009b). Ag-NPs were visually detected with TEM within the EPS matrix and attached to the bacterial cells. The SRFA appeared to inactivate the biological effect of Ag-NPs. Fabrega et. al observed an increase in biofilm detachment from Ag-NP exposure (pH = 7.5), however with the addition of SRFA, detachment of biofilm was suppressed (Fabrega et al., 2009b). Biofilm resistance to ENP size effects such as increased chemical reactivity is mainly due to diffusion limitations (Neal, 2008). In a model biofilm eradication study with nitric oxide releasing nano-SiO<sub>2</sub>, nitric oxide delivery increased as the particle size decreased (150 nm to 14 nm). Size limitations were also detected with FCS for 2 and 10 nm Ag-NPs; relative diffusion coefficients decreased exponentially with the square of the particle radius (Peulen and Wilkinson, 2011). Diffusion is more limited in heterogeneous biofilms compared to a single-species biofilm due to the higher complexity of the matrix (Guiot et al., 2002). In wastewater systems, mixed species biofilm at steady state should be achieved for proper processing of nutrient loads, which is expected to be beneficial in retaining Me(O)NP while maintaining the nutrient removal capability. As mentioned, retention of Me(O)NPs might be affected by biofilm dynamics. In a model MBBR, biosorption of silica coated Fe<sub>3</sub>O<sub>4</sub>-NPs reached 17% for the first 5 hours, however detachment of biofilm from carriers occurred after 5

hours, decreasing to 0.5% silica coated Fe<sub>3</sub>O<sub>4</sub>-NPs completed sorbed onto biofilms (Herrling et al., 2016).

The Me(O)NP surface functionalization can impact their fate in biofilms as well. Using model biofilm species, *Pseudomonas aeruginosa*, sulfate functionalized latex particles showed significantly greater attachment efficiency (e.g., colloidal filtration theory) than carboxylated latex particles, directly affecting the retention of these model nanoparticles in biofilm laden porous media (Tripathi et al., 2011). Surface coating can also affect biofilm formation, inhibiting more than 60% of biomass formation in a biofilm formation assay with *Pseudomonas aeruginosa*, with only 10% of the cells surviving after exposed to 180 µg mL<sup>-1</sup> of Ag-NPs (Dror-Ehre et al., 2010). By application of fluorescent CLSM, quantum dots labeled with various charges and functional groups incubated (1 hr.) with *E. coli* biofilm were observed unable to penetrate biofilm if the surface charge were neutral (PEG) or anionic (COOH<sup>-</sup>). While cationic nanoparticles (TTMA and Hexyl) freely diffused into biofilm (Li et al., 2015). TTMA coated ENPs accumulated near the bottom of biofilms, while Hexyl coated ENPs were concentrated in the middle of the biofilm.

The surface property of model biofilms also plays a role in the interaction with Me(O)NPs. Since these model bacterial species form biofilm that vary in extracellular chemistry (which may alter ENP transport), a mix of gram-negative and gram-positive model species (*P. aeruginosa* and *Bacillus cereus*) were selected to better model the natural environment (Xiao and Wiesner, 2013). Xiao & Wiesner observed the hydrophobicity of the biofilm interface correlated with the amount of proteins present. In the presence of biofilms, the attachment efficiency of certain Me(O)NPs increased, however, Me(O)NPs with dispersant coating showed little to no retention in comparison to bare Me(O)NPs (Z. Li et al., 2013). The concepts of loosely bound extracellular

polymeric substances (LB-EPS) versus tightly bound extracellular polymeric substances (TB-EPS) have been applied to further study the EPS matrix in biofilms (Geyik et al., 2015; Hou et al., 2015a; Li et al., 2012; Sheng and Liu, 2011). The addition of CuO at 50 mg L<sup>-1</sup> increases polysaccharide production in LB-EPS (Hou et al., 2015a). This increased production was reflective of a defensive reaction of the cells to added stress in their environment, as viability of cells is reduced with removal of LB-EPS (Chrzanowska and Załęska-Radziwiłł, 2014). Similar impact was also observed in activated sludge, where increased quantities of LB-EPS in activated sludge negatively affects floc structure and therefore dewaterability (Li and Yang, 2007). Interactions between heterogeneous biofilm surfaces (EPS) and various Me(O)NPs as their corona is altered, can affect biological treatment of wastewater, yet mechanisms behind these interactions deserve future research.

## **5. Me(O)NPs impact upon wastewater treatment design.**

### **5.1 Implications of Me(O)NPs in wastewater treatment processes.**

Activated sludge and biofilm studies with Me(O)NPs are paving a path to improved understanding of wastewater treatment efficiency of these pollutants. In Table 3, multiple studies identify negative Me(O)NP impacts upon both suspended and attached growth wastewater processes. For overall removal of model Me(O)NPs, activated sludge has the potential ability to achieve high removal percentages (>90%), however, with the cost of significant nutrient removal inhibition at certain Me(O)NP concentrations, especially impacting slower growing nitrifying bacteria (Tables 1 - 3). Sometimes the inhibitory effect can be somewhat reversed by other environmental factors. For example, at Ag-NP quantities near 1 mg L<sup>-1</sup>, it is expected that ammonia removal by activated sludge will be considerably inhibited, although this effect is lessened in systems with hard water (Anderson et al., 2014; Jeong et al., 2014). In comparison,

with Cu-NPs, nitrogen cycling biofilm species *Nitrosomonas europaea* are twofold more resistant compared to planktonic, and *Paracoccus denitrificans* are 40 – 50 times more resistant (Reyes et al., 2015). Adverse effects upon the microbial community are much more likely in activated sludge systems than for biofilm processes. This is not surprising, as biofilm contains a protective layer of EPS, and only when LB-EPS is removed does bacterial viability significantly decrease in the presence of Ag-NPs (Sheng and Liu, 2011). Sorption and retention of Me(O)NPs within biofilms is not well documented compared to activated sludge research. With *Pseudomonas putida* in Davis medium, approximately 10% (as maximum) Ag-NPs were retained in the biofilm (Fabrega et al., 2009a). With wastewater RBC biofilms specifically, in batch sorption experiments on glass slides, 10% of a 20 mg L<sup>-1</sup> Ag-NP solution was sorbed (Sheng and Liu, 2011). These studies agree, however, little attention was given to strategies to improve Ag-NP retention in biofilms. Mechanisms affecting this percentage such as Ag-NP aggregation and surface functionalization were not explored. Furthermore, it is still unclear how long the Ag-NPs can be sequestered within the biofilm matrix before having negative effects on the microbial community or biofilm formation. In Tennyson, Wisconsin, Labrenz et al. demonstrated nano-ZnS precipitation into biofilm at concentrations at least 10<sup>6</sup> times relative to the water column in a flooded underground mine, meeting drinking water standards for nearby wells (Labrenz et al., 2000). Just as the generation and sequestration of metal nanoparticles occurs in groundwater systems, the solution to improved retention in engineered biofilm systems may be hidden in what is already occurring in natural aqueous environments. However, these advantageous effects are yet to be explored in Me(O)NP removal using wastewater biofilms. The studies with WWTPs during short and long term exposure to Me(O)NPs laid important groundwork toward understanding the mechanisms controlling the fate of Me(O)NPs in waste

streams and waterways. Adsorption of Me(O)NPs to activated sludge flocs and removal by sedimentation is largely controlled by surface functionalization and the presence of organics either on the nanoparticle or in the waste stream. Partial removal of surface functionalized Me(O)NPs could warrant additional treatment processes, especially for direct or indirect potable reuse of wastewater. After removal from suspension, Me(O)NPs will be processed with the biosolids and must be dealt with during solids stabilization as a possible inhibitor.

As for biofilms, accumulation of Me(O)NPs can occur within the EPS matrix, as model biofilm bacteria have shown significant resistance to Ag-NPs (Choi et al., 2010). It is important to note that surface functionalized Ag-NPs do show higher toxic effects on biofilms than pristine Ag-NPs. Furthermore, nano-TiO<sub>2</sub> decreases growth rates in biofilms, but as a benefit, increases riboflavin secretion in metal-reducing bacteria (aiding the transformation of metals). Biofilms are also helpful in porous media by aiding the attachment efficiency of Me(O)NPs. Biosorption of Me(O)NP to both activated sludge and biofilm may become a possible origin for recovery of these resources from wastewater for economic applications. Establishment of real-world environmental quantities over time is critical to understand toxic levels for future regulation and treatment design alternatives.

To summarize, activated sludge processes are far superior in actual Me(O)NP removal from wastewater, however, the toxicity poses significant risk to slow growing niche microbial communities (Liang et al., 2010; Zhou et al., 2015). Biofilm has the potential to withstand the toxic effects of Me(O)NP, but more research is required. Improvements to older facilities may need to be considered in preparation for future regulatory changes upon effluent limitations.

## 5.2 Considerations in regulating Me(O)NP removal from wastewater.

After conducting prediction models, conclusions have been made that conventional WWTPs can process Ag-NP levels at least three times higher than the current average loads (Benn and Westerhoff, 2008). However, accumulation in biosolids may exceed EPA total concentration standards in the US, which then limits land application (L. Li et al., 2013). There is an alarming lack of pertinent data regarding how to incorporate Me(O)NPs into such regulations as the Clean Water Act, Clean Air Act, Resources Conservation and Recovery Act (RCRA), and the Toxic Substances Control Act (TSCA). The EPA has proposed reporting and record keeping requirements for nanoscale materials (US EPA, 2015b). It will require companies or persons that intend to process or manufacture chemicals in the nanoscale form notify the EPA of the volume, size, chemical type, and safety information. Unfortunately, much of the application of certain Me(O)NPs is for food or cosmetics; these products are categorized for regulation under the FDA which provide minimal guidance documents for encouraging manufacturers to communicate with EPA. Unlike the US, the EU has developed new legislations that apply specifically to nanoparticles. In 2007, legislation for Registration, Evaluation, Authorization and Restriction of Chemicals (REACH) was passed. It requires businesses to report on the hazards and properties of both industrial and domestic substances (*i.e.*, electronics, clothing) which includes ENPs. From a holistic viewpoint, researchers have yet to identify possible correlations between differing levels of regional effluent regulations for nutrients and Me(O)NP concentrations in the effluent. This is complicated by the lack of WWTP surveys connecting effluent Me(O)NP quantities and treatment processes. Less than  $25 \mu\text{g L}^{-1}$  nano-TiO<sub>2</sub> was measured in effluent of WWTPs with varying treatment processes throughout Arizona; treated effluent from membrane systems showed highest levels of nano-TiO<sub>2</sub> removal (Westerhoff et al., 2011). This study found

that the two plants with greater than  $10 \mu\text{g L}^{-1}$  effluent levels achieved only nitrification, but not denitrification. From this observation, it is reasonable to predict that regional regulatory nutrient limits on WWTP effluent may govern the quantities of Me(O)NP released from WWTP effluent streams. Further study into correlating regional nutrient limitations and Me(O)NP removal will also aid in predicting environmental impacts of Me(O)NPs.

## Notes

The authors declare no competing financial interest.

### Nomenclature

Ag-NPs	silver nanoparticles
Au-NPs	gold nanoparticles
BNR	biological nutrient removal
BOD	biochemical oxygen demand
COD	chemical oxygen demand
Cu-NPs	copper nanoparticles
ENP	engineered nanoparticle
EPA	Environmental Protection Agency
EPS	extracellular polymeric substances
ESEM	environmental scanning electron microscope
EU	European Union
FCS	fluorescence correlation spectroscopy
FDA	Food and Drug Administration
Fe <sub>3</sub> O <sub>4</sub> -NPs	iron oxide nanoparticles
Hexyl	dimethylhexyl ammonium terminus
ICP-MS	inductively coupled plasma mass spectrometry
IUPAC	International Union of Pure and Applied Chemistry
MBBR	moving bed biofilm reactor
Me(O)NPs	metal/metal oxide nanoparticles
nano-Al <sub>2</sub> O <sub>3</sub>	aluminum oxide nanoparticles
nano-CeO <sub>2</sub>	cerium oxide nanoparticles
nano-SiO <sub>2</sub>	silicon dioxide nanoparticles
nano-TiO <sub>2</sub>	titanium dioxide nanoparticles
nano-ZnO	zinc oxide nanoparticles
NZVI	nano zero valent iron
pH <sub>pzc</sub>	point of zero charge for adsorption
RBC	rotating biological contactor
SBR	sequencing batch reactor
SEM	scanning electron microscopy

SRFA	Suwannee River fulvic acid
TEM	transmission electron microscopy
TF	trickling filter
TTMA	trimethyl ammonium terminus
WWTP	wastewater treatment plant
XAS	x-ray absorption spectroscopy

### **Acknowledgements**

This manuscript is based upon work supported by the U.S. Geological Survey under grant agreement No. G16AP00040 and administered by the Arkansas Water Resources Center. The views and conclusions contained in this document are those of the authors and should not be interpreted as representing the opinions or policies of the U.S. Geological Survey. Mention of trade names or commercial products does not constitute endorsement by the U.S. Geological Survey. The authors would also like to extend gratitude towards the five anonymous reviewers and the associate editor who handled this publication.



## Figures and Tables

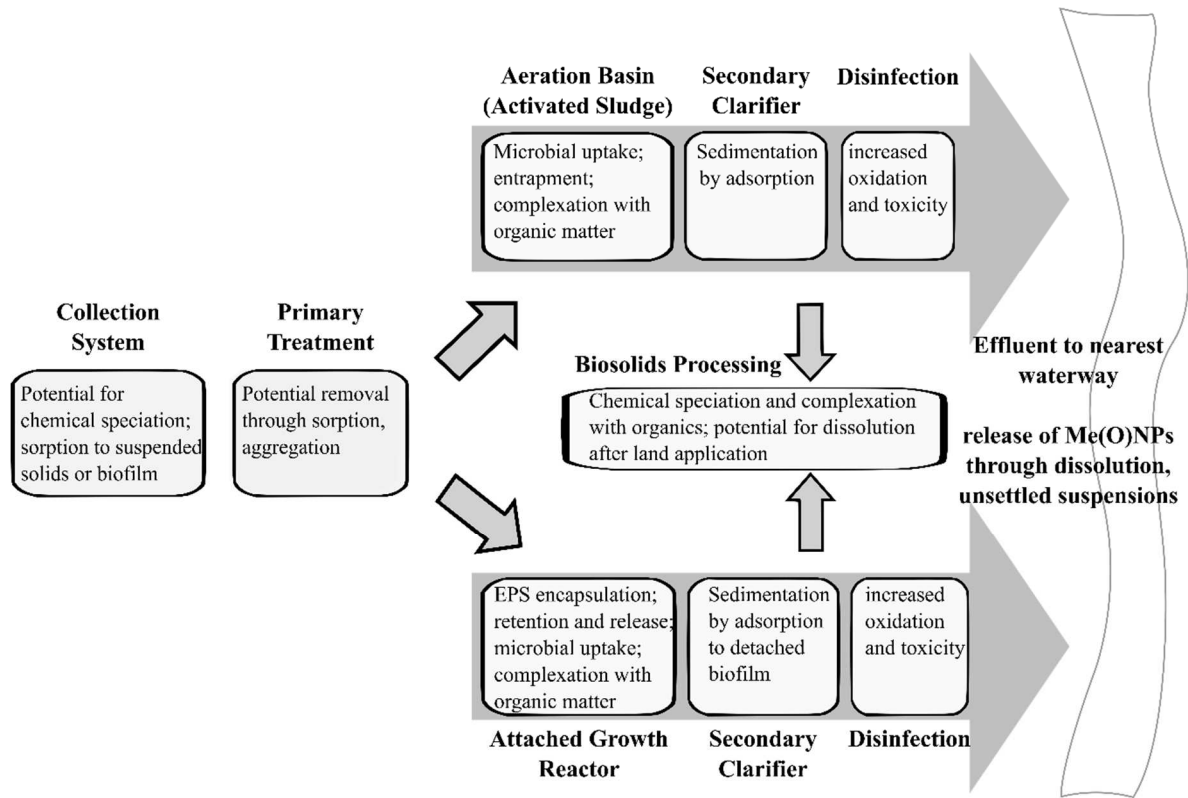


**Figure 1.** Typical fate of Me(O)NPs in WWTPs for both activated sludge and biofilm processes.

**Table 1.** Summarized results of studies focusing on the fate of Me(O)NPs in wastewater treatment design.

Process/location	Nanoparticle Tested	Stabilizing Agent	Mean Size (nm)	Quantities Added/Spiked	Process Implications	Source
Full scale WWTP; 10 Full scale biological WWTPs; Model WWTP (biological treatment)	Titanium*	**	*	Initial influent conc. (0.185 mg L <sup>-1</sup> ); No spike. Actual concentrations ranged 181-1233 µg L <sup>-1</sup>	Approx. 91% of Titanium is captured in primary solids, sludge biomass, and secondary solids; Effluents contained from 2-20 µg L <sup>-1</sup> ; trickling filters and activated sludge play a large role in removal of titanium	(Kiser et al., 2009; Limbach et al., 2008; Westerhoff et al., 2011)
	Cerium	Acryl polymer; Benzyl sulfonic acid	20-100	100 mg L <sup>-1</sup>	Up to 6% wt. of Cerium was identified in the treated wastewater; Accumulation of Cerium occurred in the biosolids	
Anaerobic digestion and sludge processing	Zinc	Capric/caprylic triglyceride, Cobalt	30-40	1000 mg kg <sup>-1</sup>	ZnO-NPs transform into complexes with citrate, cysteine, phosphate and sulfide in the same manner as 'native' zinc in wastewater	(Lombi et al., 2013, 2012)
	Silver	Citrate, PVS, MSA <sup>a</sup>	6.4-10.7, 200	50 mg kg <sup>-1</sup>	Formation of stable silver sulfides	
Pilot WWTP	Zinc	**	20-40	0.12 mg L <sup>-1</sup> (124 mg d <sup>-1</sup> )	Over 90% of both were found in solids leaving the plant; found little difference in speciation when comparing ionic and NP forms of the metal added, therefore land application regulations should not be impacted by nano versus non-nano metals	(R. Ma et al., 2013a)
	Silver	PVP	80	0.01 mg L <sup>-1</sup> (11 mg d <sup>-1</sup> )		
Full Scale Treatment Plant	Silver	**	5-20	None Added	Nanosized silver sulfides were identified in sewage sludge; 95% of Ag-NPs were reduced from influent stream	(Kim et al., 2010; L. Li et al., 2013)

**Table 1 (cont.)**

Process/location	Nanoparticle Tested	Stabilizing Agent	Mean Size (nm)	Quantities Added/Spiked	Process Implications	Source
Sewage sludge Biosolids	Titanium*	**	40-300	None Added	96.9-4510 mg kg <sup>-1</sup> identified in sewage sludge 810 mg kg <sup>-1</sup> found in Class A biosolids	(Kim et al., 2012)
Biosolids (Bench Scale)	Aluminum Cerium Silica	**	<50 50 10-20	75 – 92 mg L <sup>-1</sup>	29% nano-Al <sub>2</sub> O <sub>3</sub> , 51% nano-CeO <sub>2</sub> , and 8% nano-SiO <sub>2</sub> were removed with biosolids	(Rottman et al., 2012)
Activated Sludge (Bench Scale)	Cerium Copper Titanium Silver	** ** ** **	50 50-100 40 13	55 mg L <sup>-1</sup> 10 mg L <sup>-1</sup> 0.5 mg L <sup>-1</sup> 0.6 mg L <sup>-1</sup>	96.6% nano-CeO <sub>2</sub> were removed by aggregation and biosorption 95% Cu-NPs were removed by aggregation and settling, not biosorption 23% Titanium removed by biosorption 96±1% Silver removed by biosorption	(Ganesh et al., 2010; Gómez-Rivera et al., 2012; Kiser et al., 2010)
Membrane Bioreactor	Zinc	**	66	1.0, 10.0 mg L <sup>-1</sup>	>98% ZnO-NPs removed by biosorption	(Tan et al., 2015)

\*denotes studies focusing on total concentration regardless of speciation and form.

\*\*denotes stabilizing agent was either not used or not included in the methods.

<sup>a</sup>mercaptosuccinic acid

**Table 2.** Studies focusing on the toxicity of Me(O)NPs in activated sludge.

Target microbial group	Nanoparticle Tested	Stabilizing Agent	Mean Size (nm)	Quantities Added/Spiked	Toxicity (inhibition of metabolic activity)	Source
Heterotrophic bacteria only	Cerium	HMT	12	640 mg L <sup>-1</sup>	100% inhibition	(García et al., 2012)
	Titanium	TMAOH	7.5	840 mg L <sup>-1</sup>	Zero/low toxicity	
	Silver	Citrate	30	75 mg L <sup>-1</sup>	Approx. 33% inhibition	
	Gold	Citrate	20	130 mg L <sup>-1</sup>	Zero/low toxicity	
Nitrifying bacteria	Silver	PVA	21	1 mg L <sup>-1</sup>	Ag-NP inhibited nitrifying bacteria by 41.4%, whereas Ag <sup>+</sup> ion caused only 13.5% inhibition of nitrifying bacteria  <i>Bacterioidetes</i> and <i>proteobacteria</i> for BOD removal are inhibited	(Liang et al., 2010)
Nitrifying bacteria ( <i>Nitrosomonas</i> and <i>Nitrosococcus</i> )	Silver	**	5	0.05 mg L <sup>-1</sup>	Significant decrease in abundance of <i>Nitrosomonas</i> , complete absence of <i>Nitrosococcus</i> ; community shift toward more silver tolerant species	(Yang et al., 2014)
		**	35	40 mg L <sup>-1</sup>		
Activated sludge biomass	Titanium	**	21	1 mg L <sup>-1</sup>	Significant inhibition immediately by ZnO upon microbial respiration over 4.5 hours, delayed significant inhibition of respiration by TiO <sub>2</sub>	(Zhou et al., 2015)
	Zinc	**	<100	100 mg L <sup>-1</sup>		
Activated sludge niche species	Titanium	**	70 – 90	50 mg L <sup>-1</sup>	Significant reduction in abundance of ammonia oxidizing bacteria and nitrifying bacteria community	(Zheng et al., 2011a)
Heterotrophic and nitrifying communities	Silver	PVP	13	0.1 – 50 mg L <sup>-1</sup>	Loss of microbial diversity over time (50 days), severe inhibition of ammonia removing bacteria at Ag-NP concentrations <1 mg L <sup>-1</sup>	(Jeong et al., 2014)
Activated Sludge DOC elimination and nitrification	Titanium	SHP	<250	1 mg L <sup>-1</sup>	No significant inhibition	(Gartiser et al., 2014)

\*\*denotes stabilizing agent was either not used or not included in the methods.

**Table 3.** Summarized results of studies focusing on the implications of Me(O)NPs in wastewater treatment processes.

Process/location	Nanoparticle Tested	Stabilizing Agent	Mean Size (nm)	Quantities Added/Spiked	Process Implications	Source
Activated sludge - (Anaerobic)	Copper	**	220	0.1-10 mg L <sup>-1</sup>	Enhanced TN removal; Reduction of N <sub>2</sub> O generation	(Chen et al., 2012; Zheng et al., 2011b)
	Zinc	**	89	1, 50 mg L <sup>-1</sup>	Long term exposure at 50 mg/L decreased TN removal efficiency; no effect on phosphorous removal	
	Zinc	SDBS <sup>a</sup>	140	0, 10, 50, 100, 200 mg g <sup>-1</sup> (TSS); 10, 50 mg L <sup>-1</sup>	EPS and methane production are negatively impacted at concentrations above 100 mg g <sup>-1</sup> TSS, severely inhibiting methane production; Decreased nitrogen removal efficiencies; inhibition of phosphorous accumulating organisms due to release of zinc ions	(Mu et al., 2012)
Activated sludge - (Model sequencing batch reactors)	Silver	Citrate	52	1 – 67 µg mL <sup>-1</sup> for all; 0.1 – 20 mg L <sup>-1</sup>	No significant cytotoxic or genotoxic effects from SBR effluents or biosolids to A549 human lung cells; Negligible inhibitory effects.	(Alito and Gunsch, 2014; Hwang et al., 2011; Ma et al., 2015, 2014; Wang et al., 2012)
	Iron	**	46			
	Titanium	**	21			
	Cerium	**	33			
	Iron oxide	Surfactants	10			
	Silver	Gum arabic, Citrate	32, 15	0.2 and 2 mg L <sup>-1</sup>	Increase in effluent COD, turbidity Ammonia removal decreased by 30% in the short term only	
Activated sludge - Membrane Bioreactor	Zinc	**	66	1.0, 10.0 mg L <sup>-1</sup>	Long term nutrient removal inhibition	(Tan et al., 2015)
Biofilm - Aerobic biofilms (Rotating Biological Contactors)	Silver	PVP	15	0 – 200 mg L <sup>-1</sup>	RBC bacteria protected by EPS are not impacted by high concentrations; viability decreases significantly when EPS is not present	(Hou et al., 2014; Sheng and Liu, 2011)
	Zinc	**	51-469	0, 5, 50 mg L <sup>-1</sup>	Only 50 mg/L inhibited the outmost (200 µm) biofilm layer while also enhancing activity in deeper parts of the biofilm	

**Table 3 (cont.)**

Process/location	Nanoparticle Tested	Stabilizing Agent	Mean Size (nm)	Quantities Added/Spiked	Process Implications	Source
Biofilm - Wastewater channel (sewer);	Silver	citrate, PVP	10, 100	Approx. 53 mg L <sup>-1</sup> ; 100 mg L <sup>-1</sup>	Ag-NPs favor sorption TSS in wastewater stream than to sewer pipe biofilms Adsorption to sewer biofilms minimal.	(Brunetti et al., 2015;
bench scale sewer transfer system	Silver ZnO	citrate **	26 64; 240	90 µg L <sup>-1</sup> 700 µg L <sup>-1</sup>	1-2% adsorption, rapid speciation to sulfides, with some cysteine and histidine bound species	Kaegi et al., 2013)
Periphytic biofilm as a biosorbent	ZnO	**	37-735	50 mg L <sup>-1</sup>	Biosorption increased with removal of LB-EPS, increased biosorption occurs with lowers organic content at neutral or acidic pH	(Miao et al., 2014)

\*\* denotes stabilizing agent was either not used or not included in the methods.

<sup>a</sup>sodium dodecylbenzene sulfonate (SDBS)

## References

- A.D. McNaught, A. Wilkinson, 2007. IUPAC. Compendium of Chemical Terminology, 2nd. Ed. (the “Gold Book”) Online corrected version. ed. Blackwell Scientific Publications.
- Aitken, R.J., Chaudhry, M.Q., Boxall, A.B.A., Hull, M., 2006. Manufacture and use of nanomaterials: current status in the UK and global trends. *Occup Med (Lond)* 56, 300–306. doi:10.1093/occmed/kql051
- Aldeek, F., Mustin, C., Balan, L., Roques-Carmes, T., Fontaine-Aupart, M.-P., Schneider, R., 2011. Surface-engineered quantum dots for the labeling of hydrophobic microdomains in bacterial biofilms. *Biomaterials* 32, 5459–5470.
- Alito, C.L., Gunsch, C.K., 2014. Assessing the Effects of Silver Nanoparticles on Biological Nutrient Removal in Bench-Scale Activated Sludge Sequencing Batch Reactors. *Environ. Sci. Technol.* 48, 970–976. doi:10.1021/es403640j
- Anderson, J.W., Semprini, L., Radniecki, T.S., 2014. Influence of Water Hardness on Silver Ion and Silver Nanoparticle Fate and Toxicity Toward *Nitrosomonas europaea*. *Environmental Engineering Science* 31, 403–409. doi:10.1089/ees.2013.0426
- Antignano, A., Manning, C.E., 2008. Rutile solubility in H<sub>2</sub>O, H<sub>2</sub>O–SiO<sub>2</sub>, and H<sub>2</sub>O–NaAlSi<sub>3</sub>O<sub>8</sub> fluids at 0.7–2.0 GPa and 700–1000 °C: Implications for mobility of nominally insoluble elements. *Chemical Geology* 255, 283–293. doi:10.1016/j.chemgeo.2008.07.001
- Auffan, M., Rose, J., Bottero, J., Lowry, G.V., Jolivet, J.-P., Wiesner, M.R., 2009. Towards a definition of inorganic nanoparticles from an environmental, health and safety perspective. *Nature Nanotechnology* 4, 634–641. doi:10.1038/nnano.2009.242
- Baalousha, M., Manciuola, A., Cumberland, S., Kendall, K., Lead, J.R., 2008. Aggregation and Surface Properties of Iron Oxide Nanoparticles: Influence of pH and Natural Organic Matter. *Environmental Toxicology and Chemistry* 27, 1875–82.
- Barton, L.E., Auffan, M., Bertrand, M., Barakat, M., Santaella, C., Masion, A., Borschneck, D., Olivi, L., Roche, N., Wiesner, M.R., Bottero, J.-Y., 2014a. Transformation of Pristine and Citrate-Functionalized CeO<sub>2</sub> Nanoparticles in a Laboratory-Scale Activated Sludge Reactor. *Environ. Sci. Technol.* 48, 7289–7296. doi:10.1021/es404946y
- Barton, L.E., Therezien, M., Auffan, M., Bottero, J.-Y., Wiesner, M.R., 2014b. Theory and Methodology for Determining Nanoparticle Affinity for Heteroaggregation in Environmental Matrices Using Batch Measurements. *Environmental Engineering Science* 31, 421–427. doi:10.1089/ees.2013.0472
- Battin, T.J., Kammer, F. v.d., Weilhartner, A., Ottofuelling, S., Hofmann, T., 2009. Nanostructured TiO<sub>2</sub>: Transport Behavior and Effects on Aquatic Microbial Communities under Environmental Conditions. *Environ. Sci. Technol.* 43, 8098–8104. doi:10.1021/es9017046

- Benn, T.M., Westerhoff, P., 2008. Nanoparticle Silver Released into Water from Commercially Available Sock Fabrics. *Environmental Science & Technology* 42, 4133–4139. doi:10.1021/es7032718
- Bian, S.-W., Mudunkotuwa, I.A., Rupasinghe, T., Grassian, V.H., 2011. Aggregation and Dissolution of 4 nm ZnO Nanoparticles in Aqueous Environments: Influence of pH, Ionic Strength, Size, and Adsorption of Humic Acid. *Langmuir* 27, 6059–6068. doi:10.1021/la200570n
- Boldrin, A., Hansen, S.F., Baun, A., Hartmann, N.I.B., Astrup, T.F., 2014. Environmental exposure assessment framework for nanoparticles in solid waste. *J Nanopart Res* 16, 1–19. doi:10.1007/s11051-014-2394-2
- Bondarenko, O., Juganson, K., Ivask, A., Kasemets, K., Mortimer, M., Kahru, A., 2013. Toxicity of Ag, CuO and ZnO nanoparticles to selected environmentally relevant test organisms and mammalian cells in vitro: a critical review. *Archives Of Toxicology* 87, 1181–1200. doi:10.1007/s00204-013-1079-4
- Bour, A., Mouchet, F., Silvestre, J., Gauthier, L., Pinelli, E., 2015. Environmentally relevant approaches to assess nanoparticles ecotoxicity: A review. *Journal of Hazardous Materials* 283, 764–777. doi:10.1016/j.jhazmat.2014.10.021
- Boxall, A.B.A., Chaudry, Q., Sinclair, C., Jones, A., Aitken, R., Jefferson, B., Watts, C., 2009. Current and future predicted environmental exposure to engineered nanoparticles. Central Science Laboratory, London, UK.
- Brar, S.K., Verma, M., Tyagi, R.D., Surampalli, R.Y., 2010. Engineered nanoparticles in wastewater and wastewater sludge – Evidence and impacts. *Waste Management* 30, 504–520. doi:10.1016/j.wasman.2009.10.012
- Brunetti, G., Donner, E., Laera, G., Sekine, R., Scheckel, K.G., Khaksar, M., Vasilev, K., De Mastro, G., Lombi, E., 2015. Fate of zinc and silver engineered nanoparticles in sewerage networks. *Water Research* 77, 72–84. doi:10.1016/j.watres.2015.03.003
- Burton, A., 2012. Titanium Dioxide Photocleans Polluted Air. *Environ Health Perspect* 120, a229. doi:10.1289/ehp.120-a229
- Chen, Y., Wang, D., Zhu, X., Zheng, X., Feng, L., 2012. Long-Term Effects of Copper Nanoparticles on Wastewater Biological Nutrient Removal and N<sub>2</sub>O Generation in the Activated Sludge Process. *Environ. Sci. Technol.* 46, 12452–12458. doi:10.1021/es302646q
- Chih-ping Tso, Cheng-min Zhung, Yang-hsin Shih, Young-Ming Tseng, Shian-chee Wu, Ruey-an Doong, 2010. Stability of metal oxide nanoparticles in aqueous solutions. *Water Science & Technology* 61, 127–133. doi:10.2166/wst.2010.787



- Choi, O., Deng, K.K., Kim, N.-J., Ross Jr., L., Surampalli, R.Y., Hu, Z., 2008. The inhibitory effects of silver nanoparticles, silver ions, and silver chloride colloids on microbial growth. *Water Research* 42, 3066–3074. doi:10.1016/j.watres.2008.02.021
- Choi, O., Yu, C.-P., Esteban Fernández, G., Hu, Z., 2010. Interactions of nanosilver with *Escherichia coli* cells in planktonic and biofilm cultures. *Water Research* 44, 6095–6103. doi:10.1016/j.watres.2010.06.069
- Chrzanowska, N., Załęska-Radziwiłł, M., 2014. The impacts of aluminum and zirconium nano-oxides on planktonic and biofilm bacteria. *Desalination and Water Treatment* 52, 3680–3689. doi:10.1080/19443994.2014.884528
- Conway, J.R., Adeleye, A.S., Gardea-Torresdey, J., Keller, A.A., 2015. Aggregation, Dissolution, and Transformation of Copper Nanoparticles in Natural Waters. *Environ. Sci. Technol.* 49, 2749–2756. doi:10.1021/es504918q
- de Faria, A.F., de Moraes, A.C.M., Alves, O.L., 2014. Toxicity of Nanomaterials to Microorganisms: Mechanisms, Methods, and New Perspectives, in: Durán, N., Guterres, S.S., Alves, O.L. (Eds.), *Nanotoxicology*. Springer New York, New York, NY, pp. 363–405.
- Devlin, T., Wei, V., Oleszkiewicz, J., 2015. Impact of Nanoparticle Silver in a Sequencing Batch Reactor Removing Phosphorus and Ammonia. *J. Environ. Eng.* 141, 06015001. doi:10.1061/(ASCE)EE.1943-7870.0000942
- Domingos, R.F., Tufenkji, N., Wilkinson, K.J., 2009. Aggregation of Titanium Dioxide Nanoparticles: Role of a Fulvic Acid. *Environ. Sci. Technol.* 43, 1282–1286. doi:10.1021/es8023594
- Dror-Ehre, A., Adin, A., Markovich, G., Mamane, H., 2010. Control of biofilm formation in water using molecularly capped silver nanoparticles. *Water Research* 44, 2601–2609. doi:10.1016/j.watres.2010.01.016
- Dwivedi, A.D., Dubey, S.P., Sillanpää, M., Kwon, Y.-N., Lee, C., Varma, R.S., 2015. Fate of engineered nanoparticles: Implications in the environment. *Coordination Chemistry Reviews* 287, 64–78. doi:10.1016/j.ccr.2014.12.014
- Eduok, S., Martin, B., Villa, R., Nocker, A., Jefferson, B., Coulon, F., 2013. Evaluation of engineered nanoparticle toxic effect on wastewater microorganisms: Current status and challenges. *Ecotoxicology and Environmental Safety* 95, 1–9. doi:10.1016/j.ecoenv.2013.05.022
- Fabrega, J., Fawcett, S.R., Renshaw, J.C., Lead, J.R., 2009a. Silver Nanoparticle Impact on Bacterial Growth: Effect of pH, Concentration, and Organic Matter. *Environ. Sci. Technol.* 43, 7285–7290. doi:10.1021/es803259g

- Fabrega, J., Renshaw, J.C., Lead, J.R., 2009b. Interactions of Silver Nanoparticles with *Pseudomonas putida* Biofilms. *Environ. Sci. Technol.* 43, 9004–9009. doi:10.1021/es901706j
- Fachvereinigung Betriebs- und Regenwassernutzung e.V. (fbr), 2005. Greywater Recycling: Planning Fundamentals and Operation Information. German Association for Rainwater Harvesting and Water Recycling (fbr). Darmstadt, Germany.
- Fernández-García, M., Rodríguez, J.A., 2011. Metal Oxide Nanoparticles, in: *Encyclopedia of Inorganic and Bioinorganic Chemistry*. John Wiley & Sons, Ltd.
- Ganesh, R., Smeraldi, J., Hosseini, T., Khatib, L., Olson, B.H., Rosso, D., 2010. Evaluation of Nanocopper Removal and Toxicity in Municipal Wastewaters. *Environ. Sci. Technol.* 44, 7808–7813. doi:10.1021/es101355k
- García, A., Delgado, L., Torà, J.A., Casals, E., González, E., Puentes, V., Font, X., Carrera, J., Sánchez, A., 2012. Effect of cerium dioxide, titanium dioxide, silver, and gold nanoparticles on the activity of microbial communities intended in wastewater treatment. *Journal of Hazardous Materials* 199–200, 64–72. doi:10.1016/j.jhazmat.2011.10.057
- Gartiser, S., Flach, F., Nickel, C., Stintz, M., Damme, S., Schaeffer, A., Erdinger, L., Kuhlbusch, T.A.J., 2014. Behavior of nanoscale titanium dioxide in laboratory wastewater treatment plants according to OECD 303 A. *Chemosphere* 104, 197–204. doi:10.1016/j.chemosphere.2013.11.015
- Geyik, A.G., Kılıç, B., Çeçen, F., 2015. Extracellular polymeric substances (EPS) and surface properties of activated sludges: effect of organic carbon sources. *Environ Sci Pollut Res* 23, 1–11. doi:10.1007/s11356-015-5347-0
- Gómez-Rivera, F., Field, J.A., Brown, D., Sierra-Alvarez, R., 2012. Fate of cerium dioxide (CeO<sub>2</sub>) nanoparticles in municipal wastewater during activated sludge treatment. *Bioresource technology* 108, 300–304.
- Grillo, R., Rosa, A.H., Fraceto, L.F., 2015. Engineered nanoparticles and organic matter: a review of the state-of-the-art. *Chemosphere* 119, 608–619.
- Guiot, E., Georges, P., Brun, A., Fontaine-Aupart, M.P., Bellon-Fontaine, M.N., Briandet, R., 2002. Heterogeneity of Diffusion Inside Microbial Biofilms Determined by Fluorescence Correlation Spectroscopy Under Two-photon Excitation. *Photochemistry and Photobiology* 75, 570–578. doi:10.1562/0031-8655(2002)075<0570:HODIMB>2.0.CO;2
- Hendren, C.O., Mesnard, X., Dröge, J., Wiesner, M.R., 2011. Estimating Production Data for Five Engineered Nanomaterials As a Basis for Exposure Assessment. *Environ. Sci. Technol.* 45, 2562–2569. doi:10.1021/es103300g
- Herrling, M.P., Lackner, S., Tatti, O., Guthausen, G., Delay, M., Franzreb, M., Horn, H., 2016. Short and long term biosorption of silica-coated iron oxide nanoparticles in heterotrophic biofilms. *Sci. Total Environ.* 544, 722–729. doi:10.1016/j.scitotenv.2015.11.174

- Hou, J., Miao, L., Wang, C., Wang, P., Ao, Y., Lv, B., 2015a. Effect of CuO nanoparticles on the production and composition of extracellular polymeric substances and physicochemical stability of activated sludge flocs. *Bioresource Technology* 176, 65–70. doi:10.1016/j.biortech.2014.11.020
- Hou, J., Miao, L., Wang, C., Wang, P., Ao, Y., Qian, J., Dai, S., 2014. Inhibitory effects of ZnO nanoparticles on aerobic wastewater biofilms from oxygen concentration profiles determined by microelectrodes. *Journal of Hazardous Materials* 276, 164–170. doi:10.1016/j.jhazmat.2014.04.048
- Hou, J., You, G., Xu, Y., Wang, C., Wang, P., Miao, L., Ao, Y., Li, Y., Lv, B., 2015b. Effects of CeO<sub>2</sub> nanoparticles on biological nitrogen removal in a sequencing batch biofilm reactor and mechanism of toxicity. *Bioresource Technology* 191, 73–78. doi:10.1016/j.biortech.2015.04.123
- Hou, L., Li, K., Ding, Y., Li, Y., Chen, J., Wu, X., Li, X., 2012. Removal of silver nanoparticles in simulated wastewater treatment processes and its impact on COD and NH<sub>4</sub> reduction. *Chemosphere* 87, 248–252.
- Howard, A.G., 2010. On the challenge of quantifying man-made nanoparticles in the aquatic environment. *J. Environ. Monit.* 12, 135–142. doi:10.1039/B913681A
- Hwang, S., Martinez, D., Perez, P., Rinaldi, C., 2011. Effect of surfactant-coated iron oxide nanoparticles on the effluent water quality from a simulated sequencing batch reactor treating domestic wastewater. *Environmental Pollution* 159, 3411–3415. doi:10.1016/j.envpol.2011.08.032
- Ikuma, K., Decho, A.W., Lau, B.L., 2015. When nanoparticles meet biofilms-Interactions guiding the environmental fate and accumulation of nanoparticles. Name: *Frontiers in Microbiology* 6, 591.
- Jarvie, H.P., Al-Obaidi, H., King, S.M., Bowes, M.J., Lawrence, M.J., Drake, A.F., Green, M.A., Dobson, P.J., 2009. Fate of Silica Nanoparticles in Simulated Primary Wastewater Treatment. *Environ. Sci. Technol.* 43, 8622–8628. doi:10.1021/es901399q
- Jeong, E., Im, W.-T., Kim, D.-H., Kim, M.-S., Kang, S., Shin, H.-S., Chae, S.-R., 2014. Different susceptibilities of bacterial community to silver nanoparticles in wastewater treatment systems. *J Environ Sci Health A Tox Hazard Subst Environ Eng* 49, 685–693. doi:10.1080/10934529.2014.865454
- Jiang, X., Wang, X., Tong, M., Kim, H., 2013. Initial transport and retention behaviors of ZnO nanoparticles in quartz sand porous media coated with *Escherichia coli* biofilm. *Environmental Pollution* 174, 38–49. doi:10.1016/j.envpol.2012.11.016
- Jing, H., Mezgebe, B., Hassan, A.A., Sahle-Demessie, E., Sorial, G.A., Bennett-Stamper, C., 2014. Experimental and modeling studies of sorption of ceria nanoparticle on microbial biofilms. *Bioresource technology* 161, 109–117.

- Jokerst, J.V., Lobovkina, T., Zare, R.N., Gambhir, S.S., 2011. Nanoparticle PEGylation for imaging and therapy. *Nanomedicine (Lond)* 6, 715–728. doi:10.2217/nnm.11.19
- Kaegi, R., Voegelin, A., Ort, C., Sinnet, B., Thalmann, B., Krismer, J., Hagendorfer, H., Elumelu, M., Mueller, E., 2013. Fate and transformation of silver nanoparticles in urban wastewater systems. *Water Research, Nanotechnology for Water and Wastewater Treatment* 47, 3866–3877. doi:10.1016/j.watres.2012.11.060
- Khot, L.R., Sankaran, S., Maja, J.M., Ehsani, R., Schuster, E.W., 2012. Applications of nanomaterials in agricultural production and crop protection: A review. *Crop Protection* 35, 64–70. doi:10.1016/j.cropro.2012.01.007
- Kim, B., Murayama, M., Colman, B.P., Hochella, M.F., 2012. Characterization and environmental implications of nano- and larger TiO<sub>2</sub> particles in sewage sludge, and soils amended with sewage sludge. *Journal of Environmental Monitoring* 14, 1129. doi:10.1039/c2em10809g
- Kim, B., Park, C.-S., Murayama, M., Hochella Jr, M.F., 2010. Discovery and characterization of silver sulfide nanoparticles in final sewage sludge products. *Environmental science & technology* 44, 7509–7514.
- Kirkegaard, P., Hansen, S.F., Rygaard, M., 2015. Potential exposure and treatment efficiency of nanoparticles in water supplies based on wastewater reclamation. *Environ. Sci.: Nano* 2, 191–202. doi:10.1039/C4EN00192C
- Kiser, M.A., Ryu, H., Jang, H., Hristovski, K., Westerhoff, P., 2010. Biosorption of nanoparticles to heterotrophic wastewater biomass. *Water Research* 44, 4105–4114. doi:10.1016/j.watres.2010.05.036
- Kiser, M.A., Westerhoff, P., Benn, T., Wang, Y., Pérez-Rivera, J., Hristovski, K., 2009. Titanium Nanomaterial Removal and Release from Wastewater Treatment Plants. *Environ. Sci. Technol.* 43, 6757–6763. doi:10.1021/es901102n
- Kroll, A., Behra, R., Kaegi, R., Sigg, L., 2014. Extracellular Polymeric Substances (EPS) of Freshwater Biofilms Stabilize and Modify CeO<sub>2</sub> and Ag Nanoparticles. *PLoS One* 9, p.e110709. doi:10.1371/journal.pone.0110709
- Labrenz, M., Druschel, G.K., Thomsen-Ebert, T., Gilbert, B., Welch, S.A., Kemner, K.M., Logan, G.A., Summons, R.E., De Stasio, G., Bond, P.L., others, 2000. Formation of sphalerite (ZnS) deposits in natural biofilms of sulfate-reducing bacteria. *Science* 290, 1744–1747.
- Lee, C., Kim, J.Y., Lee, W.I., Nelson, K.L., Yoon, J., Sedlak, D.L., 2008. Bactericidal effect of zero-valent iron nanoparticles on *Escherichia coli*. *Environmental science & technology* 42, 4927–4933.

- Lerner, R.N., Lu, Q., Zeng, H., Liu, Y., 2012. The effects of biofilm on the transport of stabilized zerovalent iron nanoparticles in saturated porous media. *Water Research* 46, 975–985. doi:10.1016/j.watres.2011.11.070
- Levard, C., Hotze, E.M., Lowry, G.V., Brown, G.E., 2012. Environmental Transformations of Silver Nanoparticles: Impact on Stability and Toxicity. *Environ. Sci. Technol.* 46, 6900–6914. doi:10.1021/es2037405
- Liang, Z., Das, A., Hu, Z., 2010. Bacterial response to a shock load of nanosilver in an activated sludge treatment system. *Water Research* 44, 5432–5438. doi:10.1016/j.watres.2010.06.060
- Li, H., Wen, Y., Cao, A., Huang, J., Zhou, Q., Somasundaran, P., 2012. The influence of additives (Ca<sup>2+</sup>, Al<sup>3+</sup>, and Fe<sup>3+</sup>) on the interaction energy and loosely bound extracellular polymeric substances (EPS) of activated sludge and their flocculation mechanisms. *Bioresource Technology* 114, 188–194. doi:10.1016/j.biortech.2012.03.043
- Li, L., Hartmann, G., Döblinger, M., Schuster, M., 2013. Quantification of Nanoscale Silver Particles Removal and Release from Municipal Wastewater Treatment Plants in Germany. *Environ. Sci. Technol.* 47, 7317–7323. doi:10.1021/es3041658
- Limbach, L.K., Bereiter, R., Müller, E., Krebs, R., Gälli, R., Stark, W.J., 2008. Removal of Oxide Nanoparticles in a Model Wastewater Treatment Plant: Influence of Agglomeration and Surfactants on Clearing Efficiency. *Environ. Sci. Technol.* 42, 5828–5833. doi:10.1021/es800091f
- Liu, G., Wang, D., Wang, J., Mendoza, C., 2011. Effect of ZnO particles on activated sludge: role of particle dissolution. *Science of the total environment* 409, 2852–2857.
- Liu, X., Ray, J.R., Neil, C.W., Li, Q., Jun, Y.-S., 2015. Enhanced Colloidal Stability of CeO<sub>2</sub> Nanoparticles by Ferrous Ions: Adsorption, Redox Reaction, and Surface Precipitation. *Environ. Sci. Technol.* 49, 5476–5483. doi:10.1021/es506363x
- Li, X., Yeh, Y.-C., Giri, K., Mout, R., Landis, R.F., Prakash, Y.S., Rotello, V.M., 2015. Control of nanoparticle penetration into biofilms through surface design. *Chem. Commun.* 51, 282–285. doi:10.1039/C4CC07737G
- Li, X.Y., Yang, S.F., 2007. Influence of loosely bound extracellular polymeric substances (EPS) on the flocculation, sedimentation and dewaterability of activated sludge. *Water Research* 41, 1022–1030. doi:10.1016/j.watres.2006.06.037
- Li, Z., Aly Hassan, A., Sahle-Demessie, E., Sorial, G.A., 2013. Transport of nanoparticles with dispersant through biofilm coated drinking water sand filters. *Water Research* 47, 6457–6466. doi:10.1016/j.watres.2013.08.026
- Lombi, E., Donner, E., Taheri, S., Tavakkoli, E., Jämting, Å.K., McClure, S., Naidu, R., Miller, B.W., Scheckel, K.G., Vasilev, K., 2013. Transformation of four silver/silver chloride

- nanoparticles during anaerobic treatment of wastewater and post-processing of sewage sludge. *Environmental Pollution* 176, 193–197. doi:10.1016/j.envpol.2013.01.029
- Lombi, E., Donner, E., Tavakkoli, E., Turney, T.W., Naidu, R., Miller, B.W., Scheckel, K.G., 2012. Fate of Zinc Oxide Nanoparticles during Anaerobic Digestion of Wastewater and Post-Treatment Processing of Sewage Sludge. *Environ. Sci. Technol.* 46, 9089–9096. doi:10.1021/es301487s
- Ma, R., Levard, C., Judy, J.D., Unrine, J.M., Durenkamp, M., Martin, B., Jefferson, B., Lowry, G.V., 2013a. Fate of Zinc Oxide and Silver Nanoparticles in a Pilot Wastewater Treatment Plant and in Processed Biosolids. *Environ. Sci. Technol.* 48, 104–112. doi:10.1021/es403646x
- Ma, R., Levard, C., Michel, F.M., Brown, G.E., Lowry, G.V., 2013b. Sulfidation Mechanism for Zinc Oxide Nanoparticles and the Effect of Sulfidation on Their Solubility. *Environ. Sci. Technol.* 47, 2527–2534. doi:10.1021/es3035347
- Matamoros, V., Rodríguez, Y., Albaigés, J., 2016. A comparative assessment of intensive and extensive wastewater treatment technologies for removing emerging contaminants in small communities. *Water Research* 88, 777–785. doi:10.1016/j.watres.2015.10.058
- Maurer-Jones, M.A., Gunsolus, I.L., Meyer, B.M., Christenson, C.J., Haynes, C.L., 2013. Impact of TiO<sub>2</sub> Nanoparticles on Growth, Biofilm Formation, and Flavin Secretion in *Shewanella oneidensis*. *Anal. Chem.* 85, 5810–5818. doi:10.1021/ac400486u
- Ma, W., Zhong, D., Han, H., Wang, P., 2013. A review: inhibition of Ag NPs on wastewater treatment. *Desalination and Water Treatment* 51, 7012–7017.
- Ma, Y., Elankumaran, S., Marr, L.C., Vejerano, E.P., Pruden, A., 2014. Toxicity of engineered nanomaterials and their transformation products following wastewater treatment on A549 human lung epithelial cells. *Toxicology Reports* 1, 871–876. doi:10.1016/j.toxrep.2014.08.017
- Ma, Y., Metch, J.W., Vejerano, E.P., Miller, I.J., Leon, E.C., Marr, L.C., Vikesland, P.J., Pruden, A., 2015. Microbial community response of nitrifying sequencing batch reactors to silver, zero-valent iron, titanium dioxide and cerium dioxide nanomaterials. *Water Research* 68, 87–97. doi:10.1016/j.watres.2014.09.008
- Miao, L.Z., Wang, C., Hou, J., Wang, P.F., Qian, J., Dai, S.S., 2014. Kinetics and equilibrium biosorption of nano-ZnO particles on periphytic biofilm under different environmental conditions. *Journal of environmental informatics* 23, 1–9.
- Mitrano, D.M., Motellier, S., Clavaguera, S., Nowack, B., 2015. Review of nanomaterial aging and transformations through the life cycle of nano-enhanced products. *Environment international* 77, 132–147.

- Mu, H., Chen, Y., Xiao, N., 2011. Effects of metal oxide nanoparticles (TiO<sub>2</sub>, Al<sub>2</sub>O<sub>3</sub>, SiO<sub>2</sub> and ZnO) on waste activated sludge anaerobic digestion. *Bioresource Technology* 102, 10305–10311. doi:10.1016/j.biortech.2011.08.100
- Mu, H., Zheng, X., Chen, Y., Chen, H., Liu, K., 2012. Response of Anaerobic Granular Sludge to a Shock Load of Zinc Oxide Nanoparticles during Biological Wastewater Treatment. *Environ. Sci. Technol.* 46, 5997–6003. doi:10.1021/es300616a
- Neal, A.L., 2008. What can be inferred from bacterium–nanoparticle interactions about the potential consequences of environmental exposure to nanoparticles? *Ecotoxicology* 17, 362–371. doi:10.1007/s10646-008-0217-x
- Nevius, B.A., Chen, Y.P., Ferry, J.L., Decho, A.W., 2012. Surface-functionalization effects on uptake of fluorescent polystyrene nanoparticles by model biofilms. *Ecotoxicology* 21, 2205–2213.
- OECD, 2014. Genotoxicity of manufactured nanomaterials : Report of the OECD expert meeting (Unclassified No. 43), Series on the Safety of Manufactured Nanomaterials. OECD, Paris.
- Opportunities and Risks of Nanotechnologies (Joint Report of the Allianz Center for Technology and the OECD International Futures Programme), 2007.
- Park, H.-J., Kim, H.Y., Cha, S., Ahn, C.H., Roh, J., Park, S., Kim, S., Choi, K., Yi, J., Kim, Y., others, 2013. Removal characteristics of engineered nanoparticles by activated sludge. *Chemosphere* 92, 524–528.
- PEN, 2012. Consumer Product Inventory. Nanotechnology - Project on Emerging Nanotechnologies Woodrow Wilson International Center of Scholars [WWW Document]. URL <http://www.nanotechproject.org/> (accessed 2.13.16).
- Peulen, T.-O., Wilkinson, K.J., 2011. Diffusion of Nanoparticles in a Biofilm. *Environ. Sci. Technol.* 45, 3367–3373. doi:10.1021/es103450g
- Piella, J., Bastús, N.G., Puentes, V., 2016. Size-Controlled Synthesis of Sub-10-nanometer Citrate-Stabilized Gold Nanoparticles and Related Optical Properties. *Chem. Mater.* 28, 1066–1075. doi:10.1021/acs.chemmater.5b04406
- Powell, J.J., Ainley, C.C., Harvey, R.S., Mason, I.M., Kendall, M.D., Sankey, E.A., Dhillon, A.P., Thompson, R.P., 1996. Characterisation of inorganic microparticles in pigment cells of human gut associated lymphoid tissue. *Gut* 38, 390–395.
- Quik, J.T.K., Lynch, I., Hoecke, K.V., Miermans, C.J.H., Schamphelaere, K.A.C.D., Janssen, C.R., Dawson, K.A., Stuart, M.A.C., Meent, D.V.D., 2010. Effect of natural organic matter on cerium dioxide nanoparticles settling in model fresh water. *Chemosphere* 81, 711–715. doi:10.1016/j.chemosphere.2010.07.062

- Ratte, H.T., 1999. Bioaccumulation and toxicity of silver compounds: a review. *Environmental Toxicology and Chemistry* 18, 89–108.
- Ravishankar Rai, V., Jamuna Bai, A., 2011. Nanoparticles and their potential application as antimicrobials. *Science against microbial pathogens: communicating current research and technological advances*. FORMATEX 197–209.
- Reyes, V.C., Opot, S.O., Mahendra, S., 2015. Planktonic and biofilm-grown nitrogen-cycling bacteria exhibit different susceptibilities to copper nanoparticles. *Environmental Toxicology and Chemistry* 34, 887–897.
- Rottman, J., Shadman, F., Sierra-Alvarez, R., 2012. Interactions of inorganic oxide nanoparticles with sewage biosolids. *Water Science And Technology: A Journal Of The International Association On Water Pollution Research* 66, 1821–1827. doi:10.2166/wst.2012.354
- Ruparelia, J.P., Chatterjee, A.K., Duttagupta, S.P., Mukherji, S., 2008. Strain specificity in antimicrobial activity of silver and copper nanoparticles. *Acta biomaterialia* 4, 707–716.
- Sahai, N., 2002. Is Silica Really an Anomalous Oxide? Surface Acidity and Aqueous Hydrolysis Revisited. *Environ. Sci. Technol.* 36, 445–452. doi:10.1021/es010850u
- Sand, W., Gehrke, T., 1999. Analysis and function of the EPS from the strong acidophile *Thiobacillus ferrooxidans*, in: *Microbial Extracellular Polymeric Substances*. Springer, pp. 127–141.
- Schlegel, S., Teichgräber, B., 2000. Operational results and experience with submerged fixed-film reactors in the pretreatment of industrial effluents. *Water Science & Technology* 41, 453–459.
- Sekine, R., Khaksar, M., Brunetti, G., Donner, E., Scheckel, K.G., Lombi, E., Vasilev, K., 2013. Surface Immobilization of Engineered Nanomaterials for in Situ Study of their Environmental Transformations and Fate. *Environmental Science & Technology* 47, 9308–9316. doi:10.1021/es400839h
- Sheng, Z., Liu, Y., 2011. Effects of silver nanoparticles on wastewater biofilms. *Water Research* 45, 6039–6050. doi:10.1016/j.watres.2011.08.065
- Sheng, Z., Van Nostrand, J.D., Zhou, J., Liu, Y., 2015. The effects of silver nanoparticles on intact wastewater biofilms. *Front Microbiol* 6. doi:10.3389/fmicb.2015.00680
- Sokolov, S.V., Tschulik, K., Batchelor-McAuley, C., Jurkschat, K., Compton, R.G., 2015. Reversible or not? Distinguishing agglomeration and aggregation at the nanoscale. *Anal. Chem.* 87, 10033–10039. doi:10.1021/acs.analchem.5b02639
- Stone, V., Johnston, H., Clift, M.J.D., 2007. Air Pollution, Ultrafine and Nanoparticle Toxicology: Cellular and Molecular Interactions. *IEEE Transactions on NanoBioscience* 6, 331–340. doi:10.1109/TNB.2007.909005



- Stoodley, P., Sauer, K., Davies, D.G., Costerton, J.W., 2002. Biofilms as Complex Differentiated Communities. *Annual Review of Microbiology* 56, 187–209. doi:10.1146/annurev.micro.56.012302.160705
- Sun, T.Y., Gottschalk, F., Hungerbühler, K., Nowack, B., 2014. Comprehensive probabilistic modelling of environmental emissions of engineered nanomaterials. *Environmental Pollution* 185, 69–76.
- Sun, X., Sheng, Z., Liu, Y., 2013. Effects of silver nanoparticles on microbial community structure in activated sludge. *Science of The Total Environment* 443, 828–835. doi:10.1016/j.scitotenv.2012.11.019
- Tan, M., Qiu, G., Ting, Y.-P., 2015. Effects of ZnO nanoparticles on wastewater treatment and their removal behavior in a membrane bioreactor. *Bioresource Technology* 185, 125–133. doi:10.1016/j.biortech.2015.02.094
- Tchobanoglous, G., Burton, F.L., Stensel, H.D., Metcalf & Eddy (Eds.), 2003. *Wastewater engineering: treatment and reuse*, 4th ed. ed, McGraw-Hill series in civil and environmental engineering. McGraw-Hill, Boston.
- Thuptimrang, P., Limpiyakorn, T., McEvoy, J., Prülls, B.M., Khan, E., 2015. Effect of silver nanoparticles on *Pseudomonas putida* biofilms at different stages of maturity. *Journal of hazardous materials* 290, 127–133.
- Tong, T., Fang, K., Thomas, S.A., Kelly, J.J., Gray, K.A., Gaillard, J.-F., 2014. Chemical Interactions between Nano-ZnO and Nano-TiO<sub>2</sub> in a Natural Aqueous Medium. *Environ. Sci. Technol.* 48, 7924–7932. doi:10.1021/es501168p
- Trefalt, G., Ruiz-Cabello, F.J.M., Borkovec, M., 2014. Interaction Forces, Heteroaggregation, and Deposition Involving Charged Colloidal Particles. *The Journal of Physical Chemistry B* 118, 6346–6355. doi:10.1021/jp503564p
- Tripathi, S., Champagne, D., Tufenkji, N., 2011. Transport Behavior of Selected Nanoparticles with different Surface Coatings in Granular Porous Media coated with *Pseudomonas aeruginosa* Biofilm. *Environ. Sci. Technol.* 46, 6942–6949. doi:10.1021/es202833k
- Tso, C., Zhung, C., Shih, Y., Tseng, Y.-M., Wu, S., Doong, R., 2010. Stability of metal oxide nanoparticles in aqueous solutions. *Water Science & Technology* 61, 127. doi:10.2166/wst.2010.787
- United Kingdom Department of Environment, Food, and Rural Affairs, 2011. *Characterising the potential risks posed by engineered nanoparticles*.
- US EPA National Center for Environmental Assessment, 2001. *Sources, Emission and Exposure to Trichloroethylene (TCE) and Related Chemicals*.
- US EPA, O., 2015a. *Use and Disposal of Biosolids (Sewage Sludge) [WWW Document]*. URL <http://water.epa.gov/scitech/wastetech/biosolids/#tnss> (accessed 2.5.16).

- US EPA, O., 2015b. Monitoring and Assessment [WWW Document]. URL <http://water.epa.gov/type/wetlands/assessment/> (accessed 2.3.16).
- Vance, M.E., Kuiken, T., Vejerano, E.P., McGinnis, S.P., Hochella, M.F., Rejeski, D., Hull, M.S., 2015. Nanotechnology in the real world: Redeveloping the nanomaterial consumer products inventory. *Beilstein Journal of Nanotechnology* 6, 1769–1780. doi:10.3762/bjnano.6.181
- Vejerano, E.P., Ma, Y., Holder, A.L., Pruden, A., Elankumaran, S., Marr, L.C., 2015. Toxicity of particulate matter from incineration of nanowaste. *Environmental Science: Nano* 2, 143–154.
- Walker, H.W., Bob, M.M., 2001. Stability of particle flocs upon addition of natural organic matter under quiescent conditions. *Water Research* 35, 875–882. doi:10.1016/S0043-1354(00)00333-X
- Wang, D., Chen, Y., 2015. Critical review of the influences of nanoparticles on biological wastewater treatment and sludge digestion. *Critical Reviews in Biotechnology* 1–13.
- Wang, H., Dong, Y., Zhu, M., Li, X., Keller, A.A., Wang, T., Li, F., 2015. Heteroaggregation of engineered nanoparticles and kaolin clays in aqueous environments. *Water Research* 80, 130–138. doi:10.1016/j.watres.2015.05.023
- Wang, W., Wu, W.-Y., Zhong, X., Wang, W., Miao, Q., Zhu, J.-J., 2011. Aptamer-based PDMS–gold nanoparticle composite as a platform for visual detection of biomolecules with silver enhancement. *Biosensors and Bioelectronics* 26, 3110–3114. doi:10.1016/j.bios.2010.10.034
- Wang, Y., Westerhoff, P., Hristovski, K.D., 2012. Fate and biological effects of silver, titanium dioxide, and C60 (fullerene) nanomaterials during simulated wastewater treatment processes. *Journal of Hazardous Materials* 201–202, 16–22. doi:10.1016/j.jhazmat.2011.10.086
- Westerhoff, P.K., Kiser, M.A., Hristovski, K., 2013. Nanomaterial removal and transformation during biological wastewater treatment. *Environmental Engineering Science* 30, 109–117.
- Westerhoff, P., Song, G., Hristovski, K., Kiser, M.A., 2011. Occurrence and removal of titanium at full scale wastewater treatment plants: implications for TiO<sub>2</sub> nanomaterials. *Journal of Environmental Monitoring* 13, 1195. doi:10.1039/c1em10017c
- Wingender, J., Neu, T.R., Flemming, H.-C., 2012. *Microbial extracellular polymeric substances: characterization, structure and function*. Springer Science & Business Media.
- Wu, B., Wang, Y., Lee, Y.-H., Horst, A., Wang, Z., Chen, D.-R., Sureshkumar, R., Tang, Y.J., 2010. Comparative Eco-Toxicities of Nano-ZnO Particles under Aquatic and Aerosol Exposure Modes. *Environ. Sci. Technol.* 44, 1484–1489. doi:10.1021/es9030497

- Xiao, Y., Wiesner, M.R., 2013. Transport and Retention of Selected Engineered Nanoparticles by Porous Media in the Presence of a Biofilm. *Environ. Sci. Technol.* 47, 2246–2253. doi:10.1021/es304501n
- Yang, K., Lin, D., Xing, B., 2009. Interactions of Humic Acid with Nanosized Inorganic Oxides. *Langmuir* 25, 3571–3576. doi:10.1021/la803701b
- Yang, Y., Quensen, J., Mathieu, J., Wang, Q., Wang, J., Li, M., Tiedje, J.M., Alvarez, P.J., 2014. Pyrosequencing reveals higher impact of silver nanoparticles than Ag D on the microbial community structure of activated sludge. *water research* 48, e325.
- Yoon, K.-Y., Hoon Byeon, J., Park, J.-H., Hwang, J., 2007. Susceptibility constants of *Escherichia coli* and *Bacillus subtilis* to silver and copper nanoparticles. *Science of The Total Environment* 373, 572–575. doi:10.1016/j.scitotenv.2006.11.007
- Yu, Z., Yu, M., Zhang, Z., Hong, G., Xiong, Q., 2014. Bovine serum albumin nanoparticles as controlled release carrier for local drug delivery to the inner ear. *Nanoscale Res Lett* 9, 343. doi:10.1186/1556-276X-9-343
- Zhang, W., Yao, Y., Sullivan, N., Chen, Y., 2011. Modeling the Primary Size Effects of Citrate-Coated Silver Nanoparticles on Their Ion Release Kinetics. *Environ. Sci. Technol.* 45, 4422–4428. doi:10.1021/es104205a
- Zhang, Y., Chen, Y., Westerhoff, P., Hristovski, K., Crittenden, J.C., 2008. Stability of commercial metal oxide nanoparticles in water. *Water Research* 42, 2204–2212. doi:10.1016/j.watres.2007.11.036
- Zheng, X., Chen, Y., Wu, R., 2011a. Long-Term Effects of Titanium Dioxide Nanoparticles on Nitrogen and Phosphorus Removal from Wastewater and Bacterial Community Shift in Activated Sludge. *Environ. Sci. Technol.* 45, 7284–7290. doi:10.1021/es2008598
- Zheng, X., Wu, R., Chen, Y., 2011b. Effects of ZnO Nanoparticles on Wastewater Biological Nitrogen and Phosphorus Removal. *Environ. Sci. Technol.* 45, 2826–2832. doi:10.1021/es2000744
- Zhou, X., Huang, B., Zhou, T., Liu, Y., Shi, H., 2015. Aggregation behavior of engineered nanoparticles and their impact on activated sludge in wastewater treatment. *Chemosphere* 119, 568–576. doi:10.1016/j.chemosphere.2014.07.037
- Zook, J., Long, S., Cleveland, D., Geronimo, C., MacCuspie, R., 2011. Measuring silver nanoparticle dissolution in complex biological and environmental matrices using UV-visible absorbance. *Analytical & Bioanalytical Chemistry* 401, 1993–2002. doi:10.1007/s00216-011-5266-y

### **Chapter 3**

## **Assessing impacts of DNA extraction methods on next generation sequencing of water and wastewater samples**

## Abstract

Next Generation Sequencing (NGS) is increasingly affordable and easier to perform. However, standard protocols prior to the sequencing step are only available for few selected sample types. Here we investigated the impact of DNA extraction methods on the consistency of NGS results. Four commercial DNA extraction kits (QIAamp DNA Mini kit, QIAamp DNA Stool Mini Kit, MO BIO Power Water Kit, and MO BIO Power Soil DNA Isolation Kit) were used on sample sources including lake water and wastewater, and sample types including planktonic and biofilm bacteria communities. Sampling locations included a lake water reservoir, a trickling filter, and a moving bed biofilm reactor (MBBR). Unique genera such as *Gemmatimonadetes*, *Elusimicrobia*, and *Latescibacteria* were found in multiple samples. The Stool Mini Kit was least efficient in terms of diversity in sampling results with freshwater lake samples, and surprisingly the Power Water Kit was the least efficient across all sample types examined. Detailed NGS beta diversity comparisons indicated that the Mini Kit and PowerSoil Kit are best suited for studies that extract DNA from a variety of water and wastewater samples. We ultimately recommend application of Mini Kit or PowerSoil Kit as an improvement to NGS protocols for these sampling environments. These results are a step toward achieving accurate comparability of complex samples from water and wastewater environments by applying a single DNA extraction method, further streamlining future investigations.

## 1.0 Introduction

The study of bacteria communities reaches across a wide span of disciplines (*e.g.* immunology, engineering, environmental sciences). In recent years, technologies available for genome sequencing of bacteria have evolved in terms of affordability, speed, and accuracy (van Dijk, Auger, Jaszczyszyn, & Thermes, 2014). Advantages of genome sequencing such as identification of potential pathogens are beneficial for ensuring public safety from diseases derived from recreational water supplies or wastewater effluent mixing zones. The characterization of planktonic bacterial communities in temperate freshwater lake has revealed important genomic adaptations and novel taxa (Oh et al., 2011). Likewise, engineered systems such as wastewater treatment facilities can benefit from studies of microbial communities responses to environmental variables or xenobiotics inputs (Yu, Wu, & Chang, 2013).

DNA based technologies are known as highly dependent on the quality of DNA from extraction methods or commercial kits used for sample preparation (Knudsen et al., 2016). Moving away from the traditional phenol-chloroform DNA extraction approach, commercial kits are a less toxic option, and have been developed as a combination of independent techniques proven to minimize DNA loss while optimizing the removal of PCR inhibitors (*e.g.* spin column purification, bead beating) (Krsek & Wellington, 1999; Leff, Dana, McArthur, & Shimkets, 1995; Miller, Bryant, Madsen, & Ghiorse, 1999). Numerous studies have compared commercial extraction kits for efficiency (Cruaud et al., 2014; Huang et al., 2012; Lyautey, Lacoste, Ten-Hage, Rols, & Garabetian, 2005), and more specifically microbial diversity observed in different environments such as human intestines, soil, river biofilms, human fecal samples, sediment, and biological activated carbon (Carbonero, Nava, Benefiel, Greenberg, & Gaskins, 2011; de Liphay, Enzinger, Johnsen, Aamand, & Sørensen, 2004; Lyautey et al., 2005; McOrist, Jackson, & Bird, 2002; Mumy & Findlay, 2004; Peng et al., 2013; Zheng, Gao, & Deng, 2012). Popular

choices for analyzing extraction methods have included polymerase chain reaction (PCR) coupled with denaturing gradient gel electrophoresis (DGGE), restriction fragment length polymorphism (RFLP), or quantitative PCR (qPCR). However, in the last decade, Next Generation Sequencing (NGS) has revolutionized scientific knowledge of microbial community diversity in the environment (Cruaud et al., 2014).

Since NGS provides deep coverage of microbial diversity, use of appropriate DNA extraction methods is even more critical. To date, there is no consensus for a single DNA extraction method that can be applied for different water samples, which would improve comparability between studies. For example, out of recent publications using NGS, the MO BIO Power Water kit as well as QiaAmp Stool Mini Kit were chosen for coastal and freshwater (He et al., 2016; Malki, Bruder, & Putonti, 2015; Manzari et al., 2015). Phenol-chloroform and QiaAmp Stool Mini Kit were applied for activated sludge (Guo & Zhang, 2013; Ma et al., 2015), whereas MO BIO Power Water Kit was also chosen for activated sludge in a later study (Xu, Liu, Chen, & Ni, 2017). These previous studies set the criteria for selecting the methods compared within this study.

The objective of this study is to compare DNA extraction methods using NGS (Illumina MiSeq), and subsequently to determine the pitfalls or advantages among protocols for processing a variety of water and wastewater samples in the field of environmental engineering. Here, we selected four commercial DNA extraction kits for comparison among samples from three different environments, including both lake water and wastewater, as well as in both planktonic and attached bacteria communities. The variety of samples will provide evidence of superior DNA extraction protocols which are most suitable for use across all types with NGS analysis. It is expected the results of this study will not only confirm the most suitable DNA extraction

method(s) on multiple types of water and wastewater samples, it will also benefit the research focusing on microbial communities in various environmental settings using NGS.

## **1.1 Materials and Methods**

**1.1.1 Study sites and sampling.** Water and biofilm samples were collected from three separate locations. At each location, bulk samples were collected for both water and biofilm types. Lake water samples were collected at the southern intake structure at Beaver Lake Reservoir (Lowell, Arkansas) 3 m below water surface level using a 6 L horizontal water sampler (Wildco, Model 1960-H65, Yulee, FL). One set of wastewater and biofilm samples were collected from the moving bed bioreactor at the Waterford Estates pre-manufactured plant (Fayetteville, Arkansas), which currently processes about 356,000 L of residential wastewater per day. The other set of wastewater and biofilm samples were collected from the trickling filter reactor at the Massard Wastewater Treatment Plant (Fort Smith, Arkansas). Biofilm carriers from the moving bed reactor were scooped out of the aeration tank, and put directly on ice in the dark. Rock media from the trickling filter reactor were transported in the same fashion.

**1.1.2 Sample processing.** Biofilms were scraped with a sterile metal spatula into pre-weighed centrifuge tubes, and evenly weighed replicates were prepared preceding DNA extraction for all extraction methods. Wastewater column samples were centrifuged at 10,000  $\times$  g for 5 minutes to pellet, and 250 mg aliquots were aseptically separated for each extraction into pre-weighed sterile centrifuge tubes in the same fashion as biofilm samples.

All water column samples were stored in acid-washed 1 L brown high density polyethylene (HDPE) bottles, transported on ice from the site to laboratory, then kept at 4°C for short-term storage before filtration (Standard Method 9060 B). Samples were filtered through 0.22  $\mu$ m cellulose nitrate membrane filters (GE Healthcare Life Sciences, Buckinghamshire, UK)



(Standard Method 9020). DNA extractions were performed immediately after sample processing. All glassware used was washed in phosphorous free laboratory detergent, rinsed three times with tap water, and three times with distilled deionized (DDI) water and sterilized (Elga Process Water System (18.2 MΩ cm<sup>-1</sup>) Purelab flex, Veolia, Ireland). For sterilization, all washed glassware was autoclaved at 121°C for 30 minutes (Model 522LS Gravity Steam Sterilizer, Getinge, Rochester, NY).

**1.1.3 DNA extractions.** Four extraction kits were tested: QIAamp DNA Mini Kit (Qiagen, Hilden, Germany), QIAamp DNA Stool Mini Kit (Qiagen), MO BIO Power Water Kit (Qiagen, Carlsbad, CA) and MO BIO Power Soil DNA Isolation Kit (Qiagen). Extractions were performed in duplicate and pooled for sequencing. All final DNA concentrations were quantified by microplate reader (Synergy H1 Multi-Mode Microplate Reader, Biotek Instruments, Inc., Winooski, VT). For each location and sample type, the sample labels were correlated with extraction methods using a simplified numbering system as listed in Table 1. For example, water column (planktonic) community from the moving bed bioreactor extracted with Qiagen Stool Kit is referred to as MW2. The extraction mechanisms within each protocol are briefly described in the following paragraphs. Complete details for reproducing these methods are included on each manufacturer's website.

**1.1.3.1 QIAamp DNA Mini Kit.** With this method, cells are lysed enzymatically with Protease. A series of four spin column steps are applied in a standard microcentrifuge. Protease and lysis buffer are added to the spin column with the sample. Lysate buffering conditions adsorb DNA to the spin column membrane. Several washing steps ensure that proteins and other contaminants are not retained in the membrane and purify DNA. DNA is eluted in elution buffer (10 mM Tris-Cl, 0.5 mM EDTA, pH 9.0).

**1.1.3.2 QIAamp DNA Stool Mini Kit.** Cells are lysed enzymatically in a proprietary buffer with Protease at 70°C. This kit includes an InhibitEx matrix in tablet form for the adsorption of inhibitors and DNA degrading substances. The InhibitEx is pelleted by centrifuge and the supernatant containing DNA is purified by spin column washing steps. The purified DNA is eluted in a low salt buffer.

**1.1.3.3 MO BIO PowerSoil DNA Kit.** Environmental samples are lysed by mechanical bead-beating and chemically with SDS. Samples are vortexed in bead beating tubes for 10 minutes. The samples are then centrifuged and the supernatant is chemically lysed at 4°C. Inhibitors are removed with another solution (labeled C3) which is then followed with spin filtration steps for purification and elution of DNA.

**1.1.3.4 MO BIO PowerWater DNA Kit.** Samples are lysed mechanically by bead-beating and chemically with a proprietary solution (PW1). The whole filter is inserted into a PowerWater bead tube with a lysing solution and vortexed at maximum speed for 5 minutes. The samples are then centrifuged and washed in several steps with kit provided solutions. Inhibitors are removed and DNA purified with spin filtration steps. DNA is eluted in an elution buffer containing no EDTA.

**1.1.4 16S rRNA amplification and Illumina sequencing.** Samples were transported on ice for subsequent Illumina MiSeq processing. Community profiling was completed using Illumina MiSeq followed by bioinformatics analyses in Mothur (Kozich, Westcott, Baxter, Highlander, & Schloss, 2013; P. Schloss, Gevers, & Wescott, 2016; P. D. Schloss et al., 2009). Briefly, DNA samples were arrayed in 96-well plates, amplified by PCR with a specific combination of indexed primers, the resulting amplicons were normalized and purified (Sequalprep, ThermoFisher), pooled and quality checked (Agilent TapeStation; qPCR with KAPA Library

Quantification kit). Libraries were then sequenced on an Illumina MiSeq using the MiSeq Reagent kit V2 (500 cycles, Illumina).

The raw sequencing files obtained from Illumina MiSeq processing were processed following Mothur standard operating procedure for 16S rRNA gene amplicons (Kozich et al., 2013). Briefly, Mothur was used to join reads into contigs, eliminate ambiguous bases and reads with quality scores below 25. Chimeras were removed using the UCHIME algorithm with the Mothur command “chimera.uchime” (Edgar, Haas, Clemente, Quince, & Knight, 2011). The final sequences were clustered into operational taxonomic units (OTUs) at 85% sequence similarity to ensure coverage above 90% (Hu, Wang, Wen, & Xia, 2012). Unique sequences were referenced and assigned taxonomy using the current Silva database (Quast et al., 2013; Yilmaz et al., 2014) for 16S rRNA sequences. Alpha diversity calculations (*e.g.* (chao1, ACE, and Simpson estimators) along with Shannon diversity function) and Beta diversity (*e.g.* similarity dendrogram, Unifrac) were obtained using Mothur at a 10% dissimilarity cutoff (Lemos, Fulthorpe, Triplett, & Roesch, 2011; Lozupone & Knight). The original reporting of Simpson index varies inversely, where here we follow suggestion to report the reciprocal Simpson’s index. Hence, a greater number represents more diversity (Peet, 1974). Statistically different distances, nonparametric t-tests and PCoA were also calculated within Mothur. Significant differences in relative abundance were measured with repeated measures analysis of variance (ANOVA). Output files were opened and graphed with SigmaPlot version 12.5, from Systat Software, Inc., San Jose California USA, [www.systatsoftware.com](http://www.systatsoftware.com).

## **2.0 Results and Discussion**

This study examined the microbiota profiles of three locations with four different commercial DNA extraction kits. We selected one freshwater lake and two wastewater environments. For

these types of environmental samples, the MO BIO and Qiagen Kits have been commonly applied (Peng et al., 2013; Vanysacker et al., 2010). These commercial kits have been examined separately for accuracy (Lemarchand et al., 2005; Vandenberg & van Oorschot, 2002; Vo, USA, Jedlicka, & University of California Department of Environmental Science, 2017) but no reports have assessed their performance with wastewater biofilm communities. With Illumina sequencing, the coverage of all samples (performed at 80% dissimilarity) was larger than 91%, except for TB3 (86%, Table 2). In lieu of subsampling, all the sequences were used in the following investigation as the number of species has shown minimal influence on microbial communities (Hu et al., 2012). As a check, we examined the effect of rarefying the dataset to the lowest sample sequence number, and found no significant difference in Simpson's evenness ( $p = 0.147$ ). The effect of sequence number was examined in detail previously (Hu et al., 2012).

**2.1 Alpha diversity.** The alpha diversity evaluates the samples by comparing taxa richness and evenness. We used multiple groups of  $\alpha$ -diversity indices (Figure 1) (Peng et al., 2013). We observed several patterns among estimators. The Simpson indices from this study were similar to previous 454-pyrosequencing datasets for membrane bioreactors and activated sludge in China (Hu et al., 2012). In general, the Simpson index reflects increased diversity in biofilms compared to wastewater planktonic communities. Statistical differences between the following pairs supports this observation. Lake samples and moving bed bioreactor biofilm (MB), moving bed bioreactor water column (Stoffels, Flikweert, Stoffels, & Kroesen) and MB, trickling filter biofilm (TB) and trickling filter water column (TW) ( $p = 0.029$ ). There was no significant difference between wastewater biofilm communities (TB and MB,  $p=0.485$ ). Ace estimators were overall lower than the few previously reported values (e.g. 1218, 1152) (Wang, Miao, Kong, & Ni, 2016; Wen, Jin, Wang, & Cai, 2015). This is expected, as this study applies a

phylum level analysis. Looking at the Shannon diversity, where a larger number also represents a more diverse community, biofilms also exhibit the expected greater diversity overall compared to water column (planktonic) samples.

**2.1.1 Relative abundance.** The OTU table generated with taxonomy differences in phylum was used to compare relative abundance between samples. Taxa present in quantities less than 2% were grouped in Other/Unknown. Percent abundance for each sample reveals environmental community differences (Figure 2). These differences are detailed for each location in the succeeding sections.

**2.1.1.1 Freshwater lake.** The lake samples were dominated by Proteobacteria (15.7%±1.4), Bacteroidetes (23.4%±14.7%), and Actinobacteria (24.6%±12.9), however the large variances were mainly driven by Method 2, which favored Bacteroidetes and underestimated Actinobacteria compared to the three other extraction methods. Pairwise comparisons among samples were significantly different ( $p < 0.05$ ), except the following two pairs: Lake2 with Lake3 ( $p = 0.366$ ), and Lake1 with Lake4 ( $p = 0.132$ ). The Beaver Lake genomic profile closely compares to previously sequenced freshwater Lake Lanier (Oh et al., 2011). Gemmatimonadetes, isolated from a freshwater lake in the Gobi Desert and recently identified as a new phototrophic bacterial phylum, was identified in the Lake and TB samples (Zeng, Feng, Medová, Dean, & Koblížek, 2014). This unique phylum identified as a polyphosphate accumulating bacteria has also been isolated from a sequential batch reactor and a fluidized bed reactor for wastewater treatment (Braga, 2015; H. Zhang et al., 2003).

**2.1.1.2 Trickling filter reactor.** The trickling filter bioreactor was sampled in two ways: biofilm growth (TB) and planktonic community in the effluent (TW). As in Figure 2, variations between the communities are identified in phylum abundance analysis. Much of the phyla in TB were

identified as Proteobacteria (37.1%) and Bacteroidetes (29.5%). Firmicutes, Verrucomicrobia, Planctomycetes, Chloroflexi and Gemmatimonadetes were identified by all 4 extraction methods in abundance percentages less than 11%. Rare phyla such as Verrucomicrobia and Chloroflexi were previously detected in influent sewage with 454 pyrosequencing and relating closely to the human microbiome (Cai, Ju, & Zhang, 2014). Previous studies have identified Fusobacteria in sequencing batch reactors (Wagner et al., 2002); this phylum was not present in TB samples, but only in TW. As an obligate anaerobe, the presence of Fusobacteria in mostly aerobic conditions may indicate that coaggregation of these bacteria with other aerobic strains present in TW. The potential for a synergistic relationship between Fusobacteria and aerobes have been witnessed with oral biofilms (Bradshaw, Marsh, Watson, & Allison, 1998) and in abscess formation on mice (Brook, Hunter, & Walker, 1984). Comparing TB extraction methods, Method 3 was significantly different than the three other methods ( $p < 0.05$ ). Further, Methods 1, 2, and 4 were not significantly different from each other ( $p > 0.05$ ). For genera that occur at percentages less than 1% in TB, Method 3 failed to extract WPS-2, Elusimicrobia, Parcubacteria, Nitrospirae, and BRC1 whereas the three other methods succeeded. In TW samples, much of the phyla were also identified as Proteobacteria (41.8%) and Bacteroidetes (40.9%). Planctomycetes were identified by all extraction methods except Method 4. Method 1 and Method 3 did not identify Chloroflexi in TW which occurred at a relative abundance of 0.01%. Further, paired RM-ANOVA tests among relative abundances were not significant, except for Methods 1 and 3 which were both significantly different from Method 4 ( $p < 0.05$ ).

**2.1.1.3 Moving bed bioreactor.** Like the trickling filter, MB and MW samples were primarily Proteobacteria (40.3%, 55.9%) and Bacteroidetes (21.3%, 28.3%), respectively. The phylum Latescibacteria were found only in the MBBR environment at abundances of 5.95% in biofilm

and 0.25% suspended. It has also been identified recently with Illumina in a full scale A2O wastewater treatment plant (Tian et al., 2015). Focusing on rare genera, Method 2 and Method 4 did not extract Spirochaetes from MW, but all four methods succeeded with MB samples. Elusimicrobia was extracted in all methods with MW, but only with Method 1 at the low abundance of 0.025% from MB samples. Elusimicrobia, obligately anaerobic, were also identified in an anaerobic bio-entrapped membrane reactor (Ng, Shi, Ong, & Ng, 2016). This phylum originates from insect intestinal tracts and is hypothesized to enhance organic removal in wastewater treatment when present (Geissinger, Herlemann, Mörschel, Maier, & Brune, 2009; Ng et al., 2016).

**2.1.2 Beta diversity.**  $\beta$ -diversity compares the differences and similarities between communities within the samples. We addressed each location separately, then examined all samples as one batch. For each location, OTU  $\beta$ -diversity analysis were executed the same from one master Mothur batch command sequence detailed in Supplementary Information. These analyses include dendrograms, Metastats, and PCoA with Pearson correlation coefficients. The dendrograms describe similarities of the samples to each other, whereas PCoA (eigenvector approach) and Metastats (non-parametric T-test) identify OTU's differentially represented between samples.

**2.1.2.1 Lake community.** Dendrogram calculations identify Methods 1 and 4 as most similar with Method 3 sharing the next most similar node (Figure S1, SI). Method 2 results were least like the other 3 methods. PCoA mapping agrees with a separation between Methods 1, 3, and 4 compared to Method 2 along component 1 (Figure S2, SI). OTU's significantly responsible for shifting Method 2 negatively along Component 1 are identified as Verrucomicrobia ( $p < 0.05$ ), Sphingobacteriia ( $p = 0.032$ ), and Planctomycetes ( $p = 0.002$ ).

**2.1.2.2 MBBR biofilm community.** MB Dendrogram calculations group Methods 1 and 4 sharing a node and Methods 2 and 3 sharing another node (Figure S3, SI). Considering a greater variability between samples, Mothur PCoA mapping calculated a third axis of variation for this environment. Comparing OTU's, T-tests showed Sphingobacteria ( $p=0.001$ ) were significantly responsible for the negative shift on axis 1 and 3 (Figure S4, SI).

**2.1.2.3 MBBR planktonic community.** The dendrogram results for MW showed methods 1 and 2 are most similar (Figure S5, SI). They share the next further node with Method 3, whereas Method 4 had the least similar results from this environment. Examining the correlation coefficients of all OTU's, we found the PCoA analysis was not significantly influenced by any one specific genera. All four methods were mapped closely together at the center of the PCoA, reflecting the overall similarity between results (Figure S6, SI).

**2.1.2.4 TF biofilm community.** In the TB environment, Methods 2 and 4 shared the same node in dendrogram mapping (Figure S7, SI). The next closest node was shared with Method 1. Unlike MW and Lake samples, Method 3 was separated farthest from the opposing methods. PCoA analysis was optimized by Mothur with 3 axes. Sphingobacteria ( $p=0.01$ ) and Gammaproteobacteria ( $p=0.029$ ) were significantly responsible for positive shifts on axis 1. OTU's identified as Flavobacteria ( $p=0.008$ ), Alphaproteobacteria ( $p=0.012$ ), and Verrucomicrobia ( $p=0.015$ ) significantly correlated with negative shifts on axis 3 (Figure S8, SI). Axis 3 accounted for the differences between Methods 1 and 2 with 3 and 4.

**2.1.2.5 TF planktonic community.** Methods 1 and 2 shared the most similarities, and connect on the next closest node with method 4. Just as with TB samples, Method 3 was also the most different from all other methods (Figure S9, SI). Significant positive shifting on axis 1 which



separates Method 3 from the others are attributed to Flavobacteria and Clostridia ( $p < 0.05$ ).

Bacterioidia ( $p < 0.05$ ) significantly influenced Method 2 negatively on axis 1.

**2.1.3 Full dataset analysis.** To understand the differences between extraction methods across all sample locations, sequences were grouped into OTUs. Hierarchical clustering of these OTUs show a clear distinction between each location and sample type, except for the Lake location which only had planktonic sample types (Figure 3) (Rambaut, 2006). By ranking similarity among samples, the distance nodes reflect a pattern of Method 3 as least consistent with Methods 1, 2, and 4. Further, Method 1 joined closest nodes with Method 4 in Lake and MB environments. Method 1 joined closest nodes with Method 2 for planktonic wastewater environments. PCoA analysis agrees with cluster analysis, in which samples diverge into four separate pairings (Figure 4).

We executed the 'unifrac.unweighted' command in Mothur which implements the unweighted UniFrac algorithm to test the phylogenetic tree (See Supplementary Information). This test indicates only the probability that they have less evolutionary structure than would be expected by chance. Only four pairings resulted with  $p > 0.05$ . These pairings were: Lake3 and Lake4, MW1 and MW2, MW2 and MW4, TW1 and TW3. Note that all eight of these samples were sampled from planktonic communities, not biofilm community. This may reflect the heterogeneity that occurs in biofilms, which might impact DNA extraction results even within the same sampling batch.

#### **2.1.4 Conclusion**

NGS results showed that there is not one superior method to apply across all sample types. Chao and ace calculators for richness showed Method 3 underestimated community richness for Lake, TB, and TW locations. Diversity comparisons reflected more diverse communities in biofilm

locations, but no discernable patterns were observed across locations when comparing Shannon or Simpson diversity indices across extraction methods. Certain rare bacteria such as Chloroflexi and Gemmatimonadetes were extracted by all methods, whereas Method 3 (Power Water Kit) did not perform as well with biofilm samples. Method 3 was least successful compared to other methods in trickling filter planktonic and biofilm community analyses. In contrast, Method 1 (Qiagen Mini Kit) and Method 4 (MO BIO PowerSoil Kit) yielded more consistent results when considering multiple sample locations and types. All four methods apply a variation of these three general steps: lysis – spin column – washing. Method 4 is the only protocol that incorporates 10 minutes of bead beating with SDS during the lysis step. The only other method incorporating bead beating during lysis, Method 3, uses a proprietary chemical lysis method with only 5 minutes of bead beating. Further, the protocol for Method 1 is the simplest in terms of steps to extraction. If one were to extrapolate these results to another sample array, these traits should be considered along with the characteristics of the samples (*e.g.*, planktonic or biofilm type samples). From these results, we conclude Qiagen Mini Kit and MO BIO PowerSoil Kit are more suitable to extract DNA from a variety of freshwater and wastewater samples for NGS analysis to improve data comparability and consistency.

### **Acknowledgements**

We would like to thank Laura Walker for NGS sample processing and Daliang Ning for analytical help. This study was supported by the University of Arkansas Provost Research Grant and the University of Arkansas Doctoral Academy Fellowship.

**Table 1** Experimental matrix detailing various sampling locations and DNA extraction methods compared among sample types.

<b>Variables</b>	<b>Type</b>	<b>Label</b>
Locations	Lakewater near potable drinking water plant	Lake
	Moving bed biofilm reactor	M
	trickling filter reactor	T
Communities sampled	water column <sup>a</sup>	W
	biofilm	B
Extraction method	Qiagen Mini Kit	1
	Qiagen Stool Kit	2
	Mobio PowerWater Kit	3
	Mobio PowerSoil Kit	4

<sup>a</sup> water column in trickling filter refers to trickling filter effluent

**Table 2** Sequencing and metagenomic final sequence totals after quality filtering, removal of chimeras, and uniqueness filtering.

<b>Group</b>	<b>Quality filtered</b>	<b>Chimeras removed</b>	<b>Coverage</b>	<b>Final Number of Sequences</b>
Lake1	5439	5407	0.962	3367
Lake2	897	892	0.947	884
Lake3	1888	1779	0.928	1386
Lake4	4153	4023	0.953	2750
MB1	3916	3843	0.977	3841
MB2	2250	2215	0.961	2214
MB3	4159	4027	0.977	3974
MB4	5728	5143	0.973	5127
MW1	3258	3116	0.968	3104
MW2	2230	2121	0.958	2118
MW3	4395	4186	0.973	4113
MW4	5120	4749	0.975	4739
TB1	2440	2381	0.93	2371
TB2	3441	3350	0.947	3322
TB3	1027	962	0.864	762
TB4	2329	2175	0.911	1676
TW1	2632	2524	0.961	2514
TW2	4246	4069	0.971	4072
TW3	1472	1353	0.942	1351
TW4	3849	3698	0.966	3698

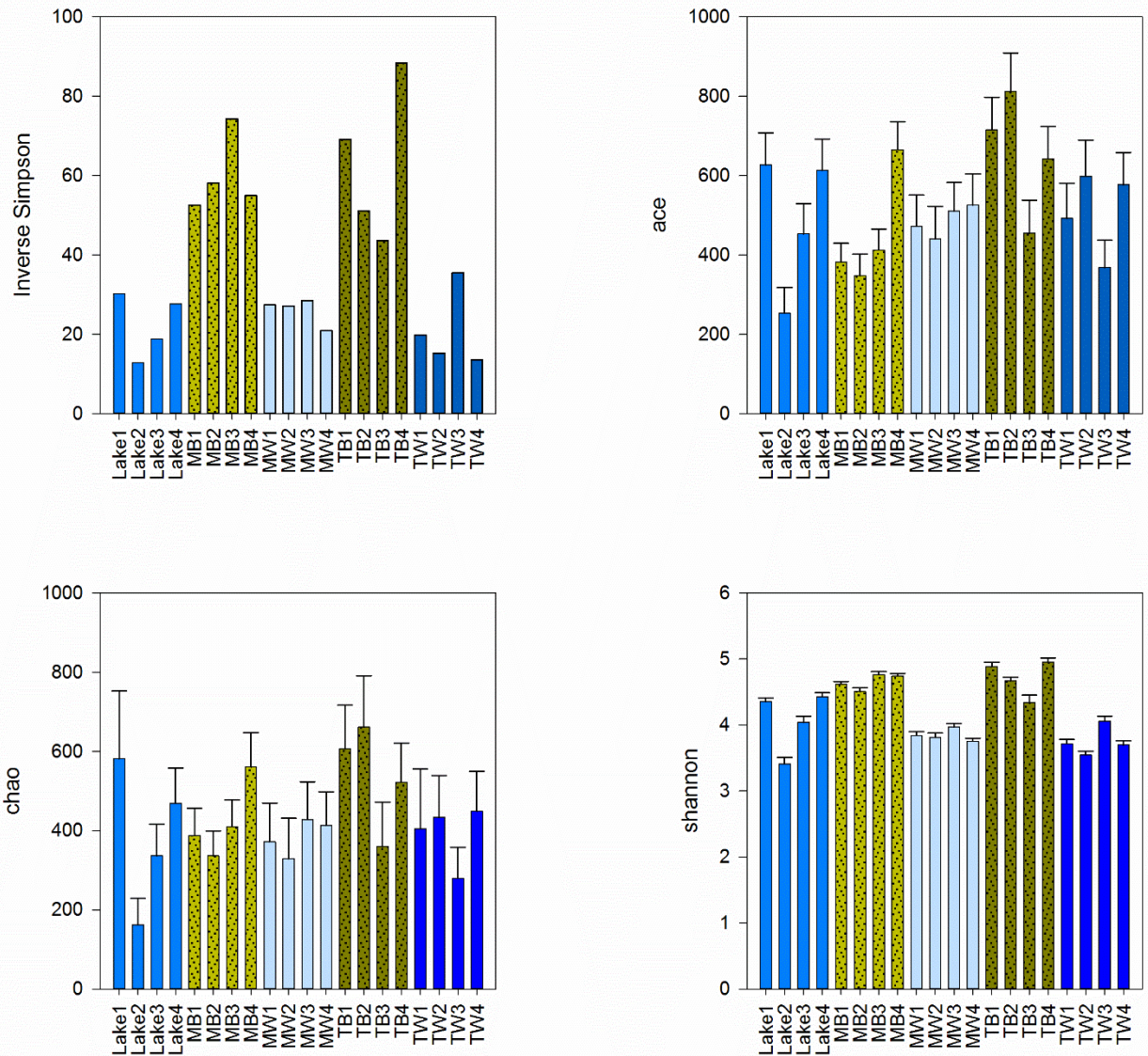


**Figure 1.** Comparison of alpha diversity indices (simpson, chao, ace, and shannon index) between all sample types and kits. Error bars represent lower and higher confidence intervals (lci, hci) calculated internally for each sequence. Confidence interval for Inverse Simpson are not visible as they are small relative to the overall value.

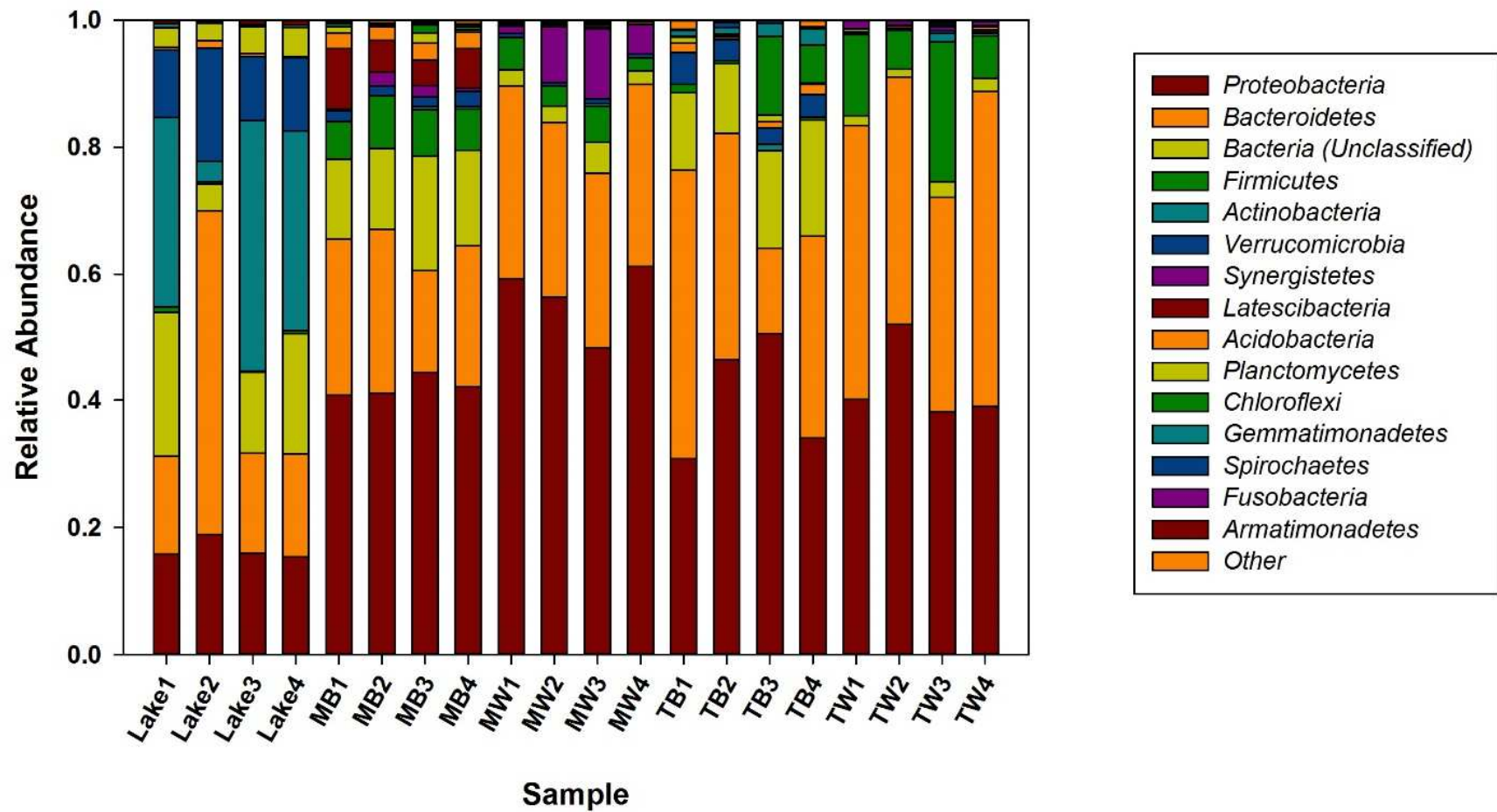


**Figure 2.** The relative abundance of microbiota variations at phylum level among location types across extraction methods.

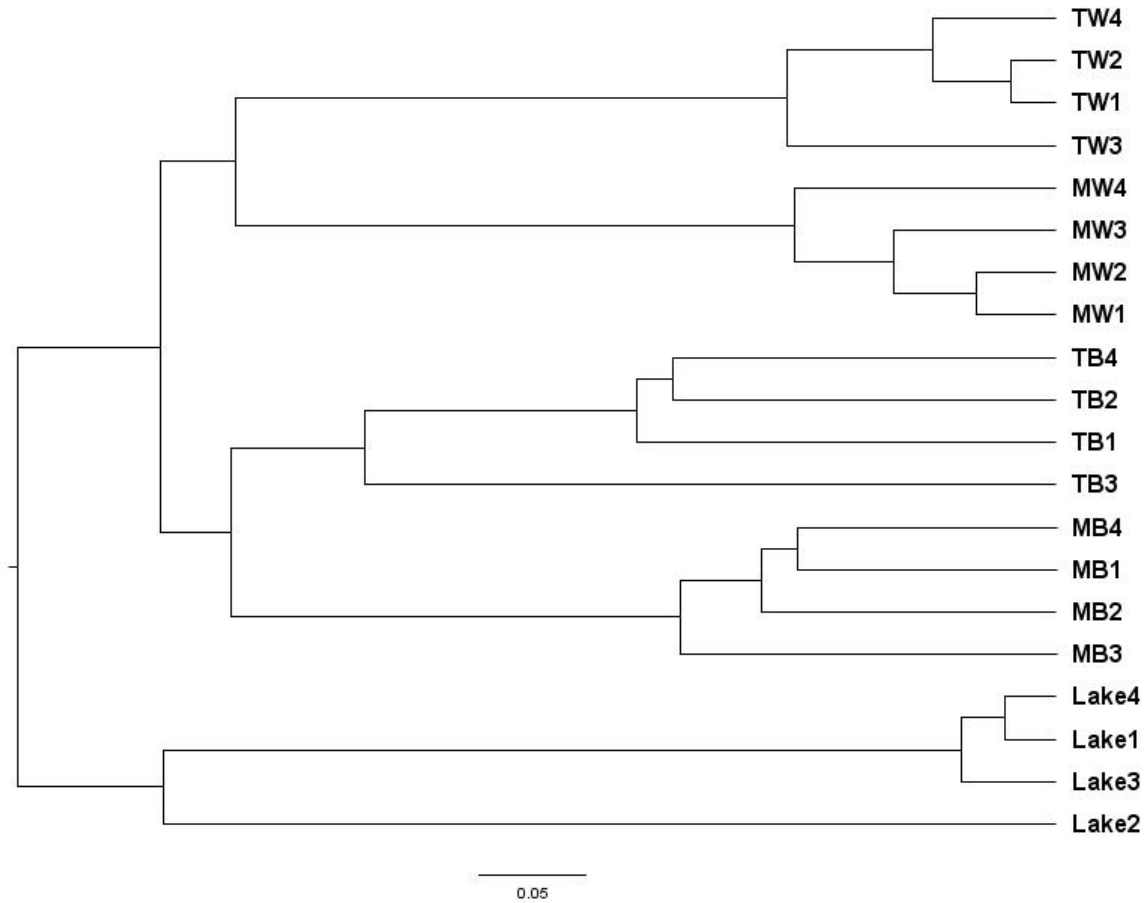


**Figure 3.** Un-weighted Pair Group Method with Arithmetic mean (UPGMA) hierarchical clustering using Euclidean similarity index to interpret the distance matrix produced from  $\beta$ -diversity analysis.

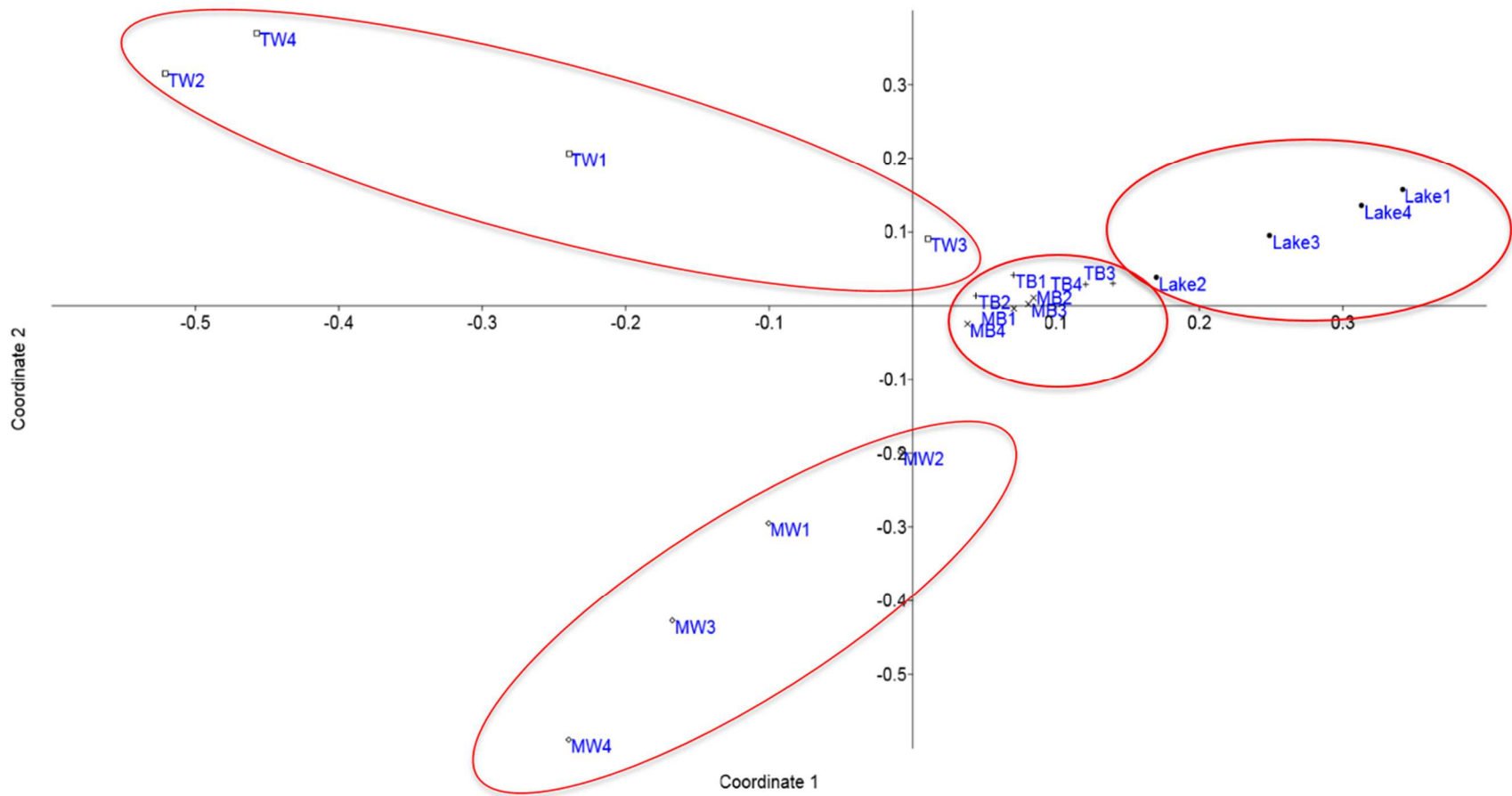


**Figure 4.** Principal components analysis (PCoA) of each community for all extraction methods where samples diverged into 4 distinct ellipses. Coordinate 1 accounts for differences occurring between water column samples (denoted W) with Lake or biofilm (denoted B) samples. Coordinate 2 accounts for the variation between TW and MW sample types.



## References

- Bradshaw, D. J., Marsh, P. D., Watson, G. K., & Allison, C. (1998). Role of *Fusobacterium nucleatum* and Coaggregation in Anaerobe Survival in Planktonic and Biofilm Oral Microbial Communities during Aeration. *Infection and Immunity*, 66(10), 4729-4732. doi:0019-9567/98/\$04.0010
- Braga, J. M., Fabricio, Silva, Edson Luiz, Amancio Varesche, Maria Bernadete. (2015). Evaluation of bacterial community from anaerobic fluidized bed reactor for the removal of linear alkylbenzene sulfonate from laundry wastewater by 454-pyrosequence. *Ecological Engineering*, 82, 231–240. doi:10.1016/j.ecoleng.2015.04.083
- Brook, I., Hunter, V., & Walker, R. I. (1984). Synergistic Effect of *Bacteroides*, *Clostridium*, *Fusobacterium*, Anaerobic Cocci, and Aerobic Bacteria on Mortality and Induction of Subcutaneous Abscesses in Mice. *The Journal of Infectious Diseases*, 149(6), 924-928. doi:10.1093/infdis/149.6.924
- Cai, L., Ju, F., & Zhang, T. (2014). Tracking human sewage microbiome in a municipal wastewater treatment plant. *Applied Microbiology and Biotechnology*, 98(7), 3317-3326.
- Carbonero, F., Nava, G. M., Benefiel, A. C., Greenberg, E., & Gaskins, H. R. (2011). Microbial DNA extraction from intestinal biopsies is improved by avoiding mechanical cell disruption. *J Microbiol Methods*, 87(1), 125-127. doi:10.1016/j.mimet.2011.07.014
- Cruaud, P., Vigneron, A., Lucchetti-Miganeh, C., Ciron, P. E., Godfroy, A., & Cambon-Bonavita, M.-A. (2014). Influence of DNA Extraction Method, 16S rRNA Targeted Hypervariable Regions, and Sample Origin on Microbial Diversity Detected by 454 Pyrosequencing in Marine Chemosynthetic Ecosystems. *Applied and environmental microbiology*, 80, 4626-4639. doi:10.1128/AEM.00592-14
- de Liphthay, J. R., Enzinger, C., Johnsen, K., Aamand, J., & Sørensen, S. J. (2004). Impact of DNA extraction method on bacterial community composition measured by denaturing gradient gel electrophoresis. *Soil Biology and Biochemistry*, 36, 1607-1614. doi:10.1016/j.soilbio.2004.03.011
- Edgar, R. C., Haas, B. J., Clemente, J. C., Quince, C., & Knight, R. (2011). UCHIME improves sensitivity and speed of chimera detection. *Bioinformatics*, 27(16), 2194-2200. doi:10.1093/bioinformatics/btr381
- Geissinger, O., Herlemann, D. P. R., Mörschel, E., Maier, U. G., & Brune, A. (2009). The Ultramicrobacterium “*Elusimicrobium minutum*” gen. nov., sp. nov., the First Cultivated

Representative of the Termite Group 1 Phylum  $\nu$  † *Appl Environ Microbiol* (Vol. 75, pp. 2831-2840).

Guo, F., & Zhang, T. (2013). Biases during DNA extraction of activated sludge samples revealed by high throughput sequencing. *Applied Microbiology and Biotechnology*, 97(10), 4607-4616.

He, X., Liu, P., Zheng, G., Chen, H., Shi, W., Cui, Y., . . . Zhang, X.-X. (2016). Evaluation of five microbial and four mitochondrial DNA markers for tracking human and pig fecal pollution in freshwater. *Scientific Reports*, 6.

Hu, M., Wang, X., Wen, X., & Xia, Y. (2012). Microbial community structures in different wastewater treatment plants as revealed by 454-pyrosequencing analysis. *Bioresource Technology*, 117, 72-79. doi:10.1016/j.biortech.2012.04.061

Huang, S.-W., Hsu, B.-M., Su, Y.-J., Ji, D.-D., Lin, W.-C., Chen, J.-L., . . . Chiu, Y.-C. (2012). Occurrence of diarrheagenic *Escherichia coli* genes in raw water of water treatment plants. *Environmental Science and Pollution Research*, 19, 2776–2783.

Knudsen, B. E., Bergmark, L., Munk, P., Lukjancenko, O., Priemé, A., Aarestrup, F. M., & Pamp, S. J. (2016). Impact of Sample Type and DNA Isolation Procedure on Genomic Inference of Microbiome Composition. *mSystems*, 1, e00095-00016. doi:10.1128/mSystems.00095-16

Kozich, J. J., Westcott, S. L., Baxter, N. T., Highlander, S. K., & Schloss, P. D. (2013). Development of a Dual-Index Sequencing Strategy and Curation Pipeline for Analyzing Amplicon Sequence Data on the MiSeq Illumina Sequencing Platform. *Applied and environmental microbiology*, 79, 5112-5120. doi:10.1128/AEM.01043-13

Krsek, M., & Wellington, E. M. (1999). Comparison of different methods for the isolation and purification of total community DNA from soil. *J Microbiol Methods*, 39(1), 1-16.

Leff, L. G., Dana, J. R., McArthur, J. V., & Shimkets, L. J. (1995). Comparison of methods of DNA extraction from stream sediments. *Applied and environmental microbiology*, 61(3), 1141-1143. doi:info:pmid/779391

Lemarchand, K., Berthiaume, F., Maynard, C., Harel, J., Payment, P., Bayardelle, P., . . . Brousseau, R. (2005). Optimization of microbial DNA extraction and purification from

- raw wastewater samples for downstream pathogen detection by microarrays. *J Microbiol Methods*, 63(2), 115-126. doi:10.1016/j.mimet.2005.02.021
- Lemos, L. N., Fulthorpe, R. R., Triplett, E. W., & Roesch, L. F. W. (2011). Rethinking microbial diversity analysis in the high throughput sequencing era. *Journal of Microbiological Methods*, 86, 42-51. doi:10.1016/j.mimet.2011.03.014
- Lozupone, C., & Knight, R. UniFrac: a New Phylogenetic Method for Comparing Microbial Communities.
- Lyautey, E., Lacoste, B., Ten-Hage, L., Rols, J.-L., & Garabetian, F. (2005). Analysis of bacterial diversity in river biofilms using 16S rDNA PCR-DGGE: methodological settings and fingerprints interpretation. *Water Research*, 39, 380-388. doi:10.1016/j.watres.2004.09.025
- Ma, Q., Qu, Y., Shen, W., Zhang, Z., Wang, J., Liu, Z., . . . Zhou, J. (2015). Bacterial community compositions of coking wastewater treatment plants in steel industry revealed by Illumina high-throughput sequencing. *Bioresource Technology*, 179, 436-443. doi:10.1016/j.biortech.2014.12.041
- Malki, K., Bruder, K., & Putonti, C. (2015). Survey of microbial populations within Lake Michigan nearshore waters at two Chicago public beaches. *Data in brief*, 5, 556-559.
- Manzari, C., Fosso, B., Marzano, M., Annese, A., Caprioli, R., D'Erchia, A. M., . . . Santamaria, M. (2015). The influence of invasive jellyfish blooms on the aquatic microbiome in a coastal lagoon (Varano, SE Italy) detected by an Illumina-based deep sequencing strategy. *Biological Invasions*, 17(3), 923-940.
- McOrist, A. L., Jackson, M., & Bird, A. R. (2002). A comparison of five methods for extraction of bacterial DNA from human faecal samples. *Journal of Microbiological Methods*, 50(2), 131-139.
- Miller, D. N., Bryant, J. E., Madsen, E. L., & Ghiorse, W. C. (1999). Evaluation and Optimization of DNA Extraction and Purification Procedures for Soil and Sediment Samples. *Applied and environmental microbiology*, 65(11), 4715-4724. doi:info:pmid/10543776
- Mumy, K. L., & Findlay, R. H. (2004). Convenient determination of DNA extraction efficiency using an external DNA recovery standard and quantitative-competitive PCR. *Journal of Microbiological Methods*, 57(2), 259-268.

- Ng, K. K., Shi, X., Ong, S. L., & Ng, H. Y. (2016). Pyrosequencing reveals microbial community profile in anaerobic bio-entrapped membrane reactor for pharmaceutical wastewater treatment. *Bioresource Technology*, 200, 1076-1079.
- Oh, S., Caro-Quintero, A., Tsementzi, D., DeLeon-Rodriguez, N., Luo, C., Poretsky, R., & Konstantinidis, K. T. (2011). Metagenomic Insights into the Evolution, Function, and Complexity of the Planktonic Microbial Community of Lake Lanier, a Temperate Freshwater Ecosystem. *Applied and environmental microbiology*, 77(17). Retrieved from <http://aem.asm.org/content/77/17/6000.full> doi:10.1128/AEM.00107-11
- Peet, R. K. (1974). The Measurement of Species Diversity. *Annual Review of Ecology and Systematics*, 5, 285-307.
- Peng, X., Yu, K.-Q., Deng, G.-H., Jiang, Y.-X., Wang, Y., Zhang, G.-X., & Zhou, H.-W. (2013). Comparison of direct boiling method with commercial kits for extracting fecal microbiome DNA by Illumina sequencing of 16S rRNA tags. *Journal of Microbiological Methods*, 95, 455-462. doi:10.1016/j.mimet.2013.07.015
- Quast, C., Pruesse, E., Yilmaz, P., Gerken, J., Schweer, T., Yarza, P., . . . Glöckner, F. O. (2013). The SILVA ribosomal RNA gene database project: improved data processing and web-based tools. doi:10.1093/nar/gks1219
- Rambaut, A. (2006). FigTree v1.4.3. Retrieved from <http://tree.bio.ed.ac.uk/software/figtree/>
- Schloss, P., Gevers, D., & Wescott, S. (2016). Reducing the Effects of PCR Amplification and Sequencing Artifacts on 16S rRNA-Based Studies. *PLoS ONE*. doi:10.1371/journal.pone.0027310
- Schloss, P. D., Westcott, S. L., Ryabin, T., Hall, J. R., Hartmann, M., Hollister, E. B., . . . Robinson, C. J. (2009). Introducing mothur: open-source, platform-independent, community-supported software for describing and comparing microbial communities. *Applied and environmental microbiology*, 75(23), 7537-7541.
- Stoffels, E., Flikweert, A., Stoffels, W., & Kroesen, G. (2002). Plasma needle: a non-destructive atmospheric plasma source for fine surface treatment of (bio) materials. *Plasma Sources Science and Technology*, 11(4), 383.
- Tian, M., Zhao, F., Shen, X., Chu, K., Wang, J., Chen, S., . . . Liu, H. (2015). The first metagenome of activated sludge from full-scale anaerobic/anoxic/oxic (A2O) nitrogen

- and phosphorus removal reactor using Illumina sequencing. *Journal of Environmental Sciences*, 35, 181-190.
- van Dijk, E. L., Auger, H., Jaszczyszyn, Y., & Thermes, C. (2014). Ten years of next-generation sequencing technology. *Trends in genetics*, 30(9), 418-426.
- Vandenberg, N., & van Oorschot, R. A. (2002). Extraction of human nuclear DNA from feces samples using the QIAamp DNA Stool Mini Kit. *J Forensic Sci*, 47(5), 993-995.
- Vanysacker, L., Declerck, S. A., J, Hellemans, B., De Meester, L., Vankelecom, I., & Declerck, P. (2010). Bacterial community analysis of activated sludge: an evaluation of four commonly used DNA extraction methods. *Applied Microbiology and Biotechnology*, 88, 299-307. doi:10.1007/s00253-010-2770-5
- Vo, A. T. E., USA, U. o. C. M. o. V. Z. a. D. o. I. B. B. C., Jedlicka, J. A., & University of California Department of Environmental Science, P., and Management Berkeley CA USA. (2017). Protocols for metagenomic DNA extraction and Illumina amplicon library preparation for faecal and swab samples. *Molecular Ecology Resources*, 14(6), 1183-1197. doi:10.1111/1755-0998.12269
- Wagner, M., Loy, A., Nogueira, R., Purkhold, U., Lee, N., & Daims, H. (2002). Microbial community composition and function in wastewater treatment plants. *Antonie van Leeuwenhoek*, 81(1-4), 665-680.
- Wang, Z.-B., Miao, M.-S., Kong, Q., & Ni, S.-Q. (2016). Evaluation of microbial diversity of activated sludge in a municipal wastewater treatment plant of northern China by high-throughput sequencing technology. *Desalination and Water Treatment*, 57(50). doi:10.1080/19443994.2015.1137232
- Wen, Y., Jin, Y., Wang, J., & Cai, L. (2015). MiSeq sequencing analysis of bacterial community structures in wastewater treatment plants. *Polish Journal of Environmental Studies*, 24(4).
- Xu, D., Liu, S., Chen, Q., & Ni, J. (2017). Microbial community compositions in different functional zones of Carrousel oxidation ditch system for domestic wastewater treatment | SpringerLink. *AMB Express*, 7(40). doi:10.1186/s13568-017-0336-y
- Yilmaz, P., Parfrey, L. W., Yarza, P., Gerken, J., Pruesse, E., Quast, C., . . . Glöckner, F. O. (2014). The SILVA and “All-species Living Tree Project (LTP)” taxonomic frameworks. doi:10.1093/nar/gkt1209

- Yu, Y., Wu, L., & Chang, A. C. (2013). Seasonal variation of endocrine disrupting compounds, pharmaceuticals and personal care products in wastewater treatment plants. *Science of the total environment*, 442, 310-316. doi:10.1016/j.scitotenv.2012.10.001
- Zeng, Y., Feng, F., Medová, H., Dean, J., & Koblížek, M. (2014). Functional type 2 photosynthetic reaction centers found in the rare bacterial phylum Gemmatimonadetes. *PNAS*, 111(21). doi:10.1073/pnas.1400295111
- Zhang, H., Sekiguchi, Y., Hanada, S., Hugenholtz, P., Kim, H., Kamagata, Y., & Nakamura, K. (2003). *Gemmatimonas aurantiaca* gen. nov., sp. nov., a Gram-negative, aerobic, polyphosphate-accumulating micro-organism, the first cultured representative of the new bacterial phylum Gemmatimonadetes phyl. nov. *International Journal of Systemic and Evolutionary Microbiology*, 53, 1155-1163. doi:doi:10.1099/ijs.0.02520-0
- Zhang, Y., Peng, H., Huang, W., Zhou, Y., & Yan, D. (2008). Facile preparation and characterization of highly antimicrobial colloid Ag or Au nanoparticles. *Journal of Colloid and Interface Science*, 325, 371-376. doi:10.1016/j.jcis.2008.05.063
- Zheng, L., Gao, N., & Deng, Y. (2012). Evaluation of DNA extraction methods for the analysis of microbial community in biological activated carbon. *Environmental Technology*, 33(4), 437-444.

## **Appendix 1.**

Supplementary Information for

“Assessing Impacts of DNA Extraction Methods on Next Generation Sequencing of Water and  
Wastewater Samples.”

## Mothur Batch Commands

```
#Batch filenames were changed for each location
#Below is one example.
make.contigs(file=comparison_MW.files, processors=8)
screen.seqs(fasta=current, group=current, maxambig=0, maxlength=275)
unique.seqs()
count.seqs(name=current, group=current)
align.seqs(fasta=current, reference=silva.v4.fasta)
screen.seqs(fasta=current, count=current, start=1968, end=11550, maxhomop=8)
filter.seqs(fasta=current, vertical=T, trump=.)
unique.seqs(fasta=current, count=current)
pre.cluster(fasta=current, count=current, diffs=2)
chimera.uchime(fasta=current, count=current, dereplicate=t)
remove.seqs(fasta=current, accnos=current)
classify.seqs(fasta=current, count=current, reference=trainset14_032015.pds.fasta,
taxonomy=trainset14_032015.pds.tax, cutoff=80)
remove.lineage(fasta=current, count=current, taxonomy=current, taxon=Chloroplast-
Mitochondria-unknown-Archaea-Eukaryota)
cluster.split(fasta=current, count=current, taxonomy=current, splitmethod=classify, taxlevel=4,
cutoff=0.15)
make.shared(list=current, count=current, label=0.07)
classify.otu(list=current, count=current, taxonomy=current, label=0.07)
phylotype(taxonomy=current)
make.shared(list=current, count=current, label=0.07)
classify.otu(list=current, count=current, taxonomy=current, label=0.07)
#do each by hand
dist.seqs(fasta=current, output=lt, processors=8)
clearcut(phylip=current)
system(rename
comparison_MW.trim.contigs.good.unique.good.filter.unique.precluster.pick.pick.an.unique_list.
shared comparison_MW.an.shared)
count.groups(shared=comparison_MW.an.shared)
summary.single(shared=current, calc=nseqs-coverage)
dist.shared(shared=current, calc=thetayc-jclass)
tree.shared(phylip=current)
pcoa(phylip=current)
nmds(phylip=current)
amova(phylip=current, design=kit_types_MW.design)
corr.axes(axes=comparison_MW.an.thetayc.0.07.lt.pcoa.axes, shared=current, numaxes=3)
metastats(shared=current, design=current)
```



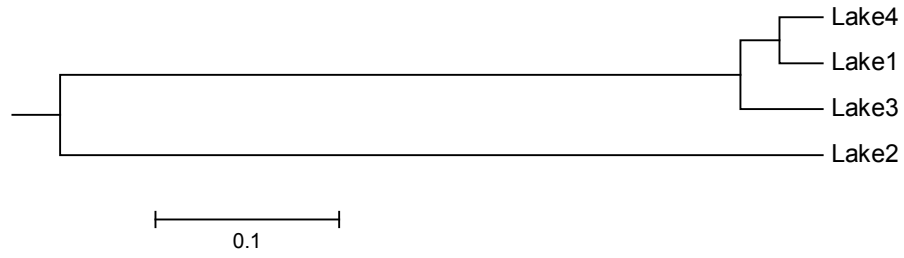


**Figure S1.** Similarity tree at 0.07 distance for freshwater Lake sample set.

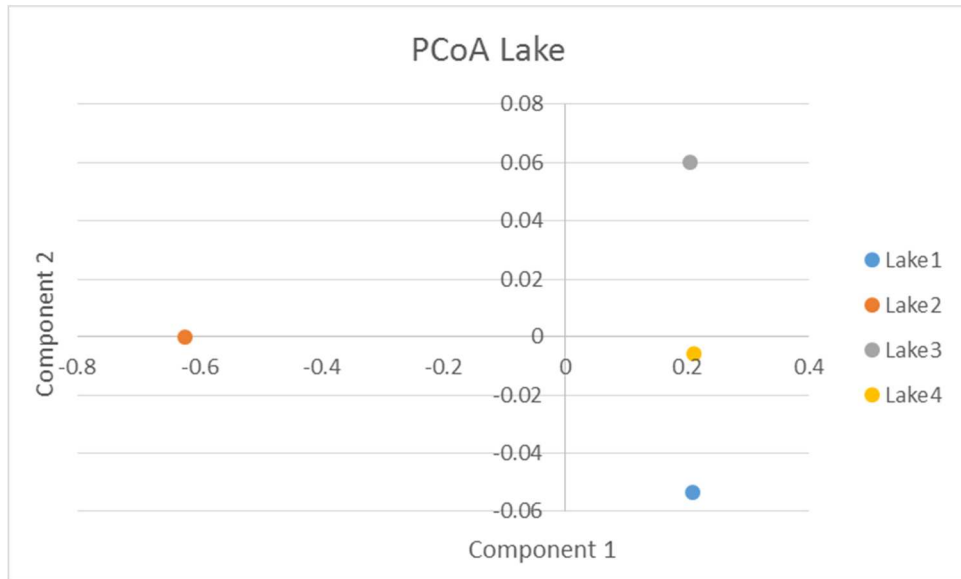


**Figure S2.** PCoA analysis of Lake samples relating each method through eigenvectors (Pearson method).

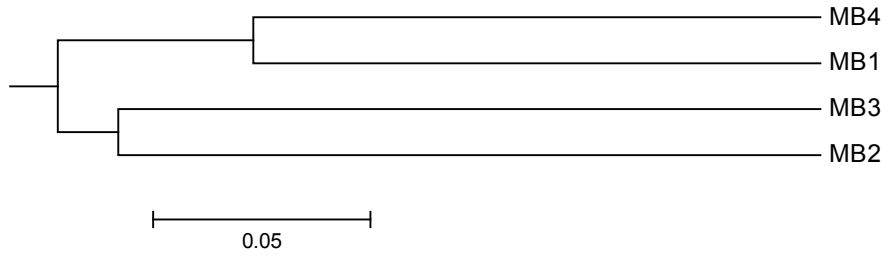


**Figure S3.** Similarity tree at 0.07 distance for MBBR wastewater biofilm environment.

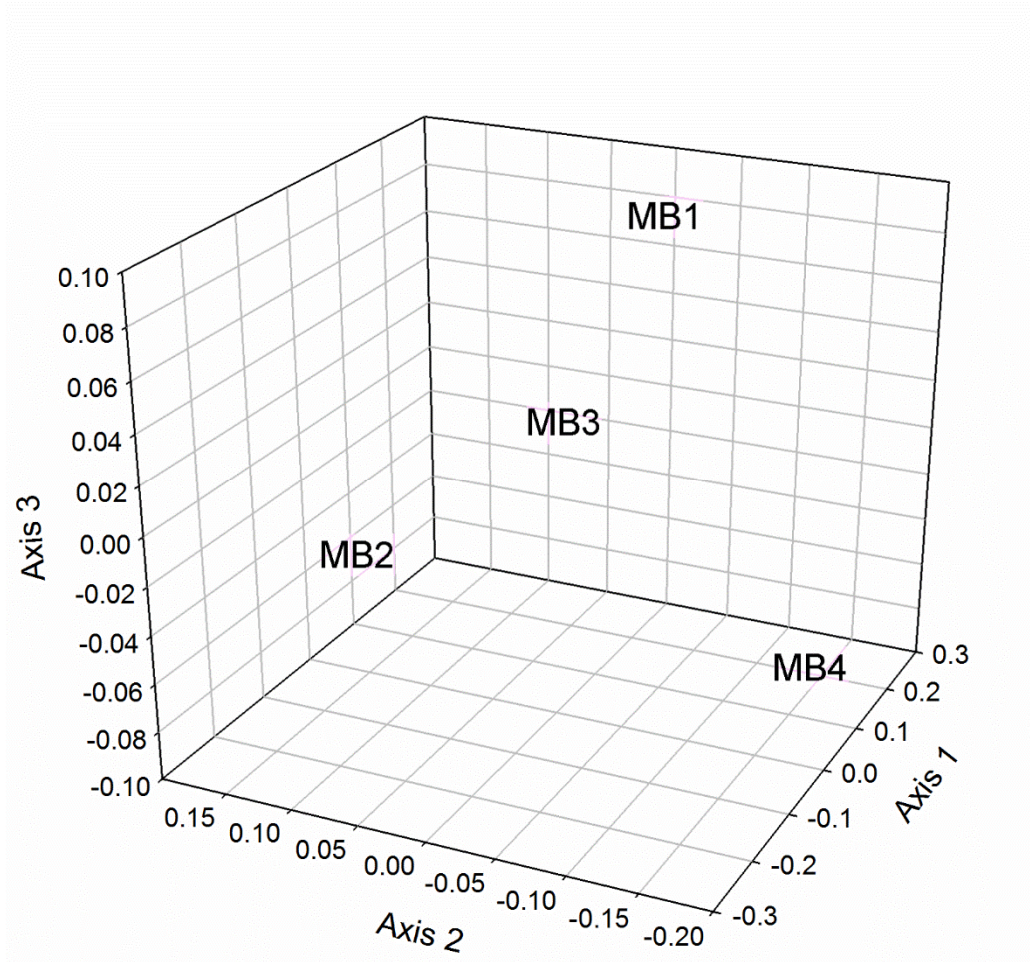


**Figure S4.** 3D PCoA analysis of MBBR biofilm samples relating each method through eigenvectors (Pearson method).

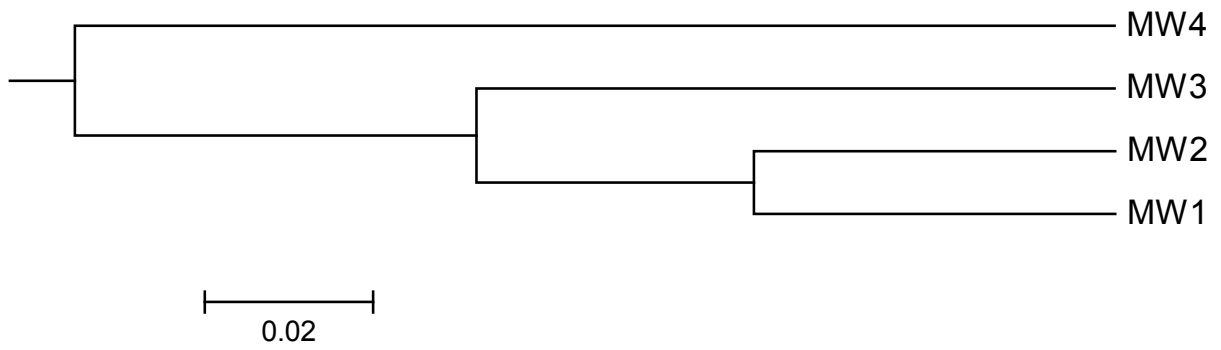


**Figure S5.** Similarity tree at 0.07 distance for MBBR suspended environment.

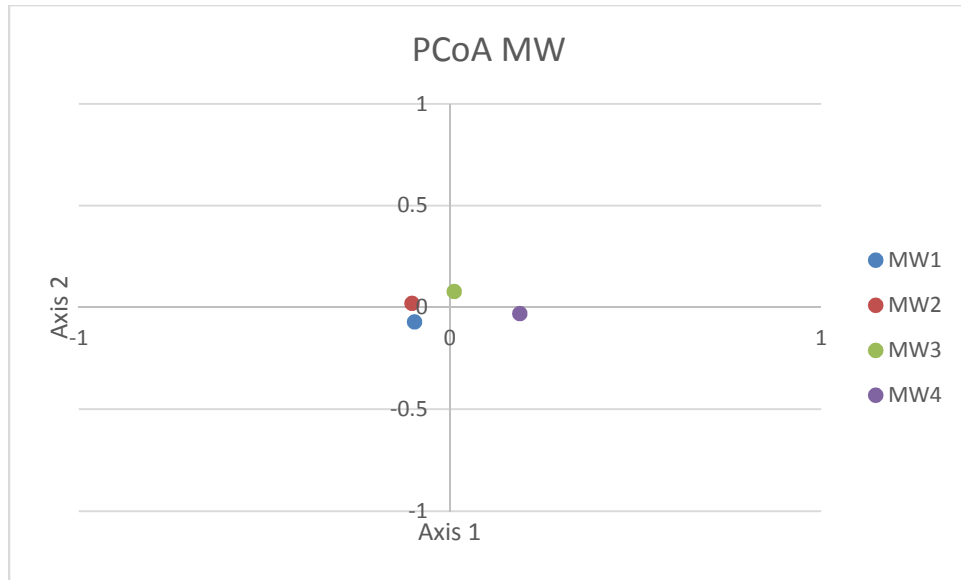


**Figure S6.** PCoA analysis of MW samples relating each method through eigenvectors (Pearson method).

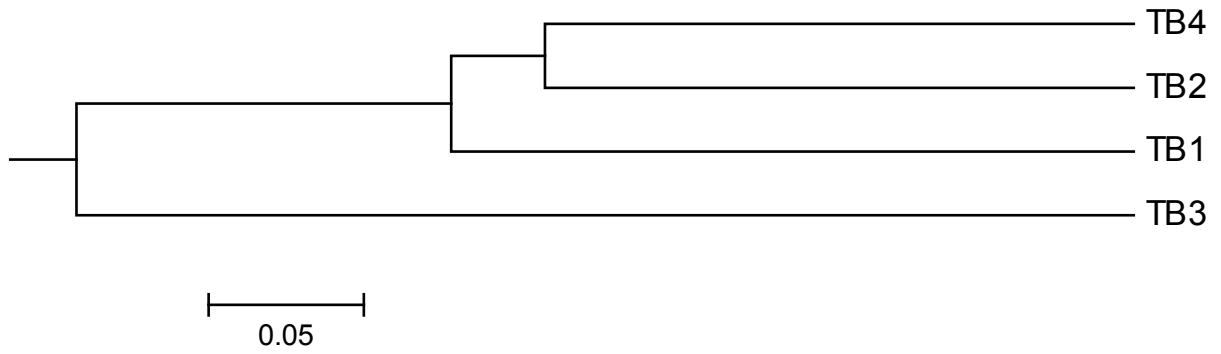


**Figure S7.** Similarity tree at 0.07 distance for TB environment.

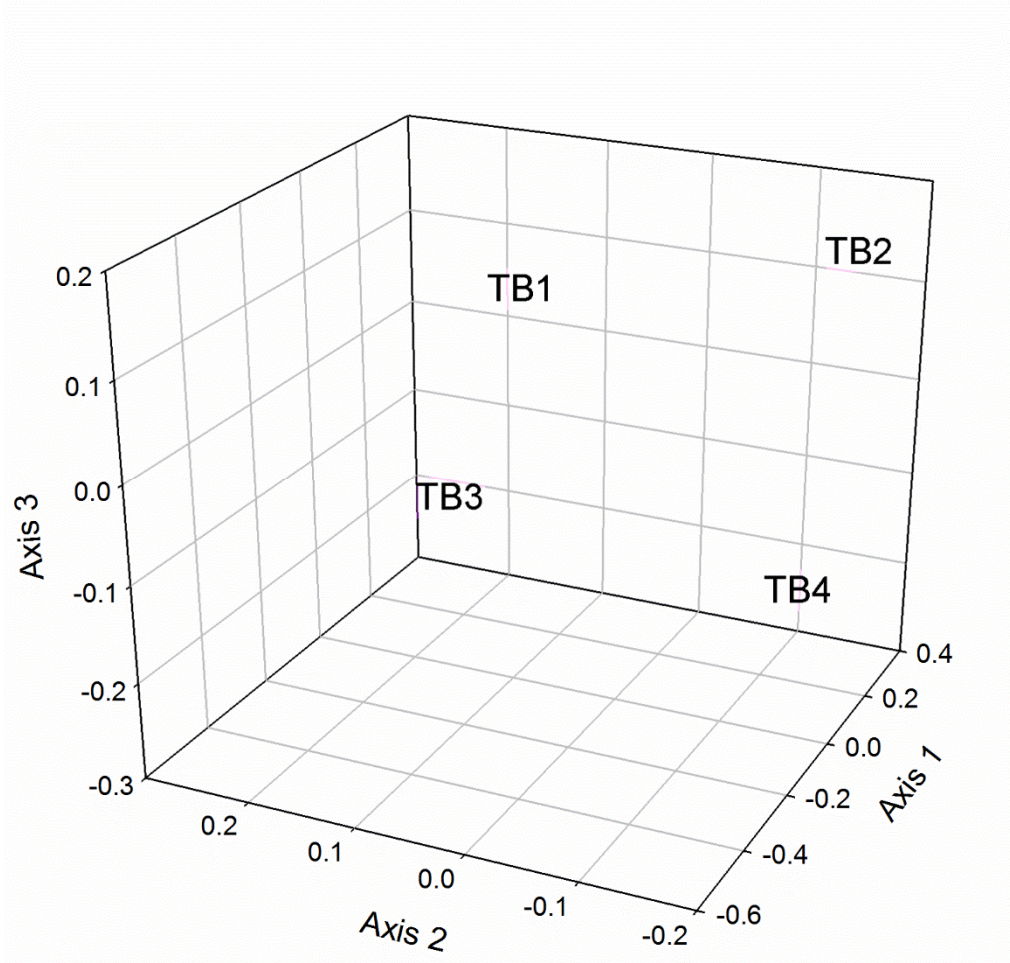


**Figure S8.** PCoA analysis of TB samples relating each method through eigenvectors (Pearson method).



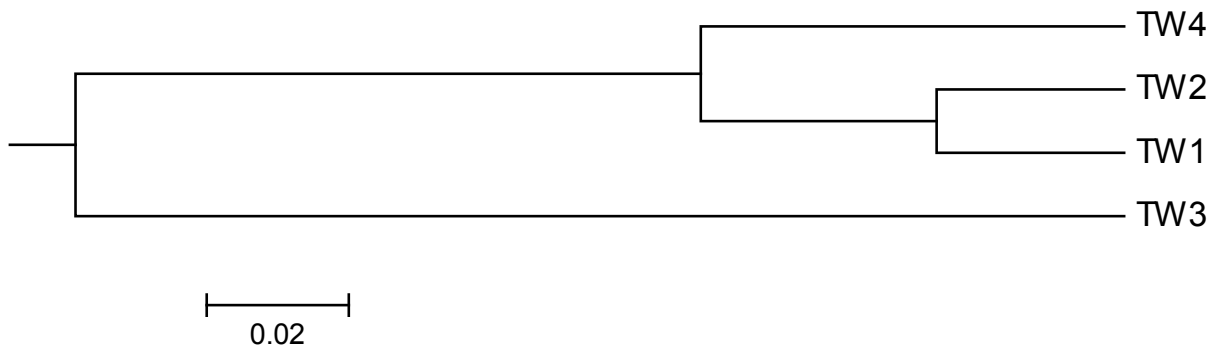


**Figure S9.** Similarity tree at 0.07 distance for TW environment.

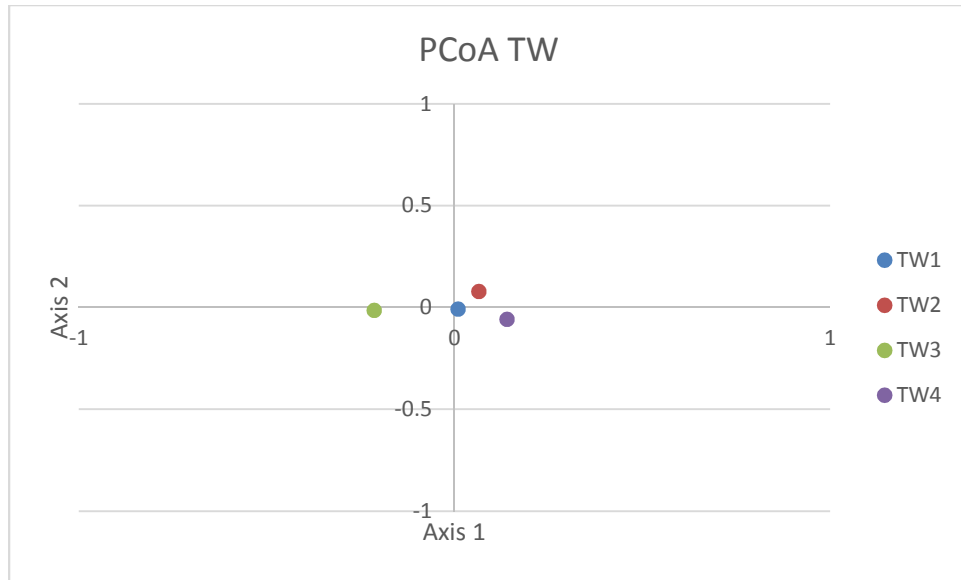


**Figure S10.** PCoA analysis of TW samples relating each method through eigenvectors (Pearson method).

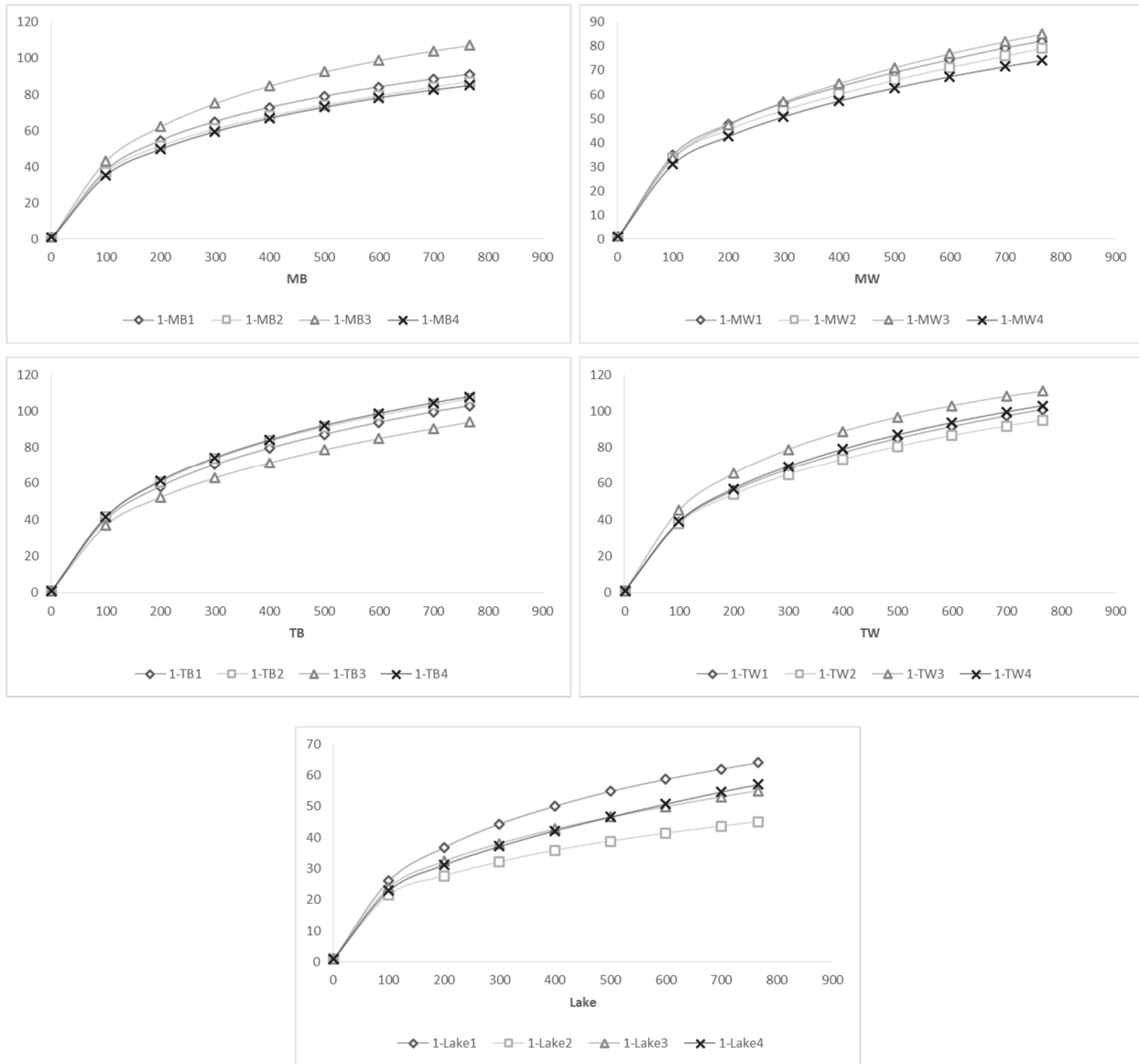


**Figure S11.** Rarefaction curves for sub-sampled dataset (n=762) at each sampling location and extraction methods.

**Table S1. LIBSHUFF analysis output**

<b>Groups</b>	<b>UWScore</b>	<b>UWSig</b>
Lake1-Lake2	0.882849	<0.0010
Lake1-Lake3	0.803128	0.003
Lake2-Lake3	0.839077	<0.0010
Lake1-Lake4	0.784939	=0.001
Lake2-Lake4	0.881001	<0.0010
Lake3-Lake4	0.7872	=0.056
Lake1-MB1	0.966836	<0.0010
Lake2-MB1	0.973201	<0.0010
Lake3-MB1	0.968862	<0.0010
Lake4-MB1	0.967906	<0.0010
Lake1-MB2	0.963085	<0.0010
Lake2-MB2	0.965103	<0.0010
Lake3-MB2	0.96551	<0.0010
Lake4-MB2	0.968388	<0.0010
MB1-MB2	0.780993	=0.003
Lake1-MB3	0.96421	<0.0010
Lake2-MB3	0.974516	<0.0010
Lake3-MB3	0.968543	<0.0010
Lake4-MB3	0.967596	<0.0010
MB1-MB3	0.796001	<0.0010
MB2-MB3	0.791046	<0.0010
Lake1-MB4	0.969331	<0.0010

**Table 1 (cont.)**

<b>Groups</b>	<b>UWScore</b>	<b>UWSig</b>
Lake2-MB4	0.979289	<0.0010
Lake3-MB4	0.975388	<0.0010
Lake4-MB4	0.972375	<0.0010
MB1-MB4	0.802661	<0.0010
MB2-MB4	0.815797	<0.0010
MB3-MB4	0.802	<0.0010
Lake1-MW1	0.963499	<0.0010
Lake2-MW1	0.968	<0.0010
Lake3-MW1	0.966885	<0.0010
Lake4-MW1	0.967436	<0.0010
MB1-MW1	0.861029	<0.0010
MB2-MW1	0.847464	<0.0010
MB3-MW1	0.874304	<0.0010
MB4-MW1	0.876381	<0.0010
Lake1-MW2	0.967812	<0.0010
Lake2-MW2	0.966925	<0.0010
Lake3-MW2	0.970046	<0.0010
Lake4-MW2	0.972213	<0.0010
MB1-MW2	0.861164	<0.0010
MB2-MW2	0.839499	<0.0010
MB3-MW2	0.868426	<0.0010
MB4-MW2	0.880447	<0.0010
MW1-MW2	0.799498	=0.079

**Table 1 (cont.)**

<b>Groups</b>	<b>UWScore</b>	<b>UWSig</b>
Lake1-MW3	0.96669	<0.0010
Lake2-MW3	0.970356	<0.0010
Lake3-MW3	0.969084	<0.0010
Lake4-MW3	0.968806	<0.0010
MB1-MW3	0.868219	<0.0010
MB2-MW3	0.861451	<0.0010
MB3-MW3	0.865035	<0.0010
MB4-MW3	0.869564	<0.0010
MW1-MW3	0.817114	<0.0010
MW2-MW3	0.811604	=0.009
Lake1-MW4	0.968701	<0.0010
Lake2-MW4	0.9729	<0.0010
Lake3-MW4	0.972635	<0.0010
Lake4-MW4	0.971241	<0.0010
MB1-MW4	0.862822	<0.0010
MB2-MW4	0.858542	<0.0010
MB3-MW4	0.869877	<0.0010
MB4-MW4	0.864545	<0.0010
MW1-MW4	0.823932	<0.0010
MW2-MW4	0.819914	=0.096
MW3-MW4	0.81785	<0.0010
Lake1-TB1	0.944111	<0.0010
Lake2-TB1	0.956309	<0.0010

**Table 1 (cont.)**

<b>Groups</b>	<b>UWScore</b>	<b>UWSig</b>
Lake3-TB1	0.950495	<0.0010
Lake4-TB1	0.948412	<0.0010
MB1-TB1	0.90527	<0.0010
MB2-TB1	0.901888	<0.0010
MB3-TB1	0.913945	<0.0010
MB4-TB1	0.920112	<0.0010
MW1-TB1	0.915322	<0.0010
MW2-TB1	0.91934	<0.0010
MW3-TB1	0.925446	<0.0010
MW4-TB1	0.92228	<0.0010
Lake1-TB2	0.945126	<0.0010
Lake2-TB2	0.95708	<0.0010
Lake3-TB2	0.950912	<0.0010
Lake4-TB2	0.95028	<0.0010
MB1-TB2	0.928231	<0.0010
MB2-TB2	0.920687	<0.0010
MB3-TB2	0.9302	<0.0010
MB4-TB2	0.934584	<0.0010
MW1-TB2	0.929473	<0.0010
MW2-TB2	0.932045	<0.0010
MW3-TB2	0.934359	<0.0010
MW4-TB2	0.936242	<0.0010
TB1-TB2	0.8061	<0.0010

**Table 1 (cont.)**

<b>Groups</b>	<b>UWScore</b>	<b>UWSig</b>
Lake1-TB3	0.942537	<0.0010
Lake2-TB3	0.934891	<0.0010
Lake3-TB3	0.931568	<0.0010
Lake4-TB3	0.943624	<0.0010
MB1-TB3	0.935269	<0.0010
MB2-TB3	0.924485	<0.0010
MB3-TB3	0.938625	<0.0010
MB4-TB3	0.947063	<0.0010
MW1-TB3	0.935764	<0.0010
MW2-TB3	0.940267	<0.0010
MW3-TB3	0.946625	<0.0010
MW4-TB3	0.947057	<0.0010
TB1-TB3	0.852045	<0.0010
TB2-TB3	0.852322	<0.0010
Lake1-TB4	0.947656	<0.0010
Lake2-TB4	0.951862	<0.0010
Lake3-TB4	0.944151	<0.0010
Lake4-TB4	0.947561	<0.0010
MB1-TB4	0.936925	<0.0010
MB2-TB4	0.930609	<0.0010
MB3-TB4	0.938345	<0.0010
MB4-TB4	0.94347	<0.0010
MW1-TB4	0.94058	<0.0010



**Table 1 (cont.)**

<b>Groups</b>	<b>UWScore</b>	<b>UWSig</b>
MW2-TB4	0.943002	<0.0010
MW3-TB4	0.944933	<0.0010
MW4-TB4	0.944624	<0.0010
TB1-TB4	0.824917	<0.0010
TB2-TB4	0.801685	<0.0010
TB3-TB4	0.819623	=0.002
Lake1-TW1	0.962323	<0.0010
Lake2-TW1	0.969547	<0.0010
Lake3-TW1	0.964698	<0.0010
Lake4-TW1	0.968684	<0.0010
MB1-TW1	0.92733	<0.0010
MB2-TW1	0.921446	<0.0010
MB3-TW1	0.93773	<0.0010
MB4-TW1	0.938239	<0.0010
MW1-TW1	0.895174	<0.0010
MW2-TW1	0.900058	<0.0010
MW3-TW1	0.906152	<0.0010
MW4-TW1	0.917877	<0.0010
TB1-TW1	0.916309	<0.0010
TB2-TW1	0.922954	<0.0010
TB3-TW1	0.937149	<0.0010
TB4-TW1	0.937612	<0.0010
Lake1-TW2	0.962151	<0.0010

**Table 1 (cont.)**

<b>Groups</b>	<b>UWScore</b>	<b>UWSig</b>
Lake2-TW2	0.969539	<0.0010
Lake3-TW2	0.969329	<0.0010
Lake4-TW2	0.969615	<0.0010
MB1-TW2	0.918755	<0.0010
MB2-TW2	0.905512	<0.0010
MB3-TW2	0.925377	<0.0010
MB4-TW2	0.930426	<0.0010
MW1-TW2	0.892466	<0.0010
MW2-TW2	0.897847	<0.0010
MW3-TW2	0.902962	<0.0010
MW4-TW2	0.904454	<0.0010
TB1-TW2	0.909661	<0.0010
TB2-TW2	0.912999	<0.0010
TB3-TW2	0.942827	<0.0010
TB4-TW2	0.936307	<0.0010
TW1-TW2	0.821971	=0.009
Lake1-TW3	0.964046	<0.0010
Lake2-TW3	0.973613	<0.0010
Lake3-TW3	0.968652	<0.0010
Lake4-TW3	0.971401	<0.0010
MB1-TW3	0.928585	<0.0010
MB2-TW3	0.91458	<0.0010
MB3-TW3	0.936196	<0.0010

**Table 1 (cont.)**

<b>Groups</b>	<b>UWScore</b>	<b>UWSig</b>
MB4-TW3	0.937712	<0.0010
MW1-TW3	0.896557	<0.0010
MW2-TW3	0.896987	<0.0010
MW3-TW3	0.905875	<0.0010
MW4-TW3	0.917902	<0.0010
TB1-TW3	0.92362	<0.0010
TB2-TW3	0.928813	<0.0010
TB3-TW3	0.942914	<0.0010
TB4-TW3	0.939571	<0.0010
TW1-TW3	0.811358	=0.055
TW2-TW3	0.832218	=0.004
Lake1-TW4	0.962377	<0.0010
Lake2-TW4	0.973633	<0.0010
Lake3-TW4	0.967875	<0.0010
Lake4-TW4	0.966299	<0.0010
MB1-TW4	0.911986	<0.0010
MB2-TW4	0.906988	<0.0010
MB3-TW4	0.920195	<0.0010
MB4-TW4	0.921161	<0.0010
MW1-TW4	0.894304	<0.0010
MW2-TW4	0.899467	<0.0010
MW3-TW4	0.895728	<0.0010
MW4-TW4	0.905915	<0.0010

**Table 1 (cont.)**

<b>Groups</b>	<b>UWScore</b>	<b>UWSig</b>
TB1-TW4	0.901796	<0.0010
TB2-TW4	0.911734	<0.0010
TB3-TW4	0.938632	<0.0010
TB4-TW4	0.931207	<0.0010
TW1-TW4	0.826844	<0.0010
TW2-TW4	0.814183	=0.004
TW3-TW4	0.833921	=0.004

## Chapter 4

### Bioaccumulation of silver nanoparticles in model wastewater biofilms

## Abstract

This study explored the capacity for wastewater biofilm to accumulate and release silver nanoparticles (Ag-NPs). To test these two facets, a non-limiting synthetic wastewater (SW) was used as a feed into two reactor types: CDC biofilm reactor (CBR) and a flow cell. Using typical wastewater bacteria (*Acinetobacter calcoaceticus*, *Comamonas testosteroni*, and *Delftia acidovorans*) as a model consortium, biofilm functionality, structure, and viability were monitored with and without Ag-NPs in the CBR influent. At a design concentration of 200 ppb, no significant change in viability or functionality were observed. However, significant cell stress was detected with the generation of excess reactive oxygen species. Further, we observed a decrease in chloride ion after the addition of Ag-NPs to SW. Most likely a chemical transformation to silver salts occurred between Ag-NPs and SW. To measure accumulation, the flow cell experiments were conducted for each species singly, in dual combinations, and mixed. The single species biofilms accumulated the least amount of silver, approximately  $0.01 \text{ ng mm}^{-2}$ . The dual species, *A. calcoaceticus* and *D. acidovorans* accumulated  $0.43 \text{ ng mm}^{-2}$ , the highest measured concentration of these combinations. This combination was then further tested for the possible release of silver. After Ag-NP exposure, influent feed was switched to sterile SW. Then, biofilm detachment or sloughing was calculated from effluent cell counts, while total silver concentrations in influent and effluent were measured with inductively coupled plasma mass spectrometry (ICP-MS). While effluent cell counts did not significantly change ( $p>0.05$ ), the measured silver attached to the biofilm significantly decreased ( $p=0.04$ ). This shows that small concentrations of silver attached to biofilm, and subsequently release. Given the dynamic nature of living biofilms, this study shows that wastewater biofilms do play a small role in silver

transport in wastewater networks. Further, this work adds to the fundamental understanding of biofilm – NP interactions in wastewater environments.

## 1. Introduction

Anthropogenic influences can negatively impact long term water quality of community water resources (*i.e.* reservoirs) that serve for drinking water and recreation. When wastewater treatment plants can no longer accommodate the needs of a growing community while still maintaining environmental discharge limits, engineers are tasked with designing processes that can meet current and future wastewater discharge requirements, while minimizing the plant footprint and operating costs. Although activated sludge processes remained the popular choice in the United States since the 1970s, scientific advances have afforded engineers more options such as biofilters, tertiary membrane filtration, and enhanced phosphorus removal. A more reasonable choice, communities opt to upgrade an existing plant when possible, as opposed to building a new plant. For example, the city of Folkston, Georgia added a moving bed biofilm reactor (MBBR) into existing activated sludge tanks for increased nutrient removal capacity without adding to the plant footprint (Schwingle & P.C. Simonton, 2009). Further examples include the addition of integrated fixed film activated sludge (IFAS) processes to existing plants in locations such as Neptune Beach, FL and Narragansett Bay, RI (Wilson et al., 2012). These are just a few examples of the ways biofilm processes are incorporated into existing structures to enhance wastewater processing plants. These upgrades utilizing the benefits offered from biofilm processes can improve capacity by as much as 200% while maintaining the same land footprint. Biofilms are ubiquitous in aquatic environments such as piping systems and surface waters when microorganisms attach to a surface and exude extracellular polymeric substances (EPS) (Wingender, Neu, & Flemming, 2012). The EPS matrix includes a heterogeneous mixture of proteins, polysaccharides, phospholipids, and nucleic acids that protect the cells from possible

stressors (de Faria, de Moraes, & Alves, 2014). As plant upgrades are meant for improving treatment capacity and nutrient removal, it is important to understand the interaction between biofilms and a variety of possible contaminants. The addition of engineered nanoparticles (ENPs) into consumer products has opened the opportunity for research on the transport and accumulation of ENPs in the environment (Walden & Zhang, 2016). Without effective treatment and source water protection, the presence of ENPs and subsequent release into the ecosystem can result in bioaccumulation in crops and aquatic species, which could have implications in food web transfer. We have already seen that the partitioning of ENPs is influenced by the presence of biofilms (Ikuma, Madden, Decho, & Lau, 2014). Studies on Biofilm-ENP interactions in wastewater treatment plants have focused on toxicity and inhibitory effect on biofilm formation (Choi & Hu, 2008; Choi, Yu, Esteban Fernández, & Hu, 2010; Sheng & Liu, 2011a). Results continually agree that biofilms are more resistant to greater levels of nanoparticles than planktonic bacteria, as EPS provides a protective barrier for bacteria cells (Battin, Kammer, Weilhartner, Ottofuelling, & Hofmann, 2009; Han et al., 2016; Sheng, Van Nostrand, Zhou, & Liu, 2015). Yet, the capacity for biofilm to accumulate ENPs has not been well studied. Structural thinning was observed with single species biofilm after exposure to multiple concentrations of silver nanoparticles (Ag-NPs) (0 – 2000 ppb), while no change in viability was observed in *Pseudomonas putida* among concentrations of Ag-NPs or pH values (Fabrega, Renshaw, & Lead, 2009). In contrast, *Aquabacterium citratiphilum* (a model for freshwater biofilm) showed no significant change in biofilm thickness as exposed to Ag-NPs (0 – 2400 ppb) (Grün, Meier, Metreveli, Schaumann, & Manz, 2016). Simple, one species models are regularly sufficient for examination of biofilm systems when evaluating antimicrobial activity, toxicity tests, or antibiofilm products. Here, we developed a



mixed species wastewater biofilm as a model to further understand the capacity for wastewater biofilms to accumulate ENPs. The model biofilm, comprised of three representative species found in wastewater, was first tested for reproducibility and similarity to wastewater biofilms by considering the biofilm formation capacity of each species alone and in combinations in synthetic wastewaters. Then, the impact of ENPs on model biofilm functionality was compared to previously observed biofilm functions in the presence of ENPs. After establishing the reliability of the laboratory model, the biofilm was tested individually and in multiple combinations to quantify ENP accumulation. We also considered the possibility of re-release after ENP attachment. Ag-NPs, a common ENP in food packaging, drug delivery, and textiles, were used as a model ENP.

## 2. Materials and Methods

**Chemicals.** Glassware used for nanoparticle synthesis were acid washed in 10% hydrochloric acid, rinsed three times with distilled deionized (DDI) water and air dried [Elga Process Water System ( $18.2 \text{ M}\Omega \cdot \text{cm}^{-1}$ ) Purelab flex, Veolia, Ireland]. All laboratory glassware was cleaned in phosphorous-free detergent, rinsed three times with tap water, and three times with DDI prior to additional cleaning procedures.

Analytical grade reagents were stored as directed, and used as received. The synthetic wastewater feed solution was prepared with glucose ( $140 \text{ mg L}^{-1}$ ), Difco nutrient broth ( $300 \text{ mg L}^{-1}$ ),  $\text{KH}_2\text{PO}_4$  ( $43.9 \text{ mg L}^{-1}$ ),  $\text{NaOH}$  ( $25 \text{ mg L}^{-1}$ ),  $\text{KNO}_3$  ( $3 \text{ mg L}^{-1}$ ),  $\text{NaHCO}_3$  ( $175 \text{ mg L}^{-1}$ ),  $(\text{NH}_4)_2\text{SO}_4$  ( $118 \text{ mg L}^{-1}$ ),  $\text{CaCl}_2$  ( $133 \text{ mg L}^{-1}$ ),  $\text{FeCl}_3 \cdot 6\text{H}_2\text{O}$  ( $5 \text{ mg L}^{-1}$ ),  $\text{MgSO}_4$  ( $100 \text{ mg L}^{-1}$ ), and  $\text{MnSO}_4$  ( $12.8 \text{ mg L}^{-1}$ ) (Juang, Yang, Chou, & Chiu, 2011). Orthophosphate, nitrate, sulfate, chloride ions were measured with Ion Chromatography (Metrohm 850 IC, Switzerland). Ammonia was measured by salicylate method on a spectrophotometer (AmVer 3 Hach reagent kit, Hach, Loveland, CA).

**Microbial culture.** The strains *Comamonas testosteroni* ATCC 11996, *Acinetobacter calcoaceticus* ATCC 31926 and *Delftia acidovorans* ATCC 15668 were obtained and propagated as instructed in Difco nutrient broth at 30°C for 48 hours. Working cultures were maintained on agar plates for 30-day increments. All cell counts in liquid culture were measured in triplicate with a Multisizer 4 Coulter Counter (Beckman Coulter, CA, USA). Prior to the experiment, one colony of each species was harvested and grown in 50 mL of SW until reaching cell turbidity approximately equivalent to 0.1 using a spectrophotometer at 620 nm (Beckman Coulter DU720 UV/VIS Spectrophotometer, Beckman Coulter Inc., Brea, CA).

**Biofilm formation assay.** A 1:100 dilution of 100 µL cell suspension in SW was transferred aseptically to a sterile microtiter 96-well plate for each species with six replicates (Andersson, Dalhammar, Land, & Kuttuva Rajarao, 2009; Djordjevic, Wiedmann, & McLandsborough, 2002). Multiple combinations between these species were tested: *A. calcoaceticus*, *C. testosteroni*, *Delftia acidovorans*, *A. calcoaceticus* and *C. testosteroni*, *A. calcoaceticus* and *Delftia acidovorans*, *C. testosteroni* and *Delftia acidovorans*, as well as a combination of all three together. The microtiter plate included six wells of SW without inoculation as the negative control. The plate was incubated at 37°C for 24 hours, rinsed and stained with crystal violet (O'Toole, 2011). To quantify the biofilm, 125 µL of 30% acetic acid were added to each well and incubated for 15 minutes. Absorbance at 590 nm was recorded for each using 30% acetic acid as the blank. (Andersson et al., 2009; Stepanovic, Vukovic, Dakic, Savic, & Svabic-Vlahovic, 2000). Formation is quantified by comparing the absorbance of the inoculated cells to control cells, where biofilm adherence is categorized as the following: less than  $Abs_{control}$  is non-adherent, between  $Abs_{control}$  and  $2 \times Abs_{control}$  are weakly adherent, between  $2 \times Abs_{control}$  and  $4 \times Abs_{control}$  are moderately adherent, and greater than  $4 \times Abs_{control}$  are strongly adherent.

**Nanoparticle characterization.** Silver nanoparticles were synthesized using sodium borohydride to reduce silver nitrate with sodium citrate as a capping agent (Mulfinger et al., 2007). The formation of Ag-NPs was confirmed by scanning the absorbance from 300 – 700 nm with a UV-vis spectrophotometer (Beckman Coulter, CA, USA). Size and shape were characterized with transmission and scanning electron microscopy. Total silver concentrations were prepped by Standard Method 3500-Ag and measured with ICP-MS (iCapQ Quadrupole with Cetac ASX-560 autosampler, Arkansas Mass Spec Facility). Ionic silver and nano-particulate silver were measured separately by applying multiple separation techniques. Samples for nano-particulate measurement were filtered with 0.1  $\mu\text{m}$  Acrodisc syringe filters (Life Sciences, Colorado), where the total filtrate concentration is less than 100 nm, was compared with the total silver concentration. 2 mL samples were also loaded in 3kDa Amicon Ultra 4 centrifugal filters (Merck Millipore, Massachusetts) where the filtrate concentration is solely ionic silver.

**Experimental setup.** Preceding experimentation, synthetic wastewater pH was adjusted with a pH meter to pH=8 with 0.1 M HCl if necessary (Thermo-Scientific, Fort Collins, Colorado). All tubing and reactors were run with 10% bleach solution and allowed to sit overnight. Then, DDI water was used to rinse. Finally, the apparatus and accessories were autoclaved at 121 °C for 30 minutes (Model 522LS Gravity Steam Sterilizer, Getinge, Rochester, New York).

The CDC biofilm reactor (CBR) (Biosurface Technologies, Bozeman, MT) was used to explore biofilm functionality under dynamic conditions. The reactor is a 1-liter glass beaker with a polyethylene lid which holds 8 polyethylene rods, each with three removable polyethylene coupons serving as an attachment site for biofilm growth. The CBR operates as a continuous flow stirred tank reactor (CFSTR), where nutrients are continuously pumped in, and effluent

flowed out. This reactor setup is assumed well mixed, has a working volume of approximately 350 mL, and was operated at 2 mL min<sup>-1</sup>, resulting in a retention time of 175 minutes. Prior to the CFSTR mode, the CBR setup was run in an incubation room at 28 °C on a stirring plate set to 80 rpm in batch mode for 24 hours, allowing a mature biofilm to form. One rod containing three coupons was removed and carefully stored in sterile SW at 28 °C for microscopic analysis. Then, the CBR was operated with SW containing approximately 50 ppb Ag-NPs at a flow rate of 2 mL min<sup>-1</sup> for 3 hours, one retention time. One rod with three coupons was removed, placed in SW without Ag-NPs to remove any unattached silver, and aseptically transferred to sterile SW in a brown HDPE bottle to minimize biofilm disturbance preceding microscopy.

A custom flow cell (Figure S1) was used to analyze silver bioaccumulation for each species combination. Before experimentation, the flow cell was cleaned and sterilized in the same manner as the CBR. The flow cell experiments were replicated until each experiment showed triplicate accumulation values with standard errors less than 20%.

**Biofilm analysis.** During functionality testing in the CBR, Biofilm was also characterized by *bacLight* cell stain (Live/Dead *bacLight* Bacterial viability kit, Life Technologies, Grand Island, New York) using confocal laser scanning microscopy (CLSM). Images were obtained with a Nikon 90i upright CLSM using the 60× objective lens (Nikon, Melville, New York). 5 replicate image z-stacks were randomly selected and recorded from at least two different CBR coupons. Oxidative stress was measured with 2'-7'-dichlorofluorescein diacetate (H<sub>2</sub>-DCFDA) on a 96 well microplate reader (Synergy H1 Multi-Mode Microplate Reader, Biotek Instruments, Inc., Winooski, VT). (Aranda et al., 2013; Thuptimdang, Limpiyakorn, McEvoy, Prüss, & Khan, 2015; Wang & Joseph, 1999). Briefly, three coupons representing 3 replicates were removed and cautiously dipped in phosphate buffered solution (PBS) to remove planktonic cells. Each coupon

was placed in a sterile tube containing 2.5 mL of PBS and vortexed for 30 seconds. with 0.4  $\mu$ L of 5 mM H<sub>2</sub>-DCFDA. 200  $\mu$ L was then transferred to the 96-well microplate and incubated for 30 minutes in the dark at 37°. ROS was assessed at 495 excitation, 527 emission. A standard curve was generated with hydrogen peroxide. Control wells included Ag-NPs with (H<sub>2</sub>-DCFDA) to consider any quenching effects on the dye fluorescence emission.

**Ag-NP adsorption.** Qualitative analysis of Ag-NP attachment to biofilms was completed by fluorescently labeling Ag-NPs for visualization with CLSM with biofilm samples. To label Ag-NPs, the particle labeling procedure was tested with different amounts of EDC (1-ethyl-3-(3-dimethylaminopropyl)carbodiimide) and Sulfo-NHS (sulfo-hydroxysuccinimide) in MES sodium salt buffer as previously described (Peulen and Wilkinson, 2011). The most efficient labeling occurred with 12 mg EDC, 0.72 nmol Rh123 in 200mM MES Buffer, followed by 24 hours agitation, then 24 hours of dialysis in 9:1 ethanol solution. Particles were visualized within 8 hours of the labeling procedure.

To quantitatively measure Ag-NP accumulation, three coupons were aseptically removed from either reactor after Ag-NP exposure, suspended in a sterile tube with 5 mL of nitric acid solution, and vortexed for 5 minutes. The coupons were then removed with tweezers, and the final volume was brought to 10 mL of 2.5% nitric acid for total silver concentration using ICP-MS.

**Statistical analysis.** Data compilation and tables were generated in Microsoft Excel (Microsoft, Redmond, WA). Output files were graphed and statistical analysis was completed in SigmaPlot version 12.5 from Systat Software, Inc., San Jose California USA, [www.systatsoftware.com](http://www.systatsoftware.com).

Statistic *p* values less than 0.05 were considered significant.

### 3. Results and Discussion

**Mixed species biofilm model.** The mixed species biofilm was thoughtfully conceived from previous studies of common wastewater species. Successful isolation and identification of *Acinetobacter calcoaceticus* in hospitals, wastewater biological nutrient removal processes, and as a dominant aerobic species within soil and water samples provides evidence that *A. calcoaceticus* is significant in NP - bacterial interactions (Baumann, 1968; Maszenan et al., 1997; Constantiniu et al., 2004). Multidrug resistant and part of the normal human bacterial community dermally and within the respiratory tract, *A. calcoaceticus* has shown responsible for nosocomial infections since the 1970's (Retalliau et al., 1979). Certain strains of *Acinetobacter spp.* also display the unique ability to generate silver and platinum nanoparticles in controlled experiments (Gaidhani et al., 2014; Singh et al., 2013). The ubiquitous nature of this species along with its tolerance and ability to generate nanoparticles make this species an excellent model for examining NP – biofilm interactions (Jung and Park, 2015). *Delftia acidovorans* are strictly aerobic, non-fermentative chemo-organotrophs. *D. acidovorans* have been identified to occur in freshwater, soil, activated sludge and clinical samples (Wen et al., 1999). *D. acidovorans* have the capacity to survive in potable water system biofilms, and are a rare but possible cause of infection with intravenous drug users (Mahmood et al., 2012). *Comamonas testosteroni* are highly motile and aerobic. Interest in *C. testosteroni* centers around activated sludge, heavy metal mining soil, and organic compound remediation (Liu et al., 2015). The heavy metal resistance of this species is also of interest when examining NP – biofilm interactions. As discussed, these species individually are relevant model biofilm in wastewater, and they could help reveal the NP-biofilm interaction in complex environment such as wastewater; further, NP interactions observed with these species separately and mixed will be

applicable in environments other than wastewater, including hospitals, distribution systems, and fresh water environments.

Before investigating the NP-biofilm interactions, the biofilm formation capability of each species and their combination was studied first. The biofilm formation assay included staining of biofilm with crystal violet, followed by an absorbance measurement which correlates to the quantity of biofilm formed (Figure S2). We compared three SW recipes through a biofilm formation assay with each species to ensure the SW supports the growth of all species relatively evenly. Recipe labeled 'SW2' showed the smallest error in biofilm formation for all three species within 24 hours, thus was selected as representative of wastewater for this study.

**Silver nanoparticle characteristics.** The generated Ag-NPs exhibited a typical surface plasmon resonance with a peak UV-vis spectroscopy wavelength 398 nm (Figure S3). Transmission electron microscopy (Figure S4) particle size measurements of the stock solution showed the particle size diameter was  $14.6 \pm 0.21$  nm (Table S1). Nano-sized and ionic silver concentrations were measured for both stock solution and SW suspensions. The stock solution total silver concentration was 1.1 ppm. Stock solutions were stored in brown bottles in the dark until time for use. For quick checks, the UV-vis wavelength peak was used to verify no agglomeration occurred during storage. After dilution into SW, silver complexation occurred. ICP-MS results showed 0.98% of total silver still existed as Ag-NPs, and 1.2% was ionic silver. TEM images of SW with Ag-NPs showed precipitates and particles in clusters (Figure S5), as expected. Ag-NPs undergo chemical transformation in sewer networks with cysteine, histidine, sulfur and chlorides (Brunetti et al., 2015). Complexation of Ag-NPs occurred with this SW, which simulates environmental conditions that are expected to occur in wastewater sewers.

**3.1 CBR exposure tests.** A CBR was operated to assess changes in biofilm functionality in this model system during silver exposure. With all three species, the CBR was inoculated and operated in batch mode for 24 hours. After the biofilm was formed, sterile SW was combined with stock Ag-NPs to a designed concentration of approximately 200 ppb and pumped through the CBR at 2 mL min<sup>-1</sup>. Random influent and effluent checks ranged from 48 ppb – 67 ppb. Stock dilution was performed volumetrically by pipet, which incorporated small variations between experiments, therefore measured values are reported as needed.

**Biofilm structure and viability.** A three-dimensional view of all live cells (green) and all damaged cells (red) shows the distribution of bacteria throughout a representative image stack (Figure 1). After 3 hours of Ag-NP exposure, live:dead ratios of biofilm formed on the coupons within the reactor were 3.66±1.01, showing no significant change in viability from live:dead ratios preceding exposure ( $p=0.578$ ). This tolerance to low concentrations of Ag-NPs (at about 50 ppb) by the biofilm was expected; in fact, to achieve biofilm toxicity, concentrations were previously determined to be higher than 5 mg L<sup>-1</sup> (Thuptimdang, Limpiyakorn, & Khan, 2017). Although viability showed no change, reactive oxygen species generated as a sign of cell stress significantly increased ( $p=0.006$ ) (Figure 2). A biovolume was also calculated in terms of fluorescent intensity using CLSM. Biovolume measurements were produced from the fluorescence of live and dead stained cells, and did not include EPS. Prior to Ag-NP exposure, the biovolume per image area was 0.015±0.002  $\mu\text{m}^3 \mu\text{m}^{-2}$ , whereas after exposure the biovolume significantly increased to 0.025±0.002  $\mu\text{m}^3 \mu\text{m}^{-2}$  ( $p=0.019$ ). However, the previously reported range of biomass volumes suggests that biomass variations as these are not surprising. Biomass volume measurements in this study were relatively low compared to *pseudomonas putida* biofilm grown on 96 well plates in static conditions for 16 hours with biomass volumes ranging 7.04 –



17.56  $\mu\text{m}^3 \mu\text{m}^{-2}$  (Thuptimdang et al., 2017). Further, when comparing across biofilm studies, the stain type, growth conditions, and image processing software are important variables to consider.

**Biofilm functionality.** The capability of biofilm to remove nutrients from wastewater was studied under the exposure of Ag-NP. Cellular function was monitored without and with Ag-NPs in the influent after multiple CBR retention times (Table 1). COD reduction percentages in the presence of Ag-NPs showed no significant difference from COD reduction capabilities without Ag-NPs present ( $p>0.05$ ). Further, no significant change in pH, sulfate, or ammonia occurred in this mesocosm ( $p>0.05$ ). Without Ag-NPs, the SW showed 122.7 mg L<sup>-1</sup> chlorides, whereas with the addition of Ag-NPs in the same SW contained 66.4 mg L<sup>-1</sup> chlorides. This change is expected, as previous studies verified the formation of silver chloride and silver sulfate in wastewater influent (Brunetti et al., 2015). This model biofilm system showed similar resistance to Ag-NPs as RBC biofilms have demonstrated under much higher concentrations of 200 mg L<sup>-1</sup> with heterotrophic plate counts (Sheng & Liu, 2011b). As this biofilm community exhibited similar chemical and biological traits to environmental wastewater systems, it will next be applied for understanding sequestration of Ag-NPs from wastewater influent.

**3.2 Flow cell exposure tests.** The flow cell was inoculated with *C. testosteroni* to first qualitatively test if Ag-NPs adsorb onto/diffuse into biofilms formed on the flow cell coupons. After the biofilm was formed, the flow cell was rinsed with sterile SW and spiked with rhodamine123 protein labeled Ag-NPs (Rh-Ag-NPs) for 10 minutes and rinsed with sterile SW once again. Then, biofilm was stained with Hoescht33358 to identify all cells, and propidium iodide to identify damaged cells (Figure 3). As shown, Rh-Ag-NPs adsorbed to the surface of the biofilm. Image stacks also showed the diffusion of Rh-Ag-NPs into the biofilm structure. Biofilm structure, Ag-NP mobility, and chemical transformation are all important parameters

controlling particle diffusion into biofilms. With *pseudomonas fluorescens*, Ag-NPs have shown to diffuse into biofilms, where the diffusion coefficient changed as the particle size increased (Peulen & Wilkinson, 2011). Further, in this study chemical transformations occurring increase aggregate size, therefore will decrease the likeliness that silver species will penetrate deeply into the biofilm.

**Biofilm accumulation of silver.** With the flow cell system, we then investigated the capacity of each species individually and in combinations to accumulate silver (Figure 4). For each separate experiment, Ag-NP stock was diluted to an expected 200 ppb. ICP-MS tests showed variations from 98.8 ppb to 246.4 ppb. For all combinations of species except *A. calcoaceticus* & *D. acidovorans*, the percent of silver accumulated with biofilms compared to measured total silver ranged from 0.27%-1.26%. With the concentration of silver added being exceedingly greater than silver with biofilms, we can assume the influent variations showed minimal influence upon biofilm accumulation. For *A. calcoaceticus* & *D. acidovorans*, the greatest measured accumulation was observed at an influent total silver  $105 \pm 2.3$  ppb, where 7.8% silver sorbed to biofilm. Box plot boundaries show the 25<sup>th</sup> and 75<sup>th</sup> percentiles, where the thicker line represents the median. The flow cell was operated for single species, dual combinations, and a mixed consortia biofilm. Irrespective of which single species was grown, the silver accumulation per coupon area did not significantly vary ( $p > 0.05$ ). Total silver concentrations for single species biofilms ranged from  $0.0078 - 0.017$  ng mm<sup>-2</sup>. The greatest silver accumulation was observed with *A. calcoaceticus* and *D. acidovorans* with a mean of  $0.431$  ng mm<sup>-2</sup> per coupon. Dual species combinations which included *D. acidovorans* showed increased silver accumulations compared to the combinations without *D. acidovorans*. *D. acidovorans* is a gold associated microbe, and has been used to synthesize gold nanoparticles (Ganesh Kumar, Poornachandra, &

Mamidyala, 2014). Just as *D. acidovorans* overcomes gold toxicity, it shows here that *D. acidovorans* is also quite tolerant to silver species as well when associated with other species in a biofilm. In general, as the number of species increased in each experiment, we witnessed an increase in the capacity to accumulate silver. This is somewhat contradictory to the concept that diffusion is more limiting in heterogeneous biofilms compared to a single-species biofilm due to the higher complexity of the matrix (Guiot et al., 2002). In fact, the increase of complexity in this study shows a trend of increased adsorbed or diffused silver with the increasing heterogeneity of the biofilm structure. With previous observations that dense biofilms tend to accumulate Ag-NPs to a greater extent than loosely-attached biofilm, we can infer that with increased structural heterogeneity, the biofilm density is also increasing (Peulen & Wilkinson, 2011).

Each species was previously tested in a standard biofilm formation assay. Biofilm formation results can be classified where  $Abs \leq Abs_{control}$  are considered non-adherent (0),  $Abs_{control} < Abs \leq 2 \times Abs_{control}$  are weakly adherent (+),  $2 \times Abs_{control} < Abs \leq 4 \times Abs_{control}$  are moderately adherent (++) , and  $Abs > 4 \times Abs_{control}$  are considered strongly adherent (+++). We did not find any correlation between the capacity to form biofilm and the silver accumulated within each biofilm combination. Interestingly, *D. acidovorans* are weakly adherent when grown singly, however in combination with other species the biofilm forming capacity is increased while silver accumulation also showed higher in biofilms containing *D. acidovorans*.

***Detachment after silver exposure.*** The biofilm combination exhibiting the highest accumulation of Ag-NPs, *A. calcoaceticus* and *D. acidovorans*, was chosen for further examination for potential release of silver as well as biofilm biomass loss through cell detachment. The flow cell accumulation test protocol was repeated, then instead of harvesting the coupons for analysis, additional measurements were conducted at two different influent concentrations to monitor both

silver release and cell counts within the effluent. After exposure, the flow cell was run at with sterilized SW for 10 minutes to flush Ag-NPs from bulk liquid. Then, as SW was pumped at 2 mL min<sup>-1</sup>, effluent cell counts and silver concentrations were measured.

**Low concentration (22 ppb).** After flushing bulk liquid silver, silver concentrations for sixty minutes did not approach zero. In fact, effluent total silver averaged 2.6±0.6 ppb for sixty minutes after removing silver from influent. Effluent cell counts ranging 3.2x10<sup>6</sup> - 1x10<sup>7</sup> cells mL<sup>-1</sup> before exposure showed no significant difference from cell counts after exposure.

**High concentration (105 ppb).** At the higher concentration of 105±2.3 ppb Ag-NPs, effluent total silver after flushing averaged 7.9±0.9 ppb for 60 minutes. Effluent cell counts before exposure to this higher concentration significantly decreased from 3x10<sup>7</sup> cell mL<sup>-1</sup> to a steady cell flow averaging 1.73x10<sup>7</sup> cells mL<sup>-1</sup>.

After the 60 minutes of influent flow without silver, biofilm coupons were harvested and analyzed for total silver. At 22 and 105 ppb, total silver remaining adsorbed to biofilm were 0.016 and 0.072 ng mm<sup>-2</sup>, respectively. Compared to the flow cell accumulation average measurement 0.431 ng mm<sup>-2</sup> (Figure 4), there was significant Ag-NP detachment ( $p=0.04$ ).

Previously, silver accumulated in *Pseudomonas fluorescens* biofilm showed to associate more closely with bacterial cells, as opposed to within the EPS (Peulen & Wilkinson, 2011). As cells detach, it is reasonable to conclude that silver detachment was concurrently taking place. Here we make no correlation to the decrease in detached cells at the high concentration to a decrease in silver concentration within effluent. Overall, even after exposure to Ag-NPs for 30 minutes, it shows here that biofilms are a location for low concentrations of Ag-NPs to accumulate in the short term. As this indicates biofilm can become a source from which Ag-NPs can be released,

these concentrations are minimal compared to the total silver that does not accumulate, but passed through the system.

#### **4. Concluding Remarks**

This study aimed to answer the question of whether bioaccumulation of ENPs poses hazards to biofilm functions as well as illustrating ENP sequestration effects for multi-component ENP - biofilm systems. The increase in biofilm biovolume indicates a softening of the biofilm structure, which is also reinforced with the detection of oxidation stress. Previous studies agree that Ag-NPs at these concentrations do not affect biofilm functional processes, as we show here for this new mixed model system. Silver accumulation occurred in each type of biofilm within 30 minutes. Biofilm accumulated silver while still protecting the cells within the structure. However, these quantities of silver are minimal considering the total concentration in the wastewater column. The largest threat from bioaccumulation will be at the wastewater effluent mixing zones where there is potential for food web transfer in macrophytes.

## Tables and Figures

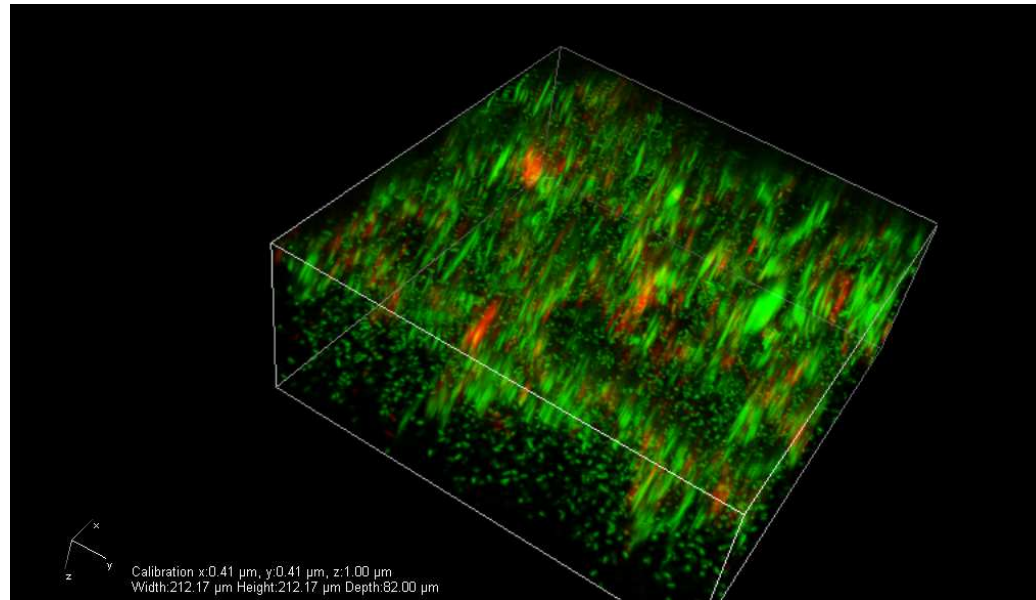


**Figure 1.** 3-dimensional view from confocal laser scanning microscopy for biovolume measurement of fluorescently stained model biofilm in the CBR after Ag-NP exposure. Green indicates live cells and red indicates damaged cells.

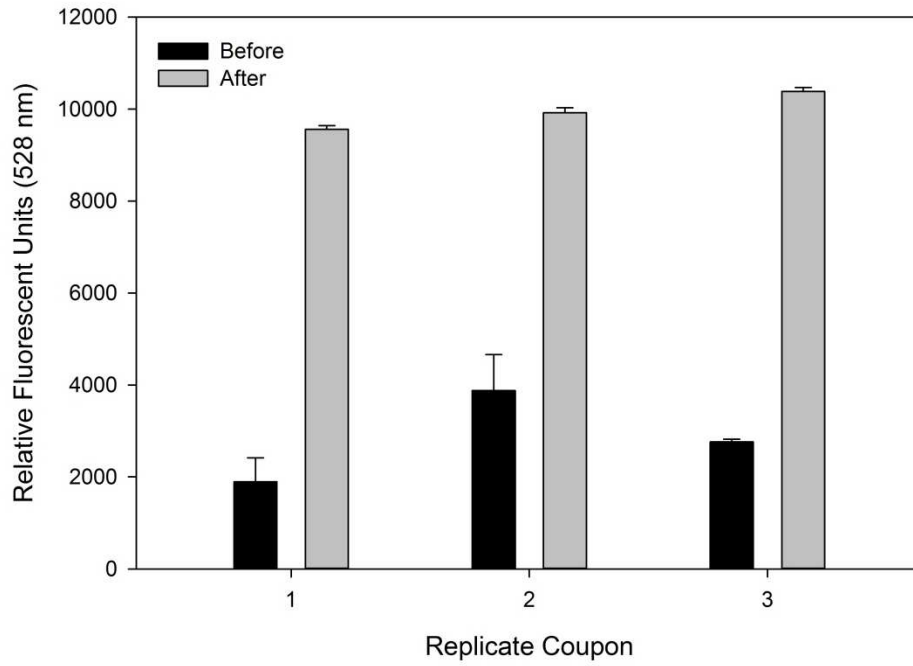


**Figure 2.** Reactive oxygen species detected before and after Ag-NP exposure to biofilms.

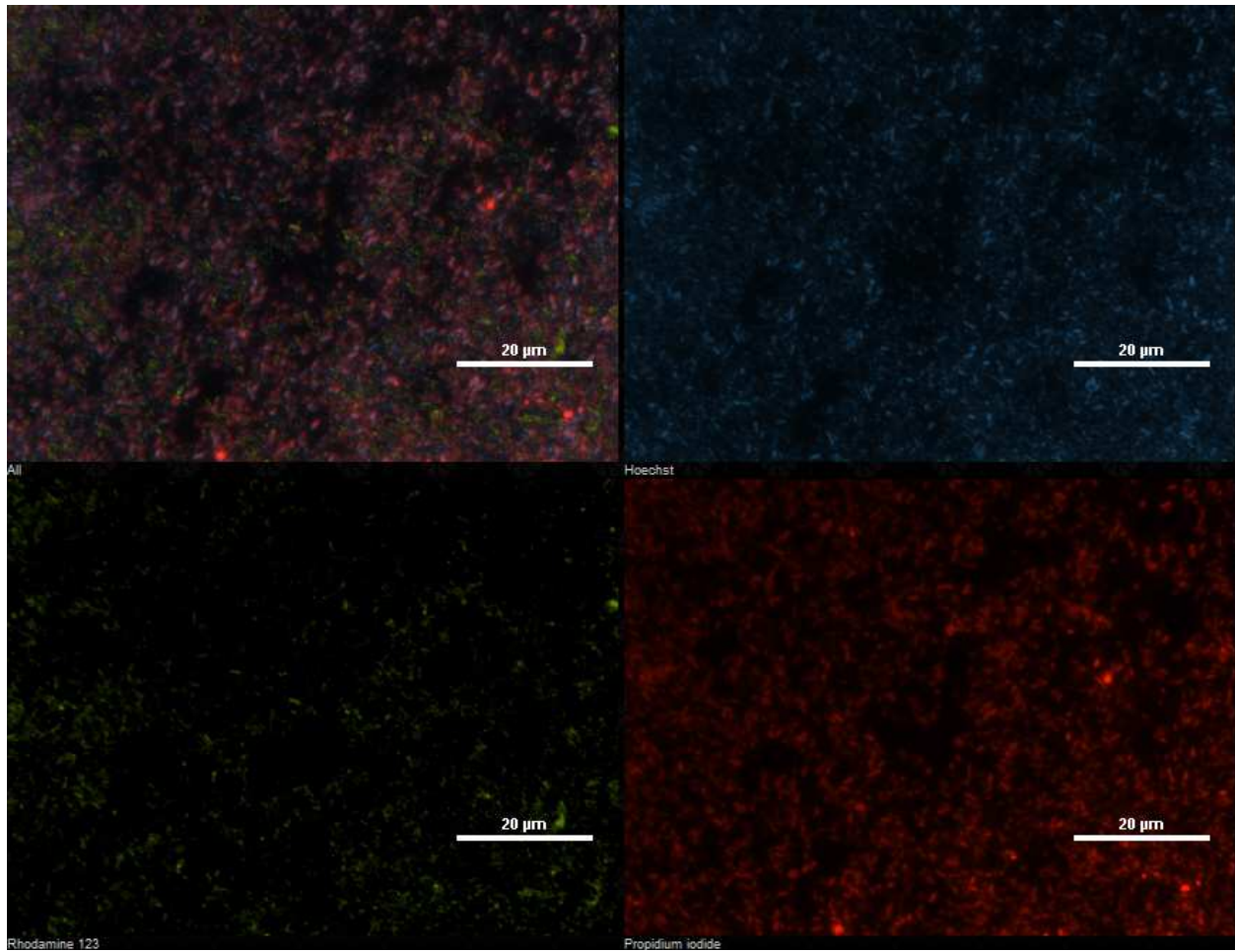


**Figure 3.** Confocal laser scanning microscope image of biofilm stained with propidium iodide (red, damaged cells) and Hoescht 33358 (blue, all cells). Ag-NPs were fluorescently labeled with rhodamine123 protein (green particles) for qualitative imaging within *C. testosteroni* biofilm matrix.



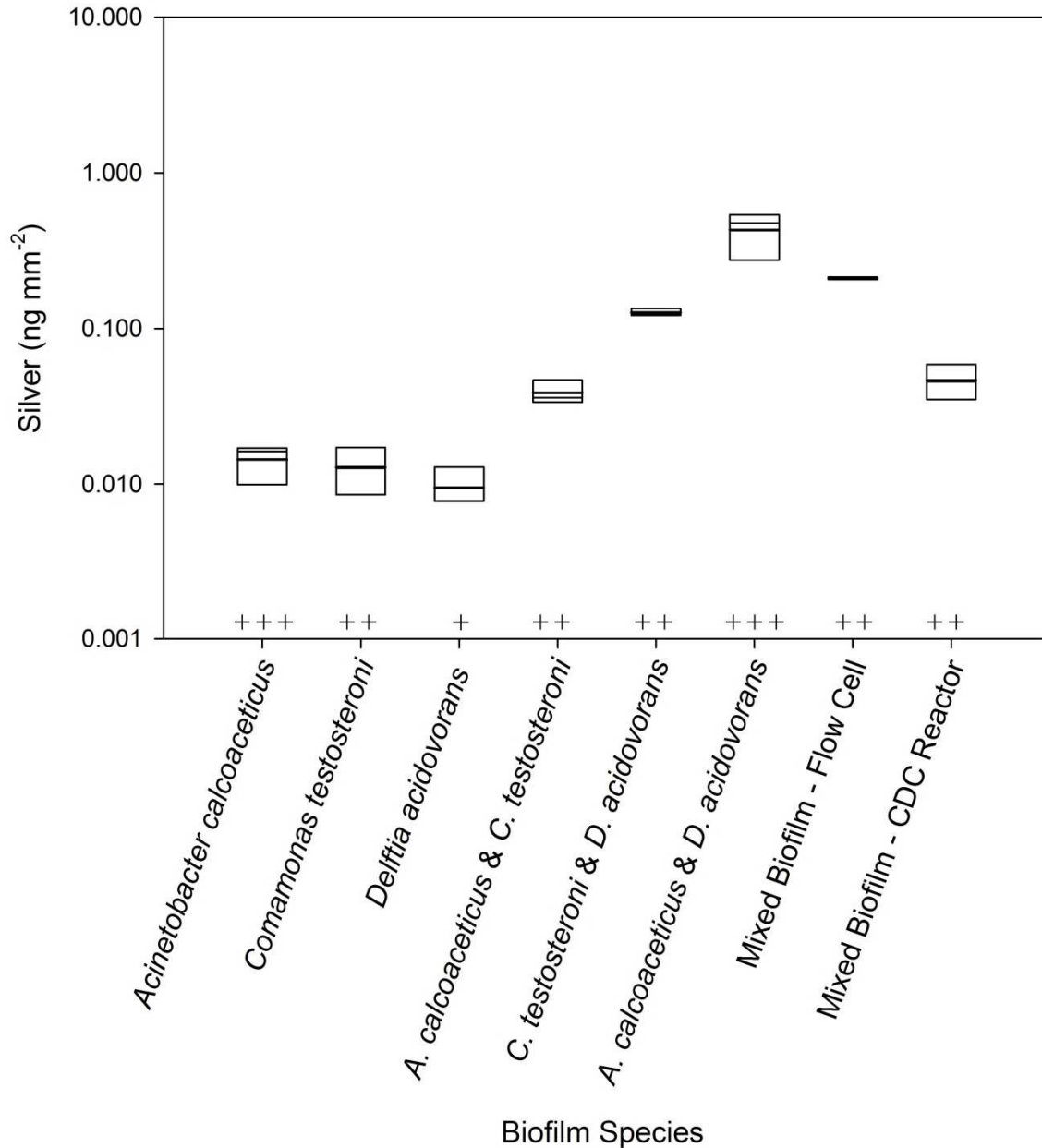


**Figure 4.** Sorption of Ag-NPs to differently formed model wastewater biofilms are expressed as the 25<sup>th</sup> and 75<sup>th</sup> percentile boxplots, with the median represented as a thicker inset bar. Biofilm formation assay results are interpreted as strongly adherent (+++), moderately adherent (++) and weakly adherent (+) as listed above each sample type.

**Table 1.** Effluent characteristics after each retention time (3 hours) of the CDC biofilm reactor for 12 hours (a) without Ag-NPs within the influent and (b) with 200 ppb Ag-NPs within the influent. All results are reported as an average of three measurements.

**(a)**

Time (hr)	COD (mg O <sub>2</sub> L <sup>-1</sup> )	pH	Ammonia (mg L <sup>-1</sup> NH <sub>3</sub> -N)	Cl <sup>-</sup>	NO <sub>3</sub> <sup>-</sup>	PO <sub>4</sub> <sup>3-</sup>	SO <sub>4</sub> <sup>2-</sup>	COD Percent Removed
0	273.5	8.6	18.5	122.7	1.4	3.2	90.2	
3	130.6	6.94	18.7	92.8	0.2	5.6	91.7	52%
6	229.1	6.47	18	75.9	0.2	2.9	89.9	16%
9	229.1	6.20	23.9	70.3	0.2	1.5	90.1	16%
12	141.0	6.26	18.9	66.2	0.3	1.4	89.6	48%

**(b)**

0	458	7.57	29.4	66.4	1.3	3.0	73.5	
3	310	6.68	28.4	66.1	0.1	4.0	79.4	32%
6	264	6.78	31.1	64.3	0.1	2.8	77.6	42%
9	275	6.95	32.2	61.3	0.1	1.9	73.7	40%
12	269	6.68	31.7	60.8	0.1	2.2	73.6	41%

## References

- Andersson, S., Dalhammar, G., Land, C. J., & Kuttuva Rajarao, G. (2009). Characterization of extracellular polymeric substances from denitrifying organism *Comamonas denitrificans*. *Applied Microbiology and Biotechnology*, 82, 535-543. doi:http://0-dx.doi.org.library.uark.edu/10.1007/s00253-008-1817-3
- Aranda, A., Sequedo, L., Tolosa, L., Quintas, G., Burello, E., Castell, J. V., & Gombau, L. (2013). Dichloro-dihydro-fluorescein diacetate (DCFH-DA) assay: A quantitative method for oxidative stress assessment of nanoparticle-treated cells. *Toxicology in Vitro*, 27, 954-963. doi:10.1016/j.tiv.2013.01.016
- Battin, T. J., Kammer, F. v., Weilhartner, A., Ottofuelling, S., & Hofmann, T. (2009). Nanostructured TiO<sub>2</sub>: transport behavior and effects on aquatic microbial communities under environmental conditions. *Environmental Science & Technology*, 43(21), 8098-8104.
- Brunetti, G., Donner, E., Laera, G., Sekine, R., Scheckel, K. G., Khaksar, M., . . . Lombi, E. (2015). Fate of zinc and silver engineered nanoparticles in sewerage networks. *Water Research*, 77, 72-84. doi:10.1016/j.watres.2015.03.003
- Choi, O., & Hu, Z. (2008). Size Dependent and Reactive Oxygen Species Related Nanosilver Toxicity to Nitrifying Bacteria. *Environmental Science & Technology*, 42, 4583-4588. doi:10.1021/es703238h
- Choi, O., Yu, C.-P., Esteban Fernández, G., & Hu, Z. (2010). Interactions of nanosilver with *Escherichia coli* cells in planktonic and biofilm cultures. *Water Research*, 44(20), 6095-6103. doi:10.1016/j.watres.2010.06.069
- de Faria, A. F., de Moraes, A. C. M., & Alves, O. L. (2014). Toxicity of Nanomaterials to Microorganisms: Mechanisms, Methods, and New Perspectives. In N. Durán, S. S. Guterres, & O. L. Alves (Eds.), *Nanotoxicology* (pp. 363-405). New York, NY: Springer New York.
- Djordjevic, D., Wiedmann, M., & McLandsborough, L. A. (2002). Microtiter Plate Assay for Assessment of *Listeria monocytogenes* Biofilm Formation. *Applied and environmental microbiology*, 68, 2950-2958. doi:10.1128/AEM.68.6.2950-2958.2002
- Ganesh Kumar, C., Poornachandra, Y., & Mamidyala, S. K. (2014). Green synthesis of bacterial gold nanoparticles conjugated to resveratrol as delivery vehicles. *Colloids and Surfaces B: Biointerfaces*, 123, 311-317. doi:10.1016/j.colsurfb.2014.09.032

- Guiot, E., Georges, P., Brun, A., Fontaine-Aupart, M. P., Bellon-Fontaine, M. N., & Briandet, R. (2002). Heterogeneity of Diffusion Inside Microbial Biofilms Determined by Fluorescence Correlation Spectroscopy Under Two-photon Excitation. *Photochemistry and Photobiology*, 75(6), 570-578. doi:10.1562/0031-8655(2002)075<0570:HODIMB>2.0.CO;2
- Han, Y., Hwang, G., Kim, D., Bradford, S. A., Lee, B., Eom, I., . . . Kim, H. (2016). Transport, retention, and long-term release behavior of ZnO nanoparticle aggregates in saturated quartz sand: Role of solution pH and biofilm coating. *Water Research*, 90, 247-257. doi:10.1016/j.watres.2015.12.009
- Ikuma, K., Madden, A. S., Decho, A. W., & Lau, B. L. T. (2014). Deposition of nanoparticles onto polysaccharide-coated surfaces: implications for nanoparticle–biofilm interactions. doi:10.1039/C3EN00075C
- Juang, D.-F., Yang, P.-C., Chou, H.-Y., & Chiu, L.-J. (2011). Effects of microbial species, organic loading and substrate degradation rate on the power generation capability of microbial fuel cells. *Biotechnology Letters*, 33, 2147. doi:10.1007/s10529-011-0690-9
- O'Toole, G. A. (2011). Microtiter Dish Biofilm Formation Assay. *Journal of Visualized Experiments : JoVE*. doi:10.3791/2437
- Peulen, T.-O., & Wilkinson, K. J. (2011). Diffusion of Nanoparticles in a Biofilm. *Environmental Science & Technology*, 45(8), 3367-3373. doi:10.1021/es103450g
- Schwingle, T., & P.C. Simonton, A. (2009, 2009-11-11). Critical biomass. *Public Works*.
- Sheng, Z., & Liu, Y. (2011a). Effects of silver nanoparticles on wastewater biofilms. *Water Research*, 45(18), 6039-6050. doi:10.1016/j.watres.2011.08.065
- Sheng, Z., & Liu, Y. (2011b). Effects of silver nanoparticles on wastewater biofilms. *Water Research*, 45, 6039-6050. doi:10.1016/j.watres.2011.08.065
- Sheng, Z., Van Nostrand, J. D., Zhou, J., & Liu, Y. (2015). The effects of silver nanoparticles on intact wastewater biofilms. *Frontiers in Microbiology*, 6. doi:10.3389/fmicb.2015.00680
- Stepanovic, S., Vukovic, D., Dakic, I., Savic, B., & Svabic-Vlahovic, M. (2000). A modified microtiter-plate test for quantification of staphylococcal biofilm formation. *Journal of Microbiological Methods*, 40, 175-179.

- Thuptim dang, P., Limpiyakorn, T., & Khan, E. (2017). Dependence of toxicity of silver nanoparticles on *Pseudomonas putida* biofilm structure. *Chemosphere*, *188*, 199-207. doi:10.1016/j.chemosphere.2017.08.147
- Thuptim dang, P., Limpiyakorn, T., McEvoy, J., Prüss s, B. M., & Khan, E. (2015). Effect of silver nanoparticles on *Pseudomonas putida* biofilms at different stages of maturity. *Journal of Hazardous Materials*, *290*, 127–133.
- Walden, C., & Zhang, W. (2016). Biofilms Versus Activated Sludge: Considerations in Metal and Metal Oxide Nanoparticle Removal from Wastewater. *Environ Sci Technol*, *50*(16), 8417-8431. doi:10.1021/acs.est.6b01282
- Wang, H., & Joseph, J. A. (1999). Quantifying cellular oxidative stress by dichlorofluorescein assay using microplate reader. *Free Radical Biology and Medicine*, *27*, 612–616.
- Wilson, M., Sandino, J., Cote, T., Brueckner, T., Boltz, J., & Michelsen, D. (2012). Design and Operational Insights of the World's Largest Integrated Fixed Film Activated Sludge (IFAS) Process for Low Nitrogen Limits. doi:info:doi/10.2175/193864712811708248
- Wingender, J., Neu, T. R., & Flemming, H.-C. (2012). *Microbial extracellular polymeric substances: characterization, structure and function*: Springer Science & Business Media.

## **Appendix 2.**

Supplementary Information for

“Bioaccumulation of Silver Nanoparticles in Model Wastewater Biofilm”

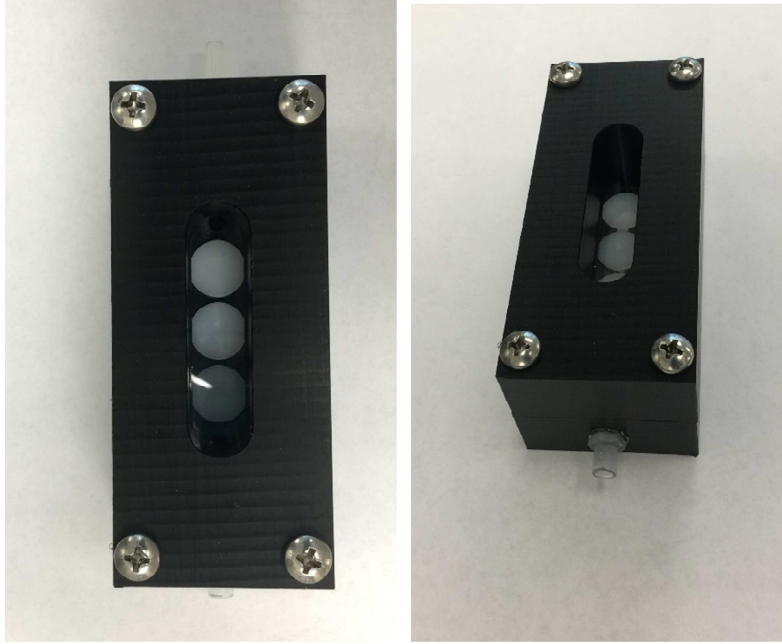


**Figure S1.** The custom flow cell with three polyethylene coupons installed. A microscope glass slide was fitted to enable real time viewing of biofilm formation.

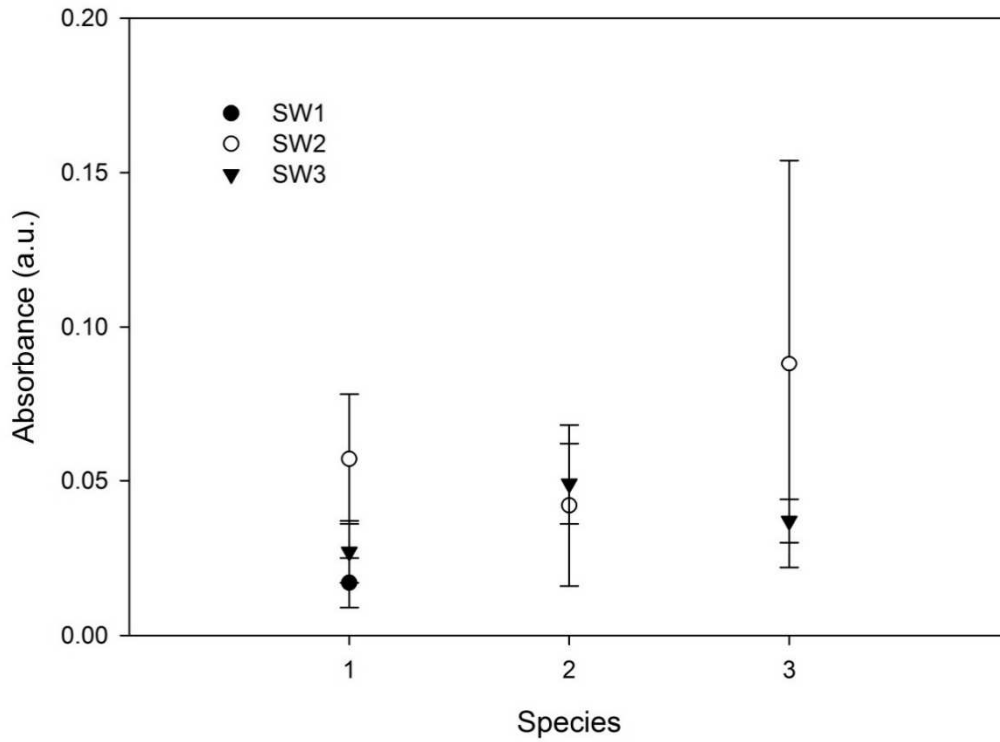


**Figure S2.** SW selection by applying a biofilm formation assay. The x-axis corresponds to (1) *Acinetobacter calcoaceticus* (2) *Comamonas testosteroni* (3) *Delftia acidovorans*.



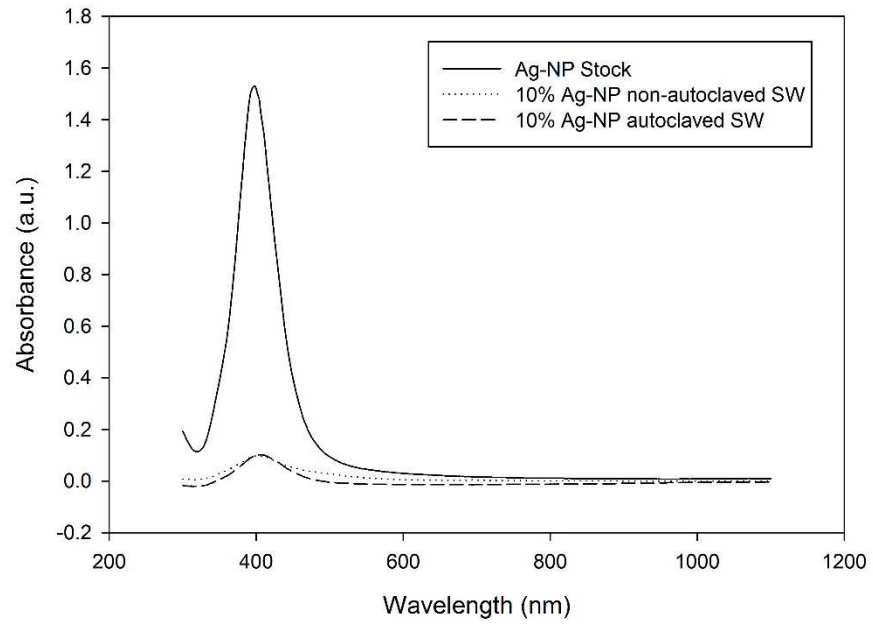
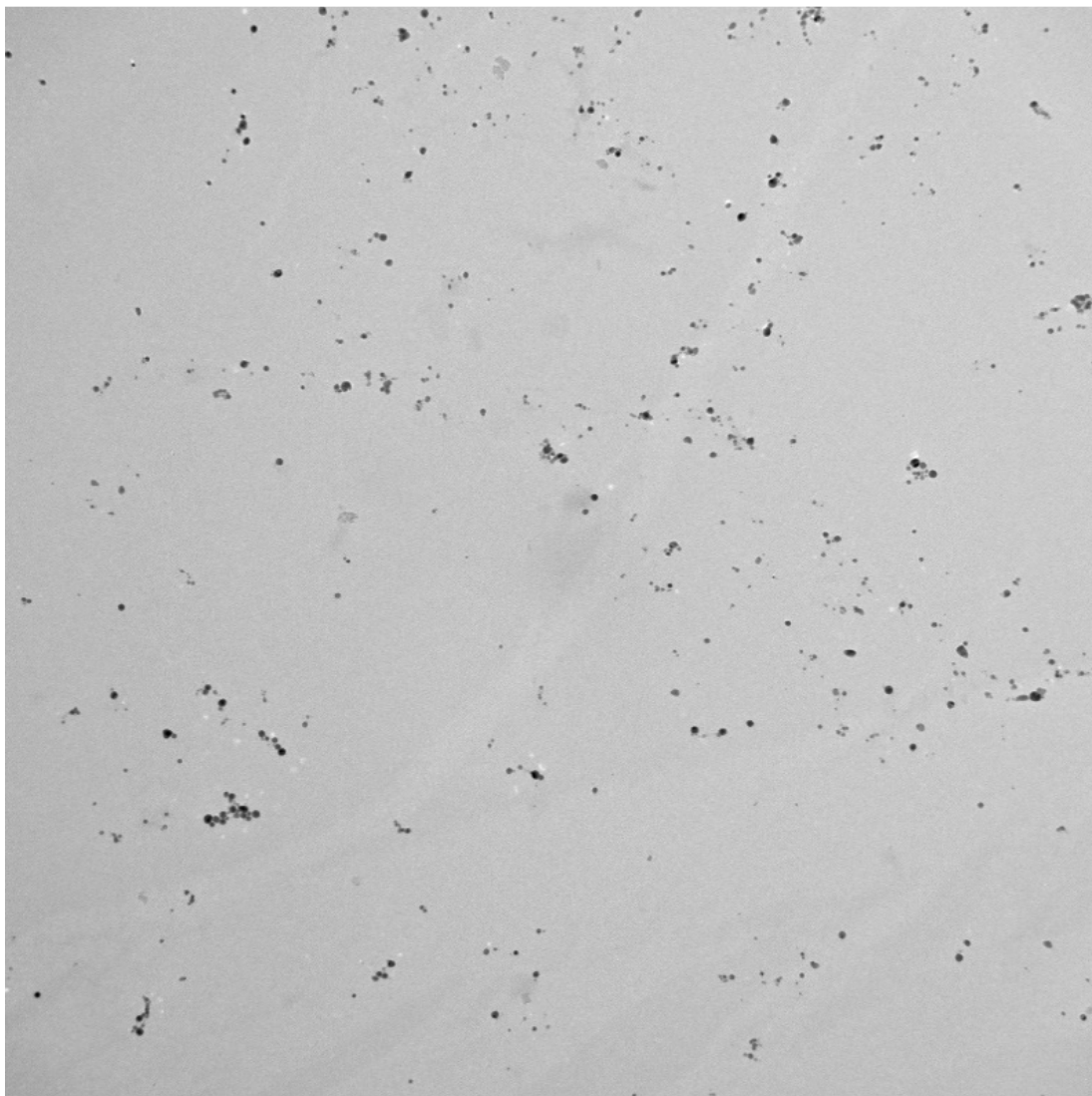


**Figure S3.** UV-Vis spectra of Ag-NP stock solution.



Pic 4.tif  
NP soln. 1:10 w/ DDI  
Print Mag: 59600x @ 7.0 in  
3:31:39 PM 7/17/2017

500 nm  
HV=100000.0kV  
Direct Mag: 50000x  
University Of Arkansas

**Figure S4.** TEM image of synthesized Ag-NP stock solution.



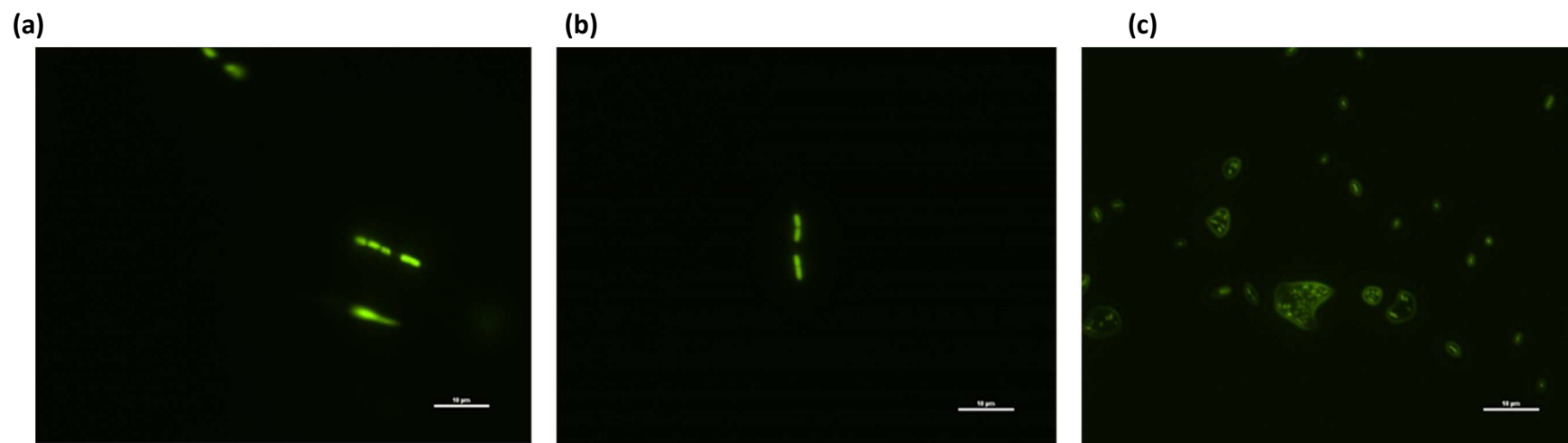


**Figure S6.** Morphology of each species in model mixed biofilm (a) *Acinetobacter calcoaceticus* (b) *Comamonas testosteroni* (c) *Delftia acidovorans*.

**Table S1.** Particle size analysis for stock Ag-NP solution.

<b>Statistics</b>		
Mean	14.59526	nm
Standard Error	0.214079	nm
Median	13.66071	nm
Mode	8.801289	nm
Standard Deviation	6.976468	nm
Sample Variance	48.67111	nm
Kurtosis	0.301524	nm
Skewness	0.654786	nm
Range	40.91322	nm
Minimum	1.876302	nm
Maximum	42.78952	nm
Count	1062	particles

**Table S2.** Particle size analysis for Ag-NPs in SW.

---

***Non -autoclaved Statistics***

---

Mean	7.050799	nm
Standard Error	0.306065	nm
Median	6.133327	nm
Mode	3.657064	nm
Standard		
Deviation	3.060648	nm
Sample Variance	9.367566	nm
Kurtosis	1.141261	nm
Skewness	1.242407	nm
Range	13.42785	nm
Minimum	3.657064	nm
Maximum	17.08491	nm
Sum	705.0799	
Count	100	particles

---

---

***Autoclaved Statistics***

---

Mean	10.01536	nm
Standard Error	0.487255	nm
Median	8.84055	nm
Mode	3.7697	nm
Standard		
Deviation	6.007287	nm
Sample Variance	36.0875	nm
Kurtosis	1.236031	nm
Skewness	1.274865	nm
Range	27.27638	nm
Minimum	3.579472	nm
Maximum	30.85585	nm
Sum	1522.335	
Count	152	particles

---

## Chapter 5

### Real-time interaction of mixed species biofilm with silver nanoparticles using QCM-D

## Abstract

Biofilm – nanoparticle interactions play an important role in nanoparticle fate and bioaccumulation into aquatic food webs. Nanoparticle release into the environment primarily occurs near wastewater treatment plant effluent streams. This study investigated the real-time changes in biofilm viscoelasticity of a mixed model wastewater biofilm in the presence of silver nanoparticles (Ag-NPs). Biofilms were monitored by a quartz crystal microbalance with dissipation monitoring (QCM-D) and measured with confocal laser scanning microscopy. A Voigt model of QCM-D change in resonant frequency  $\Delta f$  and dissipation  $\Delta D$  was developed for biofilm formation and attachment, biofilm exposed to Ag-NPs at multiple concentrations. The model showed differing biofilm viscoelastic reactions depending on the concentration. At 20 ppb, the viscosity measured at the sensor decreased from 1.02 to 0.072 kg m<sup>-1</sup>s<sup>-2</sup>. Thickness measurements from Voigt modeling also decreased from approximately 95  $\mu$ m to less than 1  $\mu$ m. At 300 ppb, the opposite reaction occurred. That is, thickness measurements increased three-fold. Further,  $\Delta D/\Delta f$  steadily increased over time. These reactions suggest that viscoelastic attachment occurring at the sensor surface is directly affected by the varying of Ag-NP concentrations. At minimal concentrations, the cell – surface interface becomes a more elastic attachment. Whereas at the greater concentration of 300 ppb, the cell – surface interface becomes more viscoelastic where the cells are more loosely attached. This allows for more fluid to encounter the sensor surface as well. To further understand such differences, a step-input experiment with increasing concentrations of Ag-NPs (127, 666, 1160, 1632 ppb) was performed. A similar pattern was observed. For low concentrations,  $\Delta D/\Delta f$  ratios decreased. At concentrations above 1 ppm, biofilm  $\Delta D/\Delta f$  responses switched to an increasing ratio. This step-input response showed a structural pattern of rigidity at low concentrations, and less rigidity of attached mass at higher concentrations.



## 1. Introduction

The quartz crystal microbalance sensor (QCM) is useful for applications in environmental studies, medical research, and the food industry where the interface between biological systems and non-living materials is of great interest. Most often, this interface is in a fluid environment and heterogeneous, increasing the difficulty of studying its characteristics. However, the acoustic technique of QCM with dissipation (QCM-D) differentiates between significantly different acoustic environments, such as the bulk liquid and organic materials (Tellechea, Johannsmann, Steinmetz, Richter, & Reviakine, 2009). The QCM-D technique measures acoustic waves from an oscillating quartz crystal to measure adsorbed mass at nanogram sensitivity. The decay of the oscillation is measured as the change in dissipation. QCM-D relies on the piezoelectric property of quartz when a voltage is applied close to the resonant frequency of the quartz sensor (Dixon, 2008). In 1986, the first quartz crystal sensor in liquid solution was coated with anti-*Candida* antibodies for the detection of *Candida albicans* (Muramatsu, Kajiwara, Tamiya, & Karube, 1986). Over the next 30 years, QCM-D improved in sensitivity and liquid loading condition measurement accuracy. QCM-D offers the advantages of eliminating the need for molecular labeling, remaining operational even with complex media, and detection of nanoscale changes in viscoelastic properties at the sensor surface (Marx, 2003).

QCM-D has shown advantageous for detecting microbes as a biosensor and monitoring bacteria biofilm growth (Dixon, 2008). Rodahl et al. (1997) first demonstrated the adhesion of small cell colonies resulted in significant shifts in dissipation. The dissipation shift was attributed to liquid trapped within the cells, cell membranes, and at the cell-surface interface. Dissipation shifts will change in response to these trapped liquids. For example, a bench scale system was constructed with a QCM-D sensor setup for online detection of *Pseudomonas cepacian*, a common

contaminant in sterile water systems. *P. cepacian* was used as a model biofilm to reproduce a contamination event in an ultrapure water system (Nivens, Chambers, Anderson, & White, 1993). Frequency and dissipation changes have also shown that ionic strength of a solution influences adhesion, as demonstrated with fimbriated and nonfimbriated *Escherichia coli* (Otto, Elwing, & Hermansson, 1999). Changes in biofilm, reflected in the ratio of change in dissipation to change in resonant frequency ( $\Delta D/\Delta f$ ) graphs versus time have also shown valuable to identify biofilm structural changes (*i.e.* biofilm attachment, response to bulk fluid changes). In a previous study over 6 days, *P. aeruginosa* biofilm was grown with QCM monitoring; the biofilm attachment, thickening, and response to bulk media changes in tap water was clearly reflected in slope changes of the ( $\Delta D/\Delta f$ ) graphs (Reipa, Almeida, & Cole, 2006). Other monolayer bacteria adhesion studies have focused on motility, hydrophobicity, and rate of adhesion (Gutman, Walker, Freger, & Herzberg, 2013; Jiang, Li, Jia, & Lei, 2010; Marcus, Herzberg, Walker, & Freger, 2012a). Multilayer studies limit film types to rigid films, as rigid multilayered assemblies are easily characterized by the frequency decrease with each layer, while dissipation remains constant (Teichroeb, Forrest, Jones, Chan, & Dalton, 2008; Yan, Liu, Wang, Ni, & Cheng, 2011). Assemblies of both rigid and viscous materials introduce complexity with differentiating between material reactions as new layers are introduced, given that dissipation changes may influence resonant frequency changes.

As engineered nanoparticles (ENPs) are now incorporated into consumer products and medical devices, they could interact with biofilm in various environments. Either to maximize the antimicrobial efficacy of ENPs such as in medical devices, or to minimize the impact on biological processes such as wastewater treatment, there is a need to form a mechanistic understanding of the ENP – biofilm interactions. Previous QCM-D investigations of ENP-

biofilm interaction use the approach of forming a rigid layer from ENPs onto the crystal, then exposing the sensor to a model biofilm. For example, silver nanoparticles (Ag-NPs) were loaded in hydrogen bonded multilayers followed by a 20-hour incubation for antimicrobial activity with *E. coli* and *Staphylococcus epidermidis* (Daeyeon Lee, Robert E. Cohen, & Michael F. Rubner\*, 2005). While model biofilm of a single species provides valuable insights to ENP-biofilm interactions, it is rarely the case in realistic environment. To the best of the authors' knowledge, we are unaware of studies that have yet to use QCM-D as a tool to fundamentally investigate the interaction between a mixed species biofilm and non-rigidly attached ENPs.

Biofilm extracellular polymeric substances (EPS) are a gel-like secretion of proteins, polysaccharides, and nucleic acids (Metcalf, and, & Eddy, 2003). EPS surrounds attached cells on a surface, providing a barrier between stressors and bacteria cells. When changes in a liquid interface occur, biofilms can experience tensile, shear, or compressive forces. The characteristics exhibited by biofilms from these forces are both viscous and elastic (viscoelastic). For stress relief, viscous deformation is irreversible over time whereas elastic stress occurs instantaneously but can return to the original state once a stress is removed (Brandon W Peterson et al., 2015). Peterson et al. hypothesized a relationship between biofilm structure and composition with viscoelastic properties. With QCM-D, viscoelastic properties are a quantifiable likeness to structure and composition. As changes in viscoelasticity are a mode of responding to chemical or mechanical stresses, a fundamental understanding of biofilm viscoelasticity as exposed to ENPs will allow for better predictions of biofilm stress responses in the presence of ENPs.

This study aims to determine the viscoelastic reaction of a mixed species biofilm in the presence of Ag-NPs. As described, the viscoelastic properties of biofilms are a key characteristic aiding in resistance to mechanical or chemical stresses (B. W. Peterson et al., 2015). Here, we apply a

quartz crystal microbalance with dissipation (QCM-D) to examine the viscoelastic response of a model wastewater biofilm with mixed species bacteria to silver nanoparticles (Ag-NPs).

## 2. Methods and Materials

**Chemicals and reagents.** Laboratory glassware used were washed in phosphorous-free laboratory detergent, rinsed three times with tap water, and three times with distilled deionized (DDI) water [Elga Process Water System ( $18.2 \text{ M}\Omega \cdot \text{cm}^{-1}$ ) Purelab flex, Veolia, Ireland]. All glassware used for nanoparticle exposure were acid washed in 10% hydrochloric acid, rinsed three times with DDI water, and air dried.

All reagents obtained were analytical grade and used as received. Synthetic wastewater (SW) feed solution was prepared with glucose ( $140 \text{ mg L}^{-1}$ ), Difco nutrient broth ( $300 \text{ mg L}^{-1}$ ),  $\text{KH}_2\text{PO}_4$  ( $43.9 \text{ mg L}^{-1}$ ),  $\text{NaOH}$  ( $25 \text{ mg L}^{-1}$ ),  $\text{KNO}_3$  ( $3 \text{ mg L}^{-1}$ ),  $\text{NaHCO}_3$  ( $175 \text{ mg L}^{-1}$ ),  $(\text{NH}_4)_2\text{SO}_4$  ( $118 \text{ mg L}^{-1}$ ),  $\text{CaCl}_2$  ( $133 \text{ mg L}^{-1}$ ),  $\text{FeCl}_3 \cdot 6\text{H}_2\text{O}$  ( $5 \text{ mg L}^{-1}$ ),  $\text{MgSO}_4$  ( $100 \text{ mg L}^{-1}$ ), and  $\text{MnSO}_4$  ( $12.8 \text{ mg L}^{-1}$ ). Phosphate, chlorides, nitrate, and ammonia were measured with Ion Chromatography (Metrohm 850 IC, Switzerland).

**Microbial culture.** The strains *Comamonas testosteroni* ATCC 11996, *Acinetobacter calcoaceticus* ATCC 31926 and *Delftia acidovorans* ATCC 15668 were obtained and propagated as instructed in Difco nutrient broth at  $30^\circ\text{C}$  for 48 hours. Working cultures were maintained on nutrient broth agar plates for 30-day increments at  $4^\circ\text{C}$ . Preceding the experiment, one colony of each species was inoculated in 100 mL of SW for 18 hours to reach exponential growth phase. Cell counts were measured by the Multisizer 4 Coulter Counter (Beckman Coulter, CA, USA).

**Nanoparticle characterization.** Silver nanoparticles were formed using sodium borohydride to reduce silver nitrate with sodium citrate as a capping agent. (Mulfinger et al., 2007). The formation of Ag-NPs was confirmed by scanning the absorbance from 300 – 700 nm with a UV-

vis spectrophotometer (Beckman Coulter, CA, USA). Size and shape were characterized with transmission electron microscopy. Total silver concentrations were measured with ICP-MS (Arkansas Mass Spec Facility). Ionic silver and nano-particulate silver were measured separately by applying multiple separation techniques with 0.1 µm Acrodisc syringe filters (Life Sciences, Colorado) and 3kDa centrifugal membranes (Merck Millipore, Massachusetts).

**Experimental setup and QCM-D analysis.** Before experimentation, synthetic wastewater pH was adjusted with a pH meter to 8 with 0.1 M hydrochloric acid if necessary (Thermo-Scientific, Fort Collins, Colorado). All SW, Ag-NPs, and PBS solutions were pre-filtered through 0.1 µm filters to eliminate background interference. Label free real-time monitoring of cell adsorption and structural changes of biofilm were measured with QCM-D (Qsense E4, Gothenburg, Sweden). QCM-D provides real-time tracking of mass changes as molecular layers form, through changes in oscillating frequency ( $\Delta f$ ) of a quartz crystal sensor. Viscoelastic properties such as structural deformation and rigidity are monitored through the energy dissipation ( $\Delta D$ ) response of the oscillating sensor. For non-porous rigid attachment, the resonant frequency is linearly related to a mass change per unit area at the QCM sensor surface according to the Sauerbrey equation:

$$\Delta f = - C_f \cdot \Delta m \quad (1)$$

Where  $C_f$  is the sensitivity factor of the sensor (56.6 Hz  $\mu\text{g}^{-1} \text{cm}^2$  for a 5MHz AT-cut quartz crystal, room temperature.) The Sauerbrey equation assumes the added mass and thickness are significantly smaller than those of the sensor, the added mass is rigid and uniform, and the measured resonance takes place in vacuum or in air. In the instances where the added mass is not rigid but a soft, porous film, the Sauerbrey equation underestimates the mass in contact with the sensor. Viscoelastic modeling with the Voigt Model corrects for this underestimation by

including dissipation changes within the model calculations (Voinova, Jonson, & Kasemo, 2002). With the Voigt Model, the correct film characteristics for viscosity, elasticity, and thickness were calculated in Q-Sense QTools (Biolin Scientific, New Jersey, USA). Models were improved by expanding the lower and upper limits for shear and viscosity fitted parameters. Models were considered acceptable when chi-squared values were minimized and modeled datasets overlay measured datasets when graphed.

A gold sensor with a titanium adhesion layer (QSX338 Au, Qsense) was pre-cleaned according to the recommended protocol: a new gold coated sensor crystal was treated with UV/Ozone for 15 minutes, submersed in a 5:1:1 solution of Millipore water, ammonia (25%) and hydrogen peroxide (30%) for 5 minutes at 75°C, thoroughly rinsed with Millipore water, dried with pure N<sub>2</sub> gas, and treated again with UV/Ozone for 15 minutes. The QSense instrument was pre-cleaned with a separate sensor mounted within the system. Approximately 10 ml of 2% SDS in water was pumped through the system followed by approximately 20 ml of Millipore water. The chamber was disassembled and visible parts were dried with N<sub>2</sub> gas. The cleaned gold sensor was mounted and resonances were found first with only air within the system followed by a phosphate buffered saline (pH=7.4) at 150 µl min<sup>-1</sup> until the frequency stabilized. After stabilization, the feed solution was switched to the mixed model consortia in SW. After biofilm thicknesses stabilized, the feed solution was switched to sterile SW for 10 minutes to ensure any planktonic bacteria were removed from the system. Then, it was switched to sterile SW containing Ag-NPs. These steps were repeated with the following Ag-NP concentrations: (1) 20 ppb (2) 300 ppb (3) incremental additions of 127 ppb, 666 ppb, 1160 ppb, 1632 ppb, and 127 ppb. After experimentation, the instrument was rinsed and cleaned while containing a replacement sensor for cleaning with 25 ml of 2% SDS, followed by 2.5% nitric acid and

thoroughly rinsed with Millipore water. The biofilm attached sensor was carefully placed on a glass microscope slide in a sterile petri dish, wrapped in foil, and placed on ice. The experiments were repeated with the same bacteria cultures to confirm reproducibility of biofilm formation results.

**Biofilm analysis and microscopy.** Cell counts were measured in triplicate for each pure culture species by Coulter Counter before combining into mixed model consortia. Equal volumes averaging  $5.3 \times 10^7$  cells  $\text{mL}^{-1}$  of each suspension were combined and brought to 50 mL with 0.1  $\mu\text{m}$  filtered sterile SW. Preceding the incremental experiment, cell counts averaged  $3.1 \times 10^5$  cells  $\text{mL}^{-1}$ . The mixed consortium was then used as the influent for QCM-D, where cells attached to the sensor over time form a biofilm. After experimentation, biofilm viability and biovolume were determined with *bacLight* Live/Dead cell stain under confocal laser scanning microscopy (CLSM) (Live/Dead *bacLight* Bacterial viability kit, Life Technologies, Grand Island, New York) (Walden, Carbonero, & Zhang, 2016). The biofilm was stained with a 50/50 mixture of propidium iodide and SYTO 9 for 30 minutes ahead of imaging. A minimum of four replicate image stacks were obtained on two different experimental days with a Nikon 90i upright CLSM using the 60 $\times$  objective lens (Nikon, Melville, New York). Total biovolume was calculated as the sum of each stained biovolume after thresholding. The area of mass was multiplied by the total distance between the layers in the stack (NIS Elements, Nikon, Melville, New York). For comparison to other studies, this biovolume was divided by the area of the image view to report final datasets in  $\mu\text{m}^3/\mu\text{m}^2$  units.

**Statistical analysis.** QCM-D datasets were modeled in Qtools with the Voigt model. Qtools models were downloaded, and data tables were generated in Microsoft Excel (Microsoft, Redmond, WA). Output files graphing and statistical analysis was completed in SigmaPlot

version 12.5 from Systat Software, Inc., San Jose California USA, [www.systatsoftware.com](http://www.systatsoftware.com).

Statistic  $p$  values less than 0.05 were considered significant. Where possible, triplicate values are reported with standard error of the mean.

### 3. Results and Discussion

The aim of this work was to evaluate the viscoelastic property changes of mixed species biofilm when exposed to silver nanoparticles. Three gram-negative species relevant to wastewater were chosen (Table 1). These bacteria are tolerant to stresses such as heavy metals and have all shown as moderate to strong biofilm formers (Andersson, Kuttuva Rajarao, Land, & Dalhammar, 2008). We chose to use a mixed species biofilm that would better represent the structural heterogeneity found in wastewater biofilms. For reproducibility, however, we limited the model to three specific species.

Before experimentation, silver nanoparticles were synthesized, where UV-vis spectra results showed the characteristic peak at 398 nm for Ag-NPs (Mulfinger et al., 2007). Shape and particle size distribution measured with TEM for the stock Ag-NP solution showed typical round particles ranging from 1.9 – 42.8 nm diameter. The final Ag-NP in SW suspension (Figure 1) contains an average Ag-NP size of  $10 \pm 0.49$  nm and less than 4 ppb of total silver was measured as silver ion. By filtering the SW through 0.1  $\mu\text{m}$  filters, the removal of precipitates improved the stability of Ag-NPs in this media. Silver stock was also filtered through a 0.1  $\mu\text{m}$  filter and remeasured to confirm that agglomeration did not occur. ICP-MS analysis reflected a concentration of approximately  $1 \text{ mg L}^{-1}$  stock Ag-NPs.

**QCM-D experiments with confocal microscopy.** Individual bacteria species was grown separately in SW for 18 hours to exponential growth phase, with cell densities ranging from  $3.7 \times 10^7$  to  $8 \times 10^7$  cells  $\text{mL}^{-1}$ . QCM-D real-time measurements reflect biofilm formation as



positive shifts in resonant frequency and dissipation occurred at the third overtone (Figure 2a). This is counter-intuitive to the negative frequency expectation when rigid mass attached increases in quantity. As biofilm attachment includes viscoelastic non-rigid attachment however, the rigid model no longer applies. Previous studies showing bacterium with surface appendages can show an increase in frequency measurements using QCM-D, despite the adherence of increasing cell numbers (Olsson, Mei, Busscher, & Sharma, 2008). In this study, two of the three species in the consortia are known to have polar or bipolar flagella, resulting in the expected frequency increase. Voigt models of the resonant frequency and dissipation changes during biofilm formation were used to calculate biofilm thicknesses over time. The QCM models reflect that after 30 minutes, biofilm thickness remained stable at  $105.6 \pm 9 \mu\text{m}$ . A previous study of Ag-NPs and *Aquabacterium citratiphilum* showed similar biofilm thicknesses (Grün, Meier, Metreveli, Schaumann, & Manz, 2016). From the beginning of attachment, the resonant frequency was changing at rates ranging  $0.094 - 0.268 \text{ Hz min}^{-1}$  (Table 2). Dissipation models among replicates for biofilm formation showed rates from  $0.146 - 0.222 \cdot 10^{-6} \text{ min}^{-1}$ . The ratio of dissipation change to resonant frequency changes ( $\Delta D/\Delta f$ ) for the control experiment with Ag-NPs alone show an exponential decrease approaching 0.25 (Figure 3a). Whereas during biofilm formation, this ratio increases in favor of greater dissipation changes compared to frequency (figure 3b).

**Exposure to nanoparticles.** Without nanoparticles, modeled biofilm thickness remained steady after about 30 minutes. The net interactions between the biofilm dynamics and nanoparticle attachment shows the biofilm structure changing differently for each concentration of Ag-NPs (Figure 4). We address each separately in the following paragraphs.

**20 ppb Ag-NPs.** The dissipation shifted negatively from approximately 0.2 to 0.1 ( $10^{-6} \text{ min}^{-1}$ ) after biofilm were exposed to 20 ppb Ag-NPs (Table 2). Viscosity also decreased from 1 ( $\text{kg ms}^{-1}$ ) to 0.072 ( $\text{kg ms}^{-1}$ ). These two changes indicate the attached structure (which may now include Ag-NPs) becoming more rigid and increasingly thin. The final biofilm thickness was modeled at  $0.97 \pm 0.004 \mu\text{m}$ . This reduction in thickness combined with decreased viscosity and dissipation suggests two possibilities: Ag-NP accumulation or cell detachment. At this low concentration, previous studies have shown no significant effect on biofilm viability (Fabrega, Renshaw, & Lead, 2009; Grün et al., 2016). Further, by graphing  $\Delta D/\Delta f$  versus time, the decrease in dissipation is reflected in a decreasing slope of  $\Delta D/\Delta f$ . This suggests the attached mass becomes more rigid over time.

**300 ppb Ag-NPs.** After exposure to 300 ppb Ag-NPs, calculated thickness increased over time, showing a final three-fold increase to  $314 \mu\text{m}$  (Figure 4). The dissipation rate slightly increased to  $0.271 (10^{-6} \text{ min}^{-1})$ , whereas viscosity remained unchanged. By comparing this increase of attached thickness to  $\Delta D/\Delta f$  graphs, we can disseminate the type of structural change occurring at the sensor interface. As nanoparticles were introduced,  $\Delta D/\Delta f$  increased over time. An increase of the  $\Delta D/\Delta f$  ratio indicates a less rigid, softer attached biofilm structure. A softer structure could be an indication of cell detachment or death.

For this concentration, the sensor was carefully removed where random fields of view were imaged from the bottom to the top of the stained biofilm cells. Biovolumes were estimated by correlating fluorescence signals with bacteria mass. Confocal image stacks measured a final biovolume of  $3.31 \pm 0.6 \mu\text{m}^3 \mu\text{m}^{-2}$ . Typical biovolumes for these species range 3.5 to  $7.3 \mu\text{m}^3 \mu\text{m}^{-2}$  when grown for 24 hours in a bioreactor. Further, we measured biofilm thickness from confocal images to confirm the modeled increase. Confocal biofilm thicknesses were  $35.6 \pm 5.0 \mu\text{m}$ , which

is less than the QCM measurements. Where confocal thickness measurements are solely stained bacteria cells, the difference could be attributed to attached nanoparticles or loosely attached cells which may have detached after cell staining. The final live:dead cell ratio was  $1.311 \pm 0.4$ , and the live/total cell percentages were  $48.2\% \pm 8.9\%$ .

The softening of the biofilm attached could suggest a detachment, where cells detaching also create more pore space within the biofilm structure. This pore space can then fill with fluid or nanoparticles. A previous study investigating the impact of the type of bacteria cell on resonant frequency showed that hydrophilic bacteria do not fully attach, and the connection between the sensor and cell are viscoelastic where a gap separates the bacteria cell and sensor (Marcus, Herzberg, Walker, & Freger, 2012b). Contrarily, if the cells fully attached, the interface at the sensor surface would respond to water release with an increase in  $\Delta f$  as the cell act points are dominated by elastic loading. We suspect a simultaneous biofilm detachment as well as Ag-NP adsorption to the remaining biofilm consortia, causing a net 'pull' away from the sensor. This would explain why the viscosity and dissipation rates did not change although modeled thickness increased. The attached mass at the sensor becomes more fluid, and an increase in shear modulus occurred.

**Step-input experiment.** With 20 ppb Ag-NPs and 300 ppb Ag-NPs elucidating two different biofilm responses, a series of Ag-NPs were chosen to study multiple responses over time. At the low end, 127 ppb Ag-NPs, and at the highest concentration was 1632 ppb. Finally, a decrease in Ag-NPs back to 127 ppb was included.

Similarities between 20 ppb and 127 ppb are reflected in  $\Delta D/\Delta f$  graphs, where the slope decreases and approaches 1.0 at 20 ppb; the slope decreases from approximately 2.8 to 2.3 at 127 ppb. Following 127 ppb, the increases were: 666 ppb, 1160 ppb, and 1632 ppb. During this step-

increase, the biofilm showed a threshold between the two highest concentrations (above 1 ppm) and the lower concentrations ranging 127-666 ppb. Below this threshold,  $\Delta D/\Delta f$  ratios decreased in a similar fashion as discussed with 20 ppb. Above this threshold,  $\Delta D/\Delta f$  ratios increased like the previous single exposure to 300 ppb. Interestingly, after 1632 ppb exposure, the step-down to 127 ppb showed a  $\Delta D/\Delta f$  response with decreasing rate as previous. This response may imply that the viscoelastic responses shown here are of an elastic stress response, where biofilm return to the previous arrangement with each change in stress. This step-input response shows a pattern of becoming rigid at low concentrations, and less rigidly attached at higher concentrations. With respect to the different responses observed comparing 20 ppb and 300 ppb exposures separately, perhaps by starting at low concentrations the biofilm structure is allowed time to acclimate to the change of Ag-NPs at the biofilm interface.

#### 4. Concluding Remarks

Different concentrations of Ag-NPs affected the viscoelastic measurements of biofilm using a quartz crystal microbalance. While there is not yet a time resolved technology to measure a dynamic biofilm with a second layer individually, this study shows a new approach to understanding biofilm-ENP interactions at the fundamental level. Previous biofilm studies with QCM-D focus on attachment characteristics of biofilm formation. Here, we step further into understanding the viscoelastic response of biofilm to environmentally relevant Ag-NP concentrations. Biofilms play an important role in biogeochemical cycling of essential nutrients. The viscoelastic properties of biofilm reflect composition and structure. Fundamental understanding of biofilm structural responses will aid in detachment research with other stressors as well, such as antimicrobial surfaces and water storage systems.

## **Acknowledgements**

The authors would like to thank the University of Arkansas National Science Foundation Seed Fund for financial support for this project. Additional thanks to Sergio Ivan Perez Bakovic for training and guidance with using the QCM-D instrument. Confocal images were obtained on an instrument provided by the P3 Center, funded through the Arkansas ASSET Initiative II (EPS-1003970) by the National Science Foundation and the Arkansas Science and Technology Authority.

## Figures and Tables

**Table 1.** Mixed model wastewater biofilm species characteristics.

Species	Taxa	Colony Type	Averaged Cell Count	Shape/Motility	Respiratory pathway	Gram Stain	Ecological Significance
<i>Acinetobacter calcoaceticus</i>	gammaproteobacteria	smooth, pale	$3.83 \times 10^7$	rods, spherical in stationary phase, non-motile.	strictly aerobic	Negative	Dominant in water, and soil; multi-drug resistant and silver tolerant
<i>Comamonas testosteroni</i>	betaproteobacteria	smooth, no pigment	$4.15 \times 10^7$	rods with polar flagella	obligately aerobic	Negative	Heavy metal resistant; relevant in organic compound remediation
<i>Delftia acidovorans</i>	gammaproteobacteria	2-4 mm no pigment	$7.94 \times 10^7$	rods with polar or bipolar flagella	obligately aerobic	Negative	Identified in freshwater and activated sludge, have shown the ability to survive in potable water systems

**Table 2.** Frequency and dissipation rates of change for mixed model biofilm under exposure to different concentrations of Ag-NPs.

	<b>Frequency (Hz min<sup>-1</sup>)</b>	<b>Dissipation (10<sup>-6</sup> min<sup>-1</sup>)</b>	<b>Viscosity (kg/ms)</b>	<b>Shear (Pa)</b>	<b>Voigt thickness (um)</b>
Biofilm (Replicate 1)	0.268	0.221	1.016	1.92x10 <sup>7</sup>	94.7
Biofilm (Replicate 2)	0.144	0.222	1.035	1.53x10 <sup>7</sup>	126.3
Biofilm (Replicate 3)	0.094	0.146	1.143	1.01x10 <sup>7</sup>	95.8
20 ppb Ag-NPs	0.107	0.107	0.072	1.50x10 <sup>7</sup>	0.4
300 ppb Ag-NPs	0.105	0.271	1.031	6.93x10 <sup>6</sup>	314.0
127 ppb Ag-NPs	-0.006	-0.094	1.064	1.47x10 <sup>7</sup>	126.4
666 ppb Ag-NPs	0.105	0.137	1.070	1.51x10 <sup>7</sup>	140.2
1160 ppb Ag-NPs	0.019	0.197	1.100	1.88x10 <sup>7</sup>	161.9
1632 ppb Ag-NPs	0.154	0.848	1.176	2.4x10 <sup>7</sup>	186.2
127 ppb Ag-NPs (step-down)	0.139	0.237	1.194	2.93x10 <sup>7</sup>	200.2

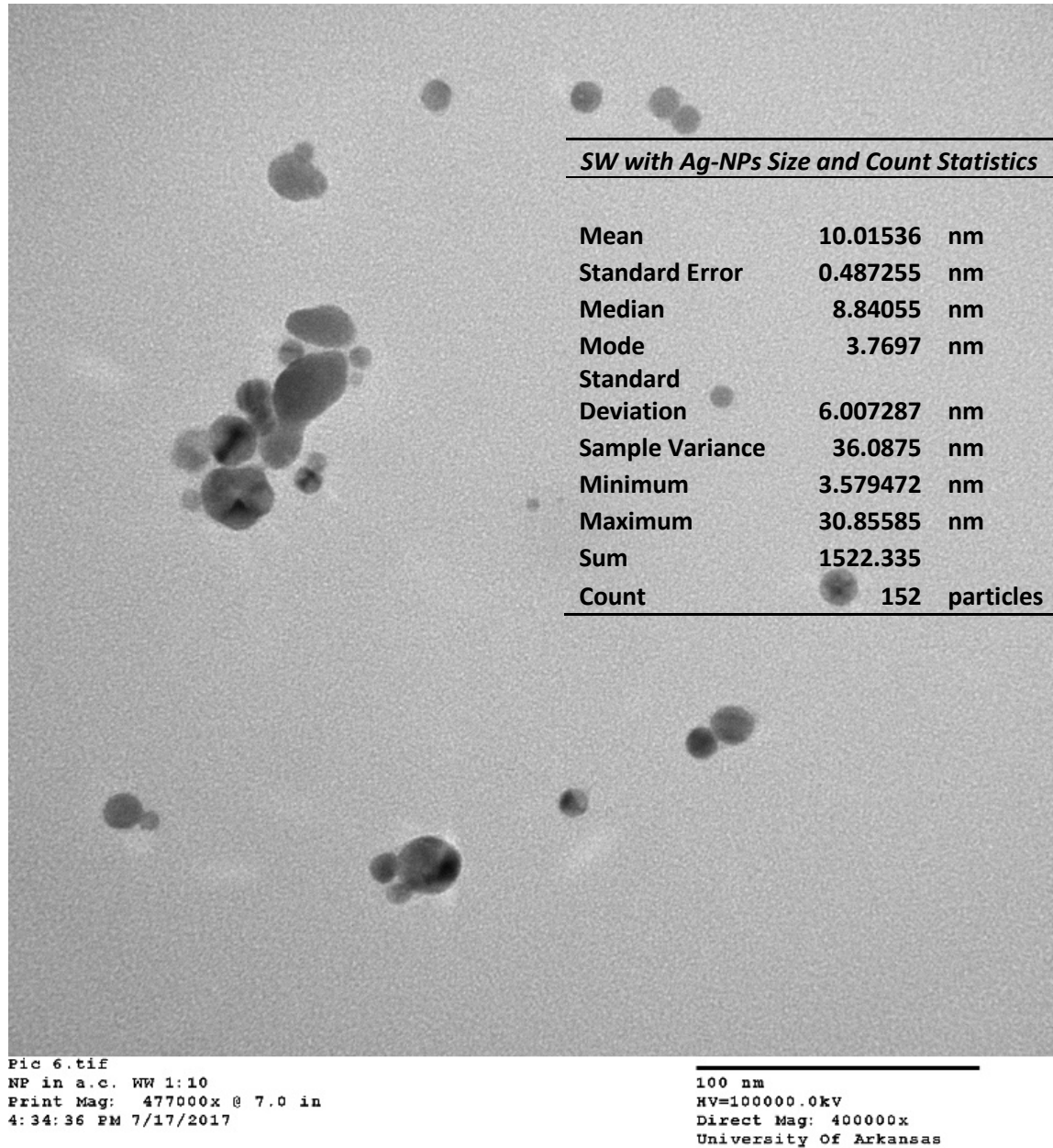


**Figure 1.** TEM image analysis of Ag-NPs in synthetic wastewater. The inset table summarizes the analysis particle counts and mean diameter from ImageJ.



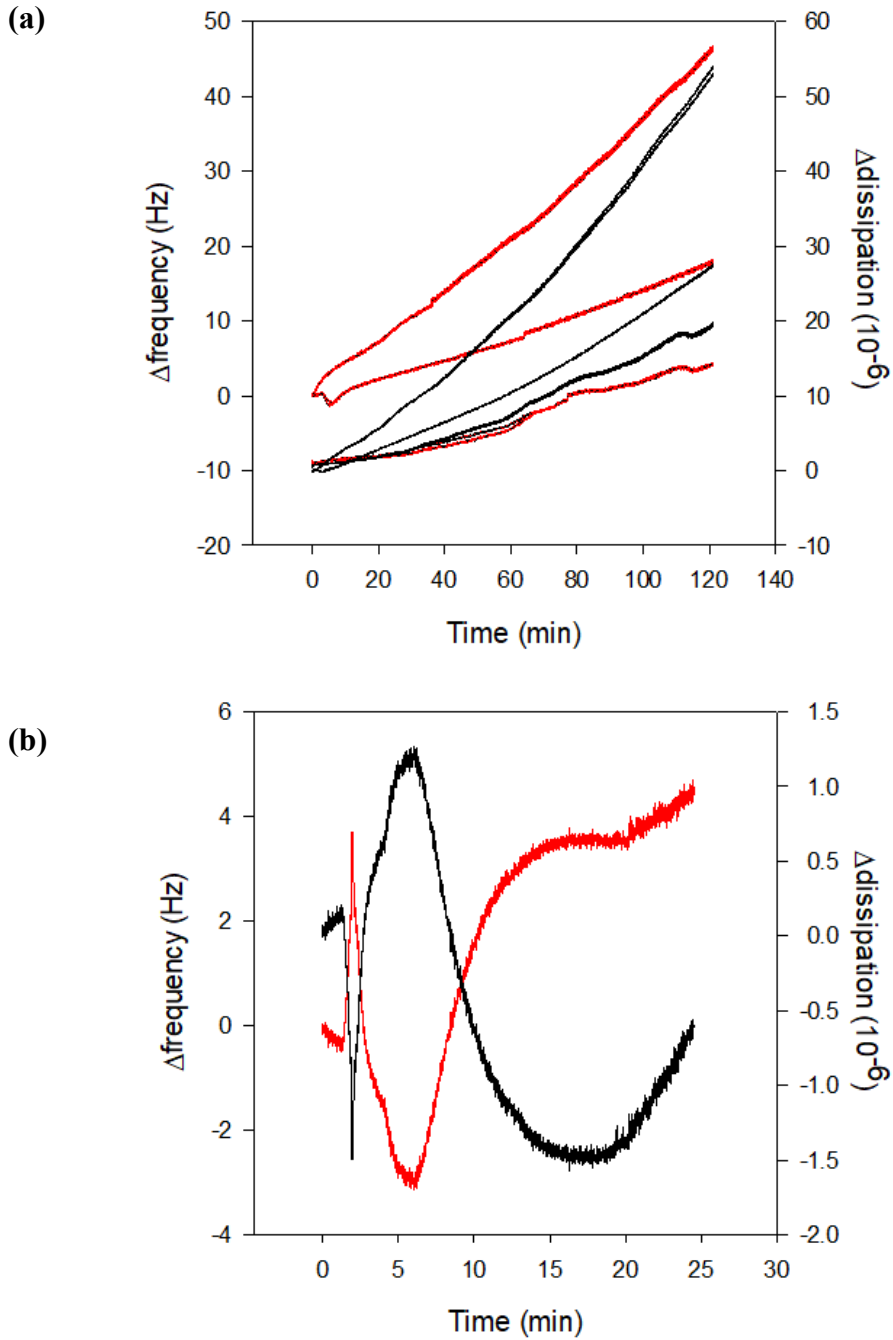


**Figure 2.** Change in frequency (red line) and change in dissipation (black line) for biofilm during Ag-NP exposure. (a) during biofilm formation (b) during biofilm exposure to SW containing 1632 ppb Ag-NPs.

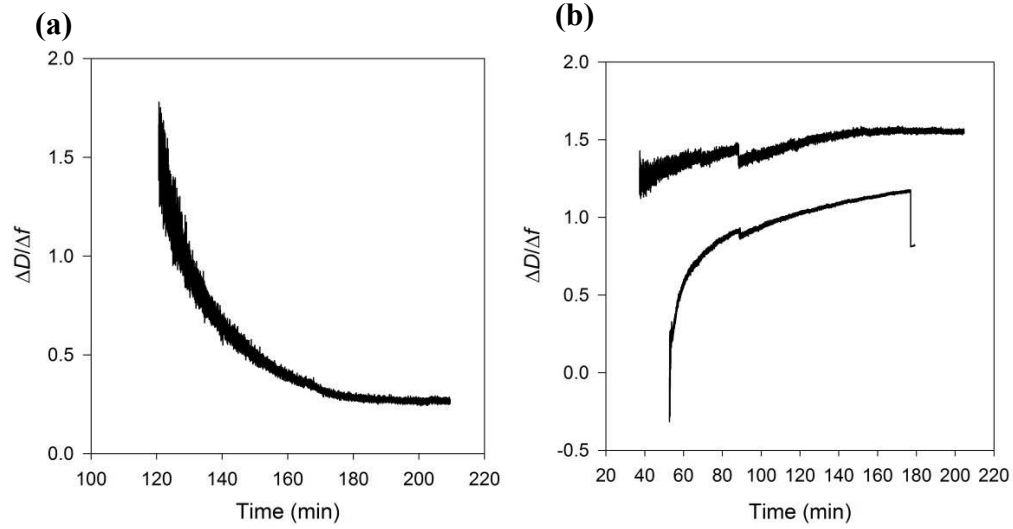


**Figure 3.**  $\Delta D/\Delta f$  over time for (a) Ag-NPs alone (b) during biofilm formation.

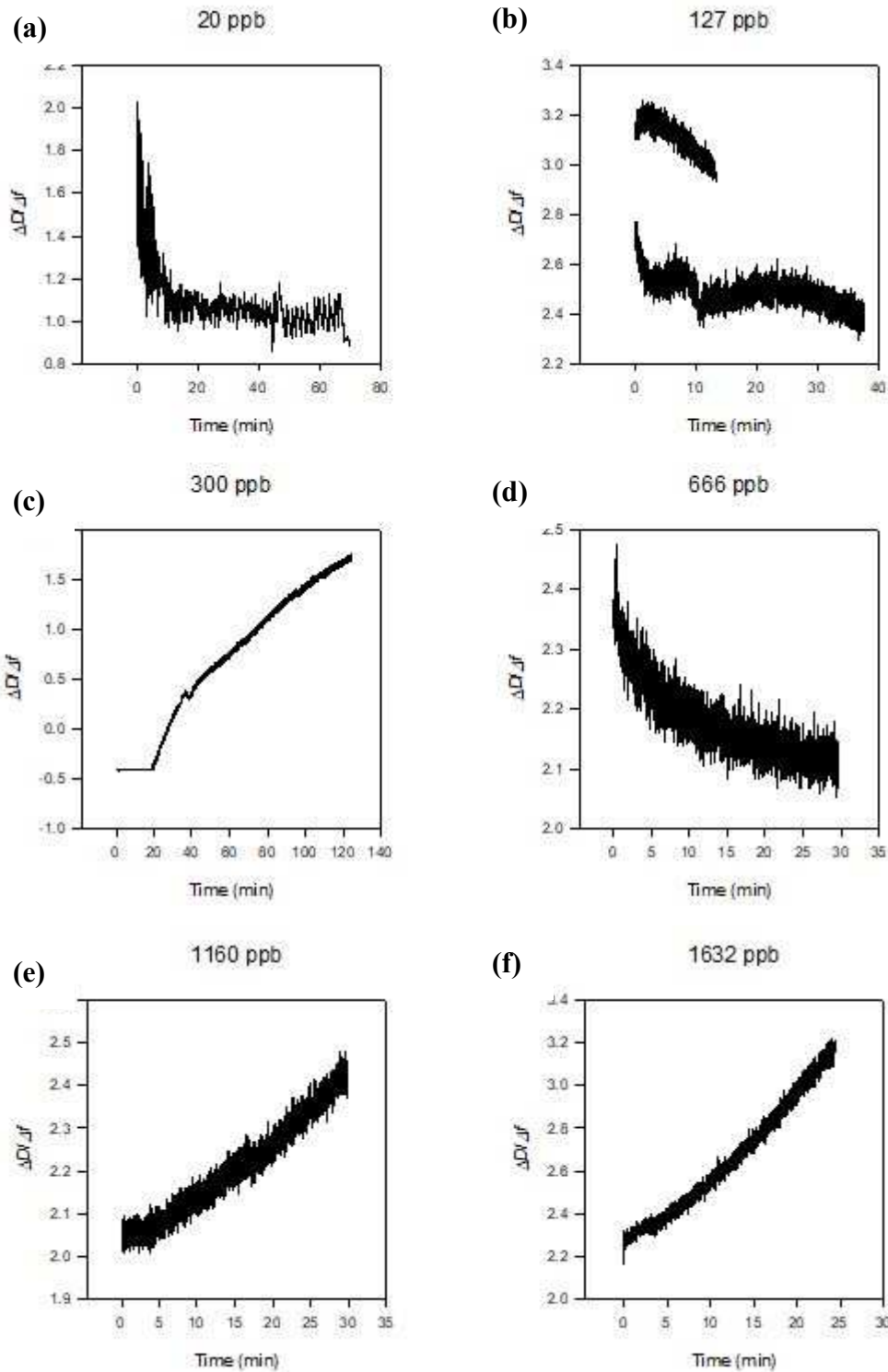


**Figure 4.**  $\Delta D/\Delta f$  over time for each Ag-NP concentration tested. (a) 20 ppb (b) 127 ppb for 30 minutes and 127 ppb final step-down for the final 10 minutes (c) 300 ppb (d) 666 ppb (e) 1160 ppb (f) 1632 ppb.

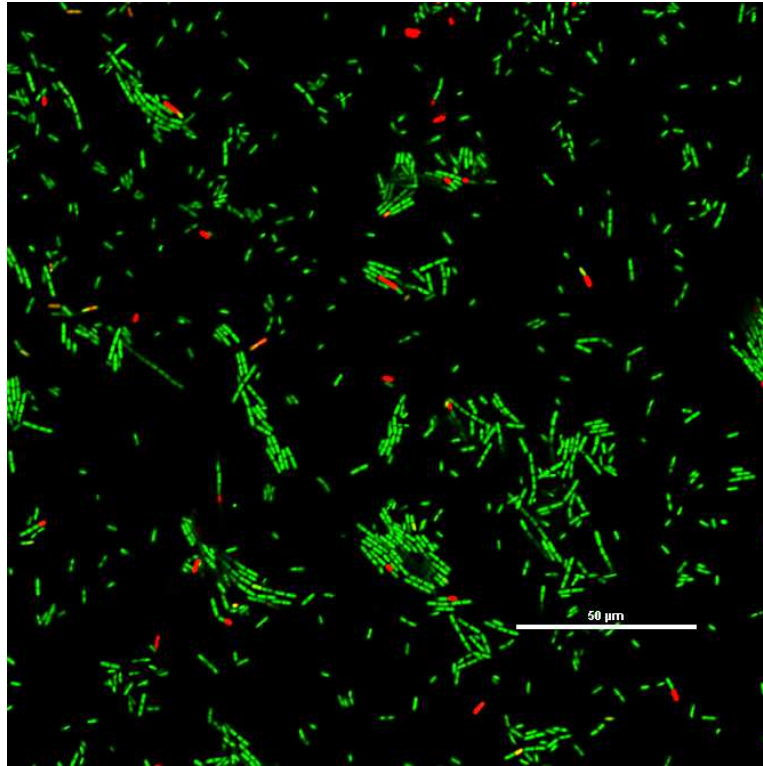
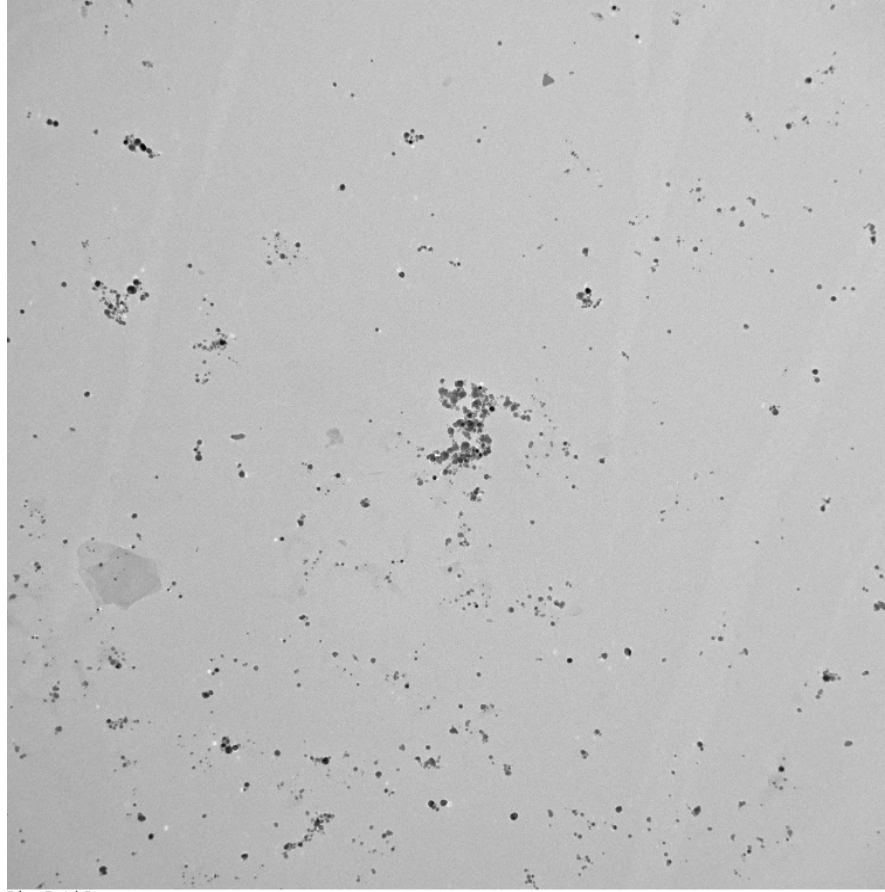


**Figure 5.** Confocal laser scanning microscope image slice from z-stacked measurements of the final attached biofilm to the quartz crystal sensor.

### **Appendix 3**

Supplementary information for

“Real-time interaction of mixed species biofilm with silver nanoparticles using QCM-D



Pic 5.tif  
NP soln. 1:10 w/ DDI  
Print Mag: 59600x @ 7.0 in  
3:33:08 PM 7/17/2017

500 nm  
HV=100000.0kV  
Direct Mag: 50000x  
University of Arkansas

**Figure S1.** TEM image of Ag-NP stock solution.

## References

- Andersson, S., Kuttuva Rajarao, G., Land, C. J., & Dalhammar, G. (2008). Biofilm formation and interactions of bacterial strains found in wastewater treatment systems: Biofilm formation and interactions of bacterial strains. *FEMS Microbiology Letters*, 283(1), 83-90. doi:10.1111/j.1574-6968.2008.01149.x
- Daeyon Lee, Robert E. Cohen, † and, & Michael F. Rubner\*. (2005). Antibacterial Properties of Ag Nanoparticle Loaded Multilayers and Formation of Magnetically Directed Antibacterial Microparticles. *Langmuir*, 21(12), 9651-9659. doi:S0743-7463(05)01330-2
- Dixon, M. C. (2008). Quartz Crystal Microbalance with Dissipation Monitoring: Enabling Real-Time Characterization of Biological Materials and Their Interactions. *J Biomol Tech*, 19(3), 151-158.
- Fabrega, J., Renshaw, J. C., & Lead, J. R. (2009). Interactions of Silver Nanoparticles with *Pseudomonas putida* Biofilms. *Environmental Science & Technology*, 43(23), 9004-9009. doi:10.1021/es901706j
- Grün, A. Y., Meier, J., Metreveli, G., Schaumann, G. E., & Manz, W. (2016). Sublethal concentrations of silver nanoparticles affect the mechanical stability of biofilms. *Environmental Science and Pollution Research*, 23, 24277-24288. doi:10.1007/s11356-016-7691-0
- Gutman, J., Walker, S. L., Freger, V., & Herzberg, M. (2013). Bacterial Attachment and Viscoelasticity: Physicochemical and Motility Effects Analyzed Using Quartz Crystal Microbalance with Dissipation (QCM-D). *Environmental Science & Technology*, 47, 398-404. doi:10.1021/es303394w
- Jiang, D., Li, B., Jia, W., & Lei, Y. (2010). Effect of inoculum types on bacterial adhesion and power production in microbial fuel cells. *Applied Biochemistry and Biotechnology*, 160, 182-196. doi:10.1007/s12010-009-8541-z
- Marcus, I. M., Herzberg, M., Walker, S. L., & Freger, V. (2012a). *Pseudomonas aeruginosa* Attachment on QCM-D Sensors: The Role of Cell and Surface Hydrophobicities. *Langmuir*. doi:10.1021/la300333c
- Marcus, I. M., Herzberg, M., Walker, S. L., & Freger, V. (2012b). *Pseudomonas aeruginosa* Attachment on QCM-D Sensors: The Role of Cell and Surface Hydrophobicities. doi:10.1021/la300333c

- Marx, K. A. (2003). Quartz Crystal Microbalance: A Useful Tool for Studying Thin Polymer Films and Complex Biomolecular Systems at the Solution–Surface Interface. *Biomacromolecules*, 4, 1099-1120. doi:10.1021/bm020116i
- Metcalf, and, & Eddy, I. (2003). *Wastewater engineering : treatment and reuse*: Fourth edition / revised by George Tchobanoglous, Franklin L. Burton, H. David Stensel. Boston : McGraw-Hill, [2003] ©2003.
- Mulfinger, L., Solomon, S. D., Bahadory, M., Jeyarajasingam, A. V., Rutkowsky, S. A., & Boritz, C. (2007). Synthesis and study of silver nanoparticles. *Journal of chemical education*, 84(2), 322.
- Muramatsu, H., Kajiwara, K., Tamiya, E., & Karube, I. (1986). Piezoelectric immuno sensor for the detection of candida albicans microbes. *Analytica Chimica Acta*, 188, 257-261. doi:10.1016/S0003-2670(00)86049-3
- Nivens, D. E., Chambers, J. Q., Anderson, T. R., & White, D. C. (1993). Long-term, on-line monitoring of microbial biofilms using a quartz crystal microbalance. *Analytical Chemistry*, 65, 65-69. doi:10.1021/ac00049a013
- Olsson, A. L. J., Mei, H. C. v. d., Busscher, H. J., & Sharma, P. K. (2008). Influence of Cell Surface Appendages on the Bacterium–Substratum Interface Measured Real-Time Using QCM-D. doi:10.1021/la803301q
- Otto, K., Elwing, H., & Hermansson, M. (1999). Effect of Ionic Strength on Initial Interactions of Escherichia coli with Surfaces, Studied On-Line by a Novel Quartz Crystal Microbalance Technique. *Journal of bacteriology*, 181, 5210-5218.
- Peterson, B. W., He, Y., Ren, Y., Zerdoum, A., Libera, M. R., Sharma, P. K., . . . Van Der Mei, H. C. (2015). Viscoelasticity of biofilms and their recalcitrance to mechanical and chemical challenges. *FEMS Microbiology Reviews*, 39(2), 234-245.
- Peterson, B. W., He, Y., Ren, Y., Zerdoum, A., Libera, M. R., Sharma, P. K., . . . Busscher, H. J. (2015). Viscoelasticity of biofilms and their recalcitrance to mechanical and chemical challenges. *FEMS Microbiol Rev*, 39(2), 234-245. doi:10.1093/femsre/fuu008
- Reipa, V., Almeida, J., & Cole, K. D. (2006). Long-term monitoring of biofilm growth and disinfection using a quartz crystal microbalance and reflectance measurements. *Journal of Microbiological Methods*, 66, 449-459. doi:10.1016/j.mimet.2006.01.016



- Rodahl, M., Höök, F., Fredriksson, C., Keller, C. A., Krozer, A., Brzezinski, P., . . . Kasemo, B. (1997). Simultaneous frequency and dissipation factor QCM measurements of biomolecular adsorption and cell adhesion. *Faraday Discussions*, *107*, 229-246. doi:10.1039/A703137H
- Teichroeb, J., Forrest, J., Jones, L., Chan, J., & Dalton, K. (2008). Quartz crystal microbalance study of protein adsorption kinetics on poly (2-hydroxyethyl methacrylate). *Journal of Colloid and Interface Science*, *325*(1), 157-164.
- Tellechea, E., Johannsmann, D., Steinmetz, N. F., Richter, R. P., & Reviakine, I. (2009). Model-Independent Analysis of QCM Data on Colloidal Particle Adsorption. *Langmuir*, *25*, 5177-5184. doi:10.1021/la803912p
- Voinova, M. V., Jonson, M., & Kasemo, B. (2002). 'Missing mass' effect in biosensor's QCM applications. *Biosensors and Bioelectronics*, *17*, 835-841. doi:10.1016/S0956-5663(02)00050-7
- Walden, C., Carbonero, F., & Zhang, W. (2016). Preliminary Assessment of Bacterial Community Change Impacted by Chlorine Dioxide in a Water Treatment Plant. *Journal of Environmental Engineering*, *142*(2), 04015077. doi:10.1061/(asce)ee.1943-7870.0001029
- Yan, M., Liu, C., Wang, D., Ni, J., & Cheng, J. (2011). Characterization of Adsorption of Humic Acid onto Alumina using Quartz Crystal Microbalance with Dissipation. *Langmuir*, *27*, 9860-9865. doi:10.1021/la1042102

## **Chapter 6**

### **Conclusion**

## 1. Summary

Chapter 2 addressed Objective 1 by critically reviewing activated sludge and biofilm treatment processes. We compared ENP toxicity and fate, while weighing advantages and disadvantages in each type of system.

Chapter 3 addressed Objective 2 with a survey of four locations pertaining to environmental engineering. We chose four methods for DNA extractions and compared such across all locations and two sample types (biofilm versus planktonic). Two extraction methods proved most reliable when comparing all sites in terms sequencing coverage, phylum identification, and community mapping. This work aids in simplifying broad research studies that include multiple sample types and locations.

Chapter 4 and Chapter 5 addressed Objective 3. ENP - biofilm interactions were studied with two bench scale reactors, as well as with QCM-D. A model biofilm was developed and tested for reproducibility and likeness to wastewater biofilm. This model biofilm was stressed with Ag-NPs, and COD removal was monitored. Flow cell tests showed Ag-NP accumulation occurring, where influent concentration fluctuations showed little impact on accumulation. Viscoelastic monitoring with QCM-D showed biofilm structural responses to multiple Ag-NP concentrations by comparing  $\Delta D/\Delta f$  ratios over time. At low concentrations,  $\Delta D/\Delta f$  ratios decreased as the attached mass became more rigid. At high concentrations,  $\Delta D/\Delta f$  ratios increased.